galaxies

MDPI

Review

High-Contrast Imaging: Hide and Seek with Exoplanets

Riccardo Claudi [1,2,*,†] **and Dino Mesa** [1,†]

[1] INAF—Astronomical Observatory of Padova, Vicolo Osservatorio, 5, 35122 Padova, Italy; dino.mesa@inaf.it
[2] Dipartimento di Matematica e Fisica, Università Roma Tre, Via della Vasca Navale 84, 00146 Roma, Italy
* Correspondence: riccardo.claudi@inaf.it
† These authors contributed equally to this work.

Abstract: So far, most of the about 5700 exoplanets have been discovered mainly with radial velocity and transit methods. These techniques are sensitive to planets in close orbits, not being able to probearge star–planet separations. μ-lensing is the indirect method that allows us to probe the planetary systems at the snow-line and beyond, but it is not a repeatable observation. On the contrary, direct imaging (DI) allows for the detection and characterization ofow mass companions at wide separation ($\leq$5–6 au). The main challenge of DI is that a typical planet–star contrast ranges from 10^{-6}, for a young Jupiter in emittedight, to 10^{-9} for Earth in reflectedight. In theast two decades, aot of efforts have been dedicated to combiningarge (D $\geq$ 5 m) telescopes (to reduce the impact of diffraction) with coronagraphs and high-order adaptive optics (to correct phase errors induced by atmospheric turbulence), with sophisticated image post-processing, to reach such a contrast between the star and the planet in order to detect and characterize cooler and closer companions to nearby stars. Building on the first pioneering instrumentation, the second generation of high-contrast imagers, SPHERE, GPI, and SCExAO, allowed us to probe hundreds of stars (e.g., 500–600 stars using SHINE and GPIES), contributing to a better understanding of the demography and the occurrence of planetary systems. The DI offers a possible clear vision for studying the formation and physical properties of gas giant planets and brown dwarfs, and the future DI (space and ground-based) instruments with deeper detectionimits will enhance this vision. In this paper, we briefly review the methods, the instruments, the main sample of targeted stars, the remarkable results, and the perspective of this rising technique.

Keywords: extrasolar planets; direct imaging; astronomical instrumentation; high-contrast imager; data reduction

Academic Editor: Alberto C. Sadun

Received: 20 September 2023
Revised: 7 November 2024
Accepted: 16 December 2024
Published: 31 December 2024

Citation: Claudi, R.; Mesa, D. High-Contrast Imaging: Hide and Seek with Exoplanets. *Galaxies* **2025**, *13*, 3. https://doi.org/10.3390/galaxies13010003

1. Introduction

Perhaps Dyson and collaborators, having observed several bright stars of the Hyades during the Sun's eclipse in 1919, went on to perform the first high-contrast astronomical observation. The total Solar eclipse allowed us to observe the Hyades stars over the coronaight background within a few arcsecs of the Sun andets the observers measure the variation of the apparent position of these stars, confirming the general relativistic prediction [1]. Also, if Dyson and collaborators exploited a total solar eclipse, they would be able to observe stars that were ateast 10^{12} fainter than the Sun. However, we had to wait until 2004 to obtain the first direct observation of a planetary-mass companion (PMC), which was taken with VLT/NACO by Chauvin et al. [2], while in 2008, Marois et al. [3] announced the first exoplanetary system (three planets) found orbiting the young A5V star HR8799, using direct imaging. This detection was fully 13 years after the first exoplanet

orbiting a Solar-like star (95 Peg b [4]) was discovered, and after that, more than 400 new worlds were indirectly discovered by radial velocity, transit, and microlensing techniques. This delay occurred mainly due to the extraordinary efforts that are necessary for the direct imaging techniques to overcome the difficulties imposed by astrophysics (planet–star contrast), physics (diffraction and scattering), and engineering (speckle noise reduction).

The high difference inuminosity and the proximity of the fainter object are the two critical elements involved in high-contrast imaging, which this technique needs to achieve in astronomical observations. In fact, directly observing very faint companions (planets or brown dwarfs) of bright stars is one of the most challenging tasks because of their small angular separation (e.g., <500 mas for a 5 au orbital radius at 10 pc) and the flux contrast between the two. For example, for the Solar System at a distance of 10 pc, the contrast can range from 10^{-3} for Jupiter in the mid-infrared to 10^{-10} for Earth in the visible spectrum (e.g., [5,6]). These difficulties pushed the use of indirect methods in searching for faint companions around stars. In fact, up to now, most of the extrasolar planets detected (about 7300 confirmed objects in August 2024, see Figure 1) have been obtained by searching for the dynamical and photometric effects that invisible companions have on the status of its host star. The most efficient indirect methods are transit (more than 6000 planets) and radial velocity (more than 1500) measurements[1]. Nevertheless, these two techniques are biased toward planets in close orbits. There are about sixty planets discovered with the radial velocity and just one, HD 75784 c, with the transit method, out of the 212 known planets with their orbital axis $>$ 5 au. On the contrary, direct imaging is biased toward thearge orbital axes with four detections of PMCs at a separation of <5 au[2]: WISE J033605.05-014350.4, a system with two BDs observed with JWST [7]; CFBDSIR J145829+101343 B, a component of another BD binary system observed with Keckaser guide star adaptive optics imaging [8]; Luhman 16 A B, a BD discovered with joint efforts of imaging, astrometry, and radial velocity techniques [9,10]; and HD 206893 c, which was also detected in this case with joint use of imaging, astrometry, optical interferometry, and radial velocity techniques [11]. Direct imaging techniques with space-based telescopes andarge ground-based telescopes in combination with adaptive optics (AO) modules is particularly well-suited for wider orbits, beyond the snowine, and younger (brighter)ow-mass companions [12–17].

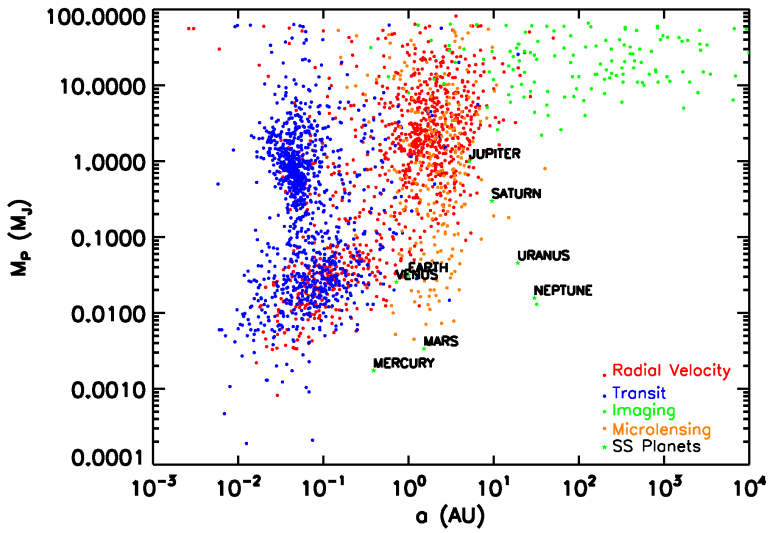

Figure 1. The distribution of the masses of exoplanets discovered so far as a function of the orbital separation. The different colors identify the different methods by which the planets have been discovered. The planets of the Solar Systems are also reported. Data are from http://exoplanet.eu/, accessed on 31 August 2024.

Direct imaging, or the direct detection of photons from the planet and/or disk picked through the glare of a host star, allows us to analyze theight reflected by the planet (visible) and, in addition, the intrinsic radiation emitted by the planet itself (infrared), by exploiting colors (by means of photometric filters) and spectra (by means of conventional or integral field spectrographs) independently of their orbital inclination and, above all, independently of the activity of the parent star. Thus, it is possible to obtain information about the physical and chemical characteristics of a planetary atmosphere without waiting for the transit (transmission spectroscopy) (e.g., [18,19]) of the planet or its occultation (emission spectroscopy) (e.g., [20]). The study of multi-band photometric images and spectra in both the visible and infrared makes it possible to estimate, under a variety of circumstances such as distance from the star, age, etc., the orbital and physical parameters of the planet, the structure and the composition of its atmosphere, its surface properties, the rotation rate, and the possible presence ofife on that planet. The planetary mass is the only parameter that the direct methods cannot measure, and generally, it is also inferred by theoretical evolutionary models (e.g., [21–23]) if it is subject to unknown initial conditions at very young ages. Large differences in the inferred value of planetary mass are foreseen between the so-called 'hot-start' and 'cold-start' models [24,25].

If an observer at distance d(pc) observes a star with a planet at projected distance δ (au) from its host star, then the angular separation between the planet and the star is $\theta = \delta/d$, where θ is expressed in arcsec. This quantity gives us an idea about the angular resolution that a telescope of diameter D should have in order to resolve any faint companion. A perfect, diffraction-limited imager can discern two sources when they are separated by ateast λ/D in angle [26]. So to resolve a planet that orbits its host star at 5 au at a distance from the observer of 10 pc, the telescope should have $\theta \leq 500$ mas, which is achievable with a 4 m class telescope in the visible band. However, if we wouldike to see a further star as close to the star as 1au, say 50 pc, we need $\theta \leq 20$ mas. Considering that most of the faint companions (e.g., extrasolar planets) are so cool that we need infrared bands to observe them, the problem becomes more difficult. Reaching such a high angular resolution is a necessary but insufficient condition. As a matter of fact, we have to fight against the glaring star and other difficulties, too. To achieve high angular resolution, two main techniques can be used: single-pupil observations witharge telescopes working close to their diffractionimit and interferometric (or multiple pupil) observations that coherently combine theight from a set of individual telescopes (two units or more) with ground separations up to a few hundred meters apart. The former case achieves typical angular resolutions of 50 mas (i.e., 5 au at 100 pc), while theatter reaches angular resolutions down to $\sim$1 mas.

The single pupil technique uses a single ground or space-based telescope with aarge primary mirror. Most of them (e.g., Palomar, CFHT, Keck, Gemini, Subaru, VLT [27]) are equipped with adaptive-optics modules coupled with coronagraphic systems to suppress or reduce the halo of the star image and can, thus, achieve high-contrast imaging.

Stellar interferometry achieves an angular resolution equal to $\lambda/2B$, with B being the separation between the telescopes, which is referred to as 'baseline' (see [28] and references therein). With baselines of about a few hundred meters, interferometry reaches resolving power equivalent to that of single telescopesarger than even the most ambitious Extremely Large Telescope projects considered so far [29]. With its angular resolution of typically 1 mas in the near-infrared on hecto-metric baselines, stellar interferometry is the tool of choice for investigating the innermost parts of circumstellar discs in nearby star-forming regions. In particular, interferometry is currently the only suitable method for directly characterizing the most important region of protoplanetary discs where dusty grains sublimate and where accretion/ejection processes originate. In principle, interferometry

also provides a sharp view of the region where terrestrial planets are supposed to be formed [29]. For more evolved planetary systems, interferometry can be used to constrain the presence of circumstellar material in the inner few au, includingarge amounts of warm dust, (sub-) stellar companions, or even hot planetary-mass companions. In this review, weimit ourselves to the description of the single pupil systems and their main results (see Section 6) due toimited space. Readers interested in optical interferometry can take into consideration the following reviews [29–33].

This review has a mainly didactical aim, and it isimited to the description of the principal difficulties in direct imaging observations and the technological solutions for overcoming them (Section 2), and the observing strategies and techniques for suppressing speckle noise (Section 3). Furthermore, we describe the present and future instrumentation that allows high-contrast imaging observations (Section 4) and the typical algorithms used for post-processing analysis of data (Section 5). In Section 6, we discuss some results with the description of some remarkable objects (at the personal evaluation of the authors), and in Section 7, we describe the surveys dedicated to the search for planets around young stars and their occurrence rate. In Section 8, we outline perspectives and conclusions. Direct imaging and high-contrast imaging have been described in several reviews (e.g., [26,34–37]) to which the reader is referred for further information.

2. Direct Observing Issues, Difficulties, and Solutions

Figure 2 shows the potentiality of the direct imaging methods. In this case, a basic stellar coronagraph and a standard spectrograph were sufficient to acquire the architecture of the system, and the spectroscopy of theow mass companion [38].

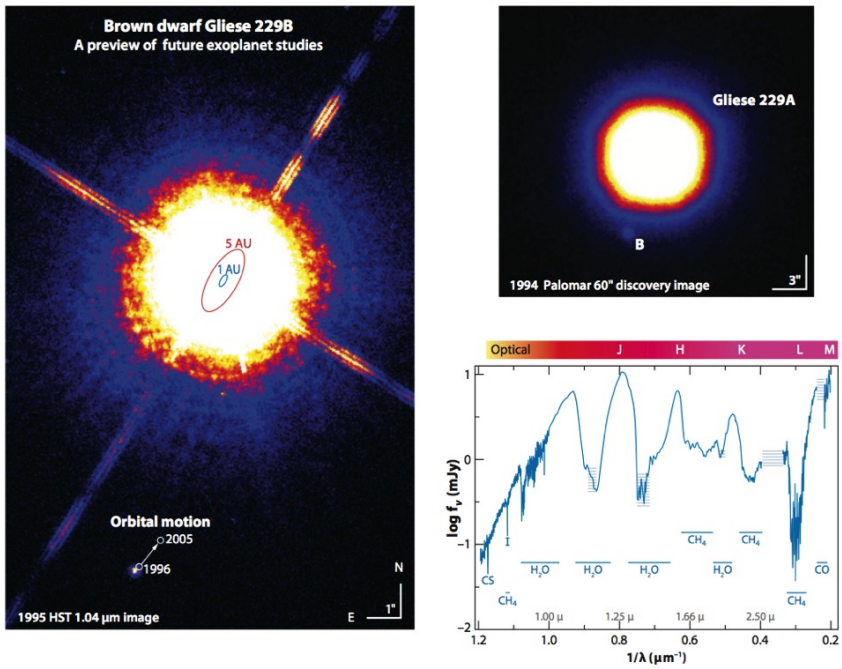

Figure 2. HST and Palomar images of the Gliese 229 system. The M-dwarf, and T-dwarf pair has been discovered with coronagraphy. Gliese 229 B is at a projected distance > 7 arcsec from its host star, and theuminosity contrast between the two objects is about 10^{-4} in the optical and NIR. This is just an example of the potentiality of DI observations. Both theimited projected separation and the high contrast made the star overcome theight of the companion; see the 1 au and 5 au orbits inside the glare of the star. **Left**: the Gliese 229 system observed with the HST. **Right—up**: the Gliese 229 system observed with Palomar. **Right—down**: the Gliese 229 B spectrum. The Picture was taken by Oppenheimer and Hinkley [26].

This example is a favorable case that is not so common if we search for planets with DI due, as already told in the previous section, to the small projected separation and to theuminosity contrast. The former depends on the evolution history of the system and it could reach a few tenths of arc-seconds for planets at a few au from stars at a distance up to 100 pc from the Sun. The contrast is a function of the wavelength λ, the properties of the planet, the apparent geometry, and the age of the system:

$$\begin{aligned} C_{OPT} &= \frac{F_{p,\,Reflected}(\lambda)}{F_{\star}(\lambda)}; \\ C_{IR} &= \frac{F_{p,\,Intrinsic}(\lambda)}{F_{\star}(\lambda)}. \end{aligned} \tag{1}$$

where C_{OPT} and C_{IR} are the contrast in the optical due to the reflected flux ($F_{p,\,Reflected}(\lambda)$) from the planet and the contrast in the IR due to the thermal or intrinsic emission ($F_{p,\,Intrinsic}(\lambda)$) of the planet respectively. $F_{\star}$ is the flux emitted by the host star. The reflected component depends on the brightness of the host star, the separation of the planet by the star, and the albedo $A(\lambda, t)$ of the planet, which depends on the wavelength and time t. The intrinsic component is defined by the temperature T_p of the planet itself.

Considering a planet with a radius R_p that orbits the host star at an orbital distance a, the flux reflected by the planets is as follows:

$$F_{p,\,Reflected} = A(\lambda, t)\phi(t)\frac{R_p^2}{4a^2}B(\lambda, T_{eff})R_{\star}^2, \tag{2}$$

where $B(\lambda, T_{eff})$ is the brightness of the host star and $R_{\star}$ is the stellar radius. $\phi(t)$ is the phase angle ($[0, \pi]$) or the angle between the observer–planet and the planet–star direction. Due to the irradiation characteristics of the host stars, the flux reflected by the planet is in the visible range. The albedo $A(\lambda, t)$ represents the fraction of the stellaright reflected by the planets, and it depends on what properties of matter are taken into consideration. Both geometrical (A_g) and Bond albedo (A_B) are considered to describe the general reflectance properties of a planetary surface. The geometrical albedo is the ratio of planet brightness at phase angle $\phi = 0$ (superior conjunction) to the brightness of a perfectly diffusing disk with the same position and apparent size as the planet. On the other hand, the Bond albedo is the ratio of theight reflected by the planet to theight incident to the planet, which is integrated over all wavelengths and on all the phase angles. The Bond and geometric albedo are correlated by means of the phase integral q: $A_B = A_g q$.

We can determine the intrinsic component of the flux emitted by a planet as that of a black body at the same temperature (T_p) as the planet itself:

$$F_{p,\,Intrinsic} = \epsilon_{IR}B(\lambda, T_p)R_p^2 \tag{3}$$

where ϵ_{IR} is the emission coefficient of the planet, and it depends on the wavelength and on the chemistry of the planetary surface and atmosphere. The value of the T_p results from the absorbed fraction of the host star radiation plus the internal heat of the planet. If theatter is negligible, the planetary temperature is named equilibrium temperature (T_{eq}). If this is not the case, it is named the effective temperature of the planet ($T_{eff,p}$) instead. In addition, the atmosphere of the planet could be a source of heat by means of the greenhouse effect, and generally, its contribution is added to the equilibrium or the effective temperature of the planet. In the Earth's case, for example, the greenhouse effect raises the temperature by about 30 degrees [39]. The fraction of the stellar radiation absorbed by the planet is $(1 - A_B)$, and assuming that the incident flux is equal to the radiated flux:

$$T_{eq} = \left(\frac{1 - A_B}{4f}\right)^{1/4} \left(\frac{R_p}{a}\right)^{1/2} T_{\star}. \quad (4)$$

f is the fraction of the area over which the heat is spread, so it is $f = 1$ for a rapid rotator and $f = 0.5$ for a tidallyocked planet. The $T_{eff,p}$ results from fitting the intrinsic emission with a black body curve. The two temperatures are generally different from each other, for example in the case of Jupiter: $T_{eq} = 110\ K$ and $T_{eff,p} = 124.4\ K$ [40]).

The expected contrast of the typical Jupiter-like measurements (for an angular separation of 0.5 arcsec) is of the order of 10^{-9} in the visible band and 10^{-6} in the NIR. On the contrary, for Earth-like planets orbiting the habitable zone of a G star (at angular separations of about 0.1 arcsec), the contrast is 10^{-10} and 10^{-7} in the visible and NIR, respectively. For further details, the interested reader is referred to [34,36]. Young planets could also be three orders of magnitude brighter than old ones (Figure 3, [41,42]). This reflects on the observational strategy (see ahead) because the contrast depends on the distance from the star for old planets with negligible intrinsic flux component, while it is independent of the distance for young planets that have high intrinsic flux. A detailed spectroscopic study of even young (∼100 Myr) and hot (∼800 K) planets of about 1 M_J requires a contrast of 10^{-8}. It depends on the distance by the host star and on the age of the system, but also if it is possible to detect one photon from the planet for every 10^6 from the star, to probe the depths of the spectral features requires ateast two more orders of magnitude in precision. The contrast is also worse for old planets, making this kind of study really challenging. In the case of Terrestrial planets, it becomes worse, requiring a contrast of 10^{-10} [26,34].

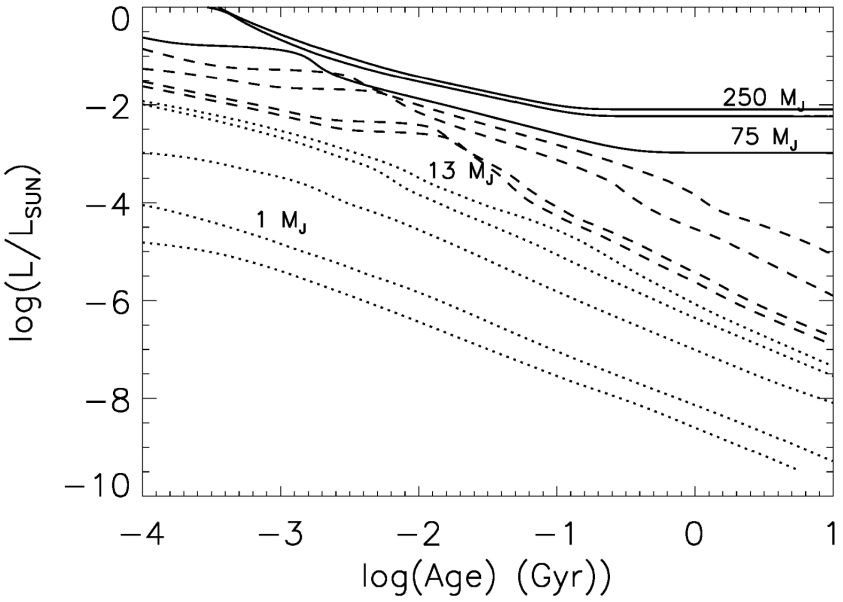

Figure 3. Theoretical models for theuminosity evolution of different structures with different masses versus age. The stars are shown in (continuous ine), while sub-stellar structures with M > 13 M_J are in (dashedline), and giant planets are in (dottedline). The masses of the structures areabeled in Jupiter mass units. Young planets are brighter by more than three orders of magnitude than old planets. The data are taken by Burrows et al. [41].

2.1. Image and Speckles Formation

Theight coming from a star far away from the observer, once it reaches the observer's telescope, could be considered as a plane wavefrontight. For example, for light coming from a 10 pc distant star, the deviation from a plane is of one part on 10^{17} [26]. Following Huygens' Principle, the telescope aperture D becomes an emission center of spherical waves that will focalize onto the telescope focal plane. In this case, considering a circular

aperture D and a wavefront with an amplitude equal to $A_1(X) = 1$, we have the following on the focal plane of the telescope (Chapter 8.5.2, [43]):

$$A_2(\theta) = \sqrt{I_0}\frac{2J_1(\pi D\theta/\lambda)}{\pi D\theta/\lambda}, \quad (5)$$

and the corresponding intensity is $I_2 = |A_2|^2$, or

$$I_2(\theta) = I_0\left[\frac{2J_1(\pi D\theta/\lambda)}{\pi D\theta/\lambda}\right]^2. \quad (6)$$

$J_1(X)$ is the Bessel function of the first order. The first angle at which the intensity is zero is $\theta_z = 1.22\lambda/D$ or the Airy disk radius. The full width at half-maximum (FWHM) of the intensity pattern is $\theta_z = 1.03\lambda/D \cong \lambda/D$. This value is often mentioned as the diameter of the diffraction-limited image of a point source of a telescope of diameter D. For a ground-based telescope, theight from a star passes through about 20 km of atmosphere, and the image of the point source is degraded to λ/r_0, where r_0 is the Fried parameter (see Section 2.2), the indicative size of the seeing cell size, typically about 10 cm in the visible band ($r_0 \propto \lambda^{6/5}$). In an atmospheric cell of radius r_0, the refraction index of air is constant but different from that of adjacent atmospheric cells. The incoming wavefront is heavily modified, and the point source image on the telescope's focal plane is degraded (seeing image). To solve the problem of seeing there are two solutions. The first is completely bypassing the Earth's atmosphere (e.g., HST, JWST, etc.). The second solution is to equip the telescope with an adaptive optics (AO) module to correct the atmospheric turbulence effect on the wavefront in real time and restore almost the full resolution of the telescope (see Section 2.2).

The image obtained using a short exposure time to image a point source without any wavefront correction is composed of an interference pattern with a shortifetime named speckles (see Figure 4). Speckles are interference patterns due to several coherent patches of size r_0 [44] that are distributed above the aperture (D) of the telescope. One aperture (sub-pupil) of dimension r_0 produces a Point Spread Function (PSF) with a FWHM$\sim\lambda/r_0$. Two such sub-pupils at a distance of $\sim D$ from each other constitute an interferometer that generates on the focal plane of the telescope an interference pattern of size $\sim\lambda/D$ with fringes that run orthogonally to the conjunction of the two apertures. Each couple of apertures causes a different system of interference fringes, and when the interference is a constructive one, it causes a bright speckle. The random phase variation of an incoming wavefront enables the movement of the interference pattern inside the dimension of the PSF, which causes the characteristic boiling of speckles and makes the intensity of speckles vary in a random way. The wavelength of the observedight and the wavefront perturbations determine the position of the speckle on the focal plane.

The fluctuations of the atmospheric diffraction index are carried along by the wind, and the timescale in which the wavefront changes depends on the wind speed in the overlying atmosphere. Typically, we have a speckleifetime of 3 ms for a wind speed of 10 m/s. The speckleifetime depends on the telescope site, the AO systems, and ancillary instrument configurations. Therefore, a ground-based telescope image of a star is formed of approximately $(D/r_0)^2$ speckles, churning on a timescale of the order of milliseconds, and spread over an angular diameter on the sky of $\sim\lambda/r_0$ or about 1 arcsec in the visible, independent of telescope diameter. Also, the telescope and instrument optics induce speckles generated by the optics surface shape errors due mainly to the manufacturing processes.

Generally, the behavior of the speckles does not follow the Poisson statistics, and they represent a noise several orders of magnitudearger than the shot noise of a perfect PSF [44]. They are evanescent and exhibit a correlated noise behavior [45]. These characteristics do

not allow blurring them, enhancing the exposure time, or using broadband observations to improve the system sensitivity to objects fainter than the speckle's background. Nevertheless, several techniques or observation strategies exist that can remove or reduce the barrier of speckles.

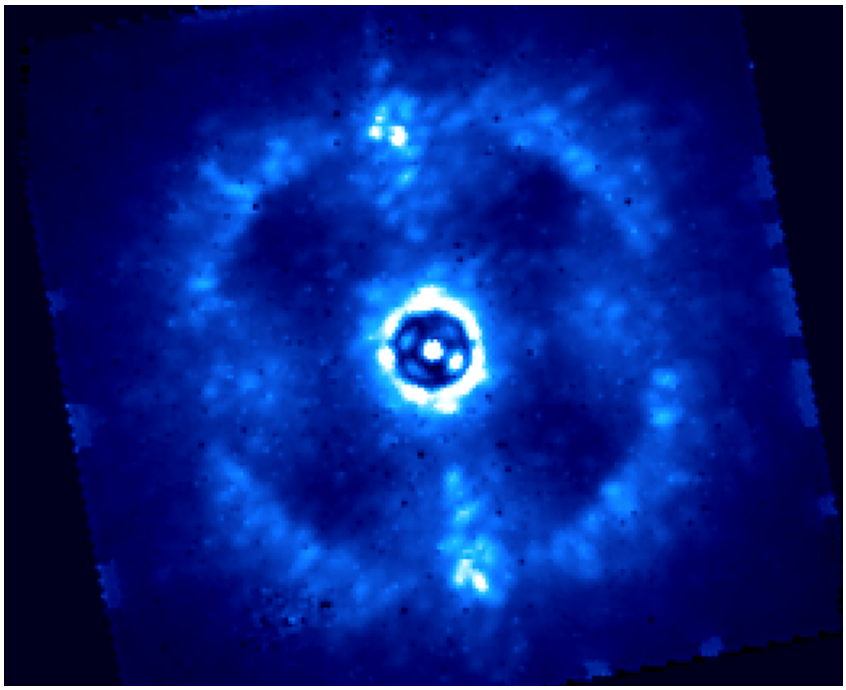

Figure 4. Image taken with a coronagraph showing the presence of speckles.

2.2. Adaptive Optics

In 1953, the astronomer Horace W. Babcock wrote: "*If we had the means of continually measuring the deviation of rays from all parts of the mirror, and of amplifying and feeding back this information so as to correctocally the figure of the mirror in response to the Schlieren pattern, we could expect to compensate both for the seeing and for any inherent imperfection of the optical figure*" ([46]). The realization of Babcock's concept had to wait until the assembly of the first astronomical AO instrument COME-ON tested at the end of 1989 at the 1.5 m telescope of the Observatoire de Haute-Provence (see Figure 5), and then it was installed on the 3.6 m ESO telescope in La Silla [47–49].

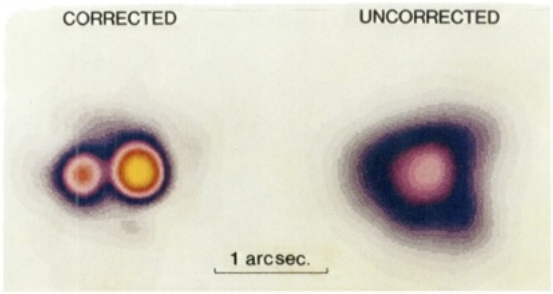

Figure 5. First image of the AO prototype 'COME–ON' system taken at 1.52 m telescope of the Observatoire de Haute Provence. γ_2 And (a binary star with a 0.5″ separation) was observed in *K* band [50].

The main elements of an AO system are the wavefront sensor (WFS), a real-time computer, and a deformable mirror (DM). A WFS allows us to measure the wavefront, providing a signal thatets us estimate the shape of the wavefront with sufficient accuracy. It generally includes a phase-sensitive optical device and aow-noise, high-quantum efficiency

photon detector. Among the different WFSs, the most used is the Shack-Hartmann WFS. It is a simple system that is able to sample a transferred pupil with aarge number of smallenses. Eachenslet forms an image of the star onto multiple quad cells or a CCD, and the position of each image caused by theocal tilt of the sampled portion of the wavefront could be measured by obtaining information on the average slope of the wavefront. Another very used type of WFS is the Pyramid one, which adopts a pyramidal prism with a veryarge apex angle to split the incoming beam into four images that will be perfectly identical in the absence of any aberration. Anyhow, any aberration in the wavefront will introduce differences in the four pupil intensity distribution that can be used to obtain information about the aberration itself [51]. This information can eventually be used to drive a DM, and a closed-loop control is established. The role of a DM is to correct for the optical path differences introduced by the turbulent atmosphere. A DM comprises an array of actuators connected to a thin reflecting surface deformed by the expansion of the actuators. The most important parameters for a DM are stroke, response time, spacing, and the number of actuators. There are some telescopes that mount the DM directly to their secondary mirrors (DMS),ike, for example, the 6.5 m Multiple Mirror Telescope (MMT) and the Large Binocular Telescope (LBT) ([52]), but typically DMs are medium-sized piezo DMs with an actuator spacing of several millimeters. SPHERE [53], the high-contrast imager of VLT, mounts this type of DM. Recently, MOEMSs (micro-optical-electrical-mechanical systems) have emerged as an alternative to DMs. They are manufactured using standard semiconductor technologies. The Gemini Planet imager (GPI [54]) at the Gemini South telescope used them (GPI is under refurbishment; see Section 4).

The primary application of AO is the real-time correction of the image seen on the focal plane of a telescope to produce a diffraction-limited image. This result is achieved in several steps, the first of which is obtained with a tip/tilt system, or finer guidance tracker, able to stabilize the stellar PSF against thearge movements (up to a few arcsec) due to the atmospheric variation and instability, and telescope vibrations. The remaining alterations of the incoming wavefront are adjusted by a DM. The AO system regulates the optical path variations (wavefront), measures the deviations from a plane wavefront with a WFS, and uses a real-time computer; it calculates and applies the appropriate correction to a DM that reaches a shape able to correct the input wavefront to a quasi-plane wavefront (see Figure 6).

The AO system performs a feedbackoop that is carried out hundreds of times per second to comply with the time scale of the atmospheric changes. The dimension of the resolution elements of the WFS (sub-apertures) and the number of the DM active sub-surfaces (actuators) projected on the telescope entrance aperture should approximately match the r_0. The efficiency of an AO system is measured by the Strehl ratio or the ratio of the peak intensity in a real image to that of a perfect image taken with the same imaging system working at the diffractionimit. Named σ_{WFE} the root mean square of the wavefront error in radians, the Strehl ratio could be expressed by the Maréchal approximation $S \sim \exp(-2\pi\sigma^2_{\mathrm{WFE}})$ when $\sigma_{\mathrm{WFE}} \ll 1$ [55]. The Strehl ratio depends on the wavelength at which the imaging system is working, or in other words, it depends on the photometric band used in the observation (e.g., [27]).

We have just described single-conjugate adaptive optics (SCAO), in which the wavefront coming from a single natural guide star (NGS) is measured. This is the technique generally used in HCI observations. Nevertheless, other than SCAO, there are other AO systems to optimize the use of the guiding star exploiting synthetic stars generated byaser beacons oraser guide stars (LGSs). This LGS technology exploits two physical mechanisms: the Rayleigh scattering in the dense regions of the atmosphere up to altitudes of about 30 km and the resonance fluorescence of sodium atoms concentrated in aayer at about

90 km height. Several telescopes around the world are now equipped with AO modules that use LGS,ike, for example, Keck II [56], VLT [57], Gemini North [58], and Subaru [59]. Other AO systems are also designed to probe different turbulent atmosphericayers with different combinations of NGSs or LGS (we just mention them inviting the interested reader to the review by Davies and Kasper [27]): the Laser Tomography Adaptive Optics (LTAO), Ground Layer Adaptive Optics (GLAO), and Multi Conjugate Adaptive Optics (MCAO).

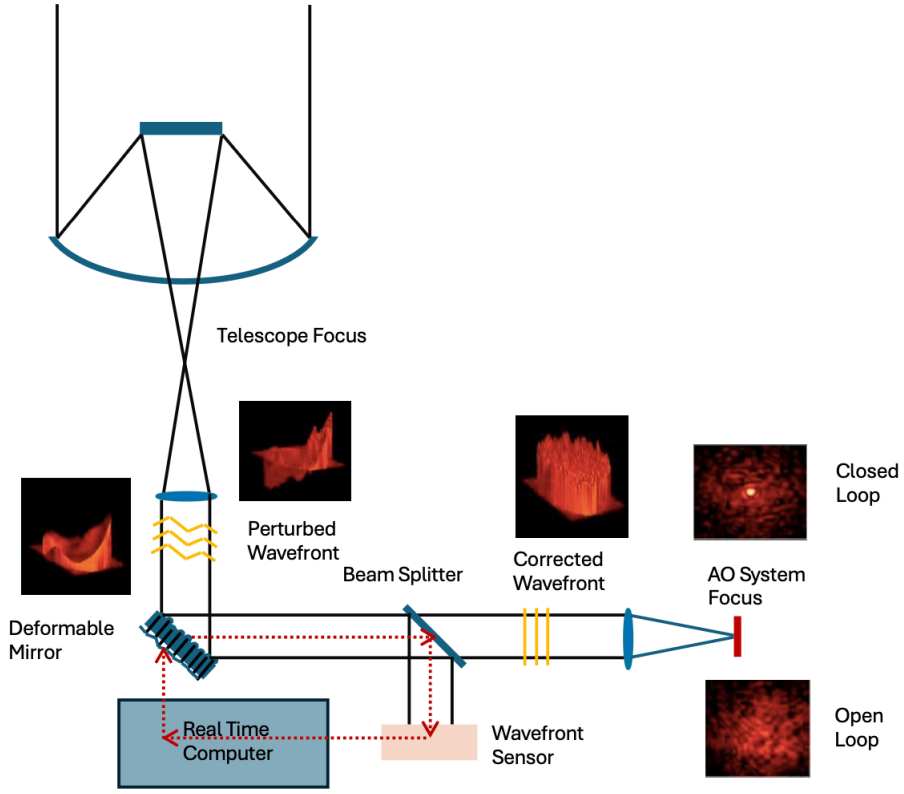

Figure 6. The principle of an Adaptive Optics System. The inserted images represent the different status of the wavefront: before the closure (perturbed wavefront) and after the closure of the AO controloop (corrected wavefront).

In theast decade, most of the new generation high-contrast imagers adopted the extreme AO (ExAO) concept. The ExAO system is built to fully correct both atmospheric and instrumental perturbations using a single star on-axis for wavefront measurement. It is not different from conventional SCAO but challenging in the technical implementation; the main aim is to provide exceptionally high performance on bright ($V < 10$ mag) stars, reaching a Strehl ratio of about 90% in the H-band [60]. These results have been obtained by optimizing the sampling of the DMs, enhancing the number of actuators, and using fast andow noise detectors such as Electron-Multiplying Charge-Coupled Devices (EMCCDs) to reduce the errors in the wavefront sensor measurements. A complete review on the ExAO is given in Guyon [60] at which the interested reader is referred.

However, the AO is necessary but not sufficient in performing high-contrast observations. This goal is reached with the introduction of a coronagraph in the imaging system.

2.3. Coronagraphy

Bernard Lyot [61], in 1930, invented the coronagraph to study the Sun, which was a telescope with a design able to block theight coming from the solar disk to see the extremely faint emission from the corona. The main part of this device is an occulting disk in the focal plane of a telescope completed by other optical parts to reduce strayight. After a few years,

coronagraphy has also been utilized in star observations, and recently become an important technique for high-contrast imaging. In fact,arge ground-based telescopes, thanks to the AO systems (see Section 2.2) obtain the diffraction image of a point source that is many orders of magnitude brighter than any faint companion which became observable after that the coronagraph suppresses the diffraction peak. The left panel of Figure 7 shows a scheme of a typical Lyot coronagraph. To achieve the suppression of starlight, it uses two masks (the occulting mask c and Lyot Stop f).

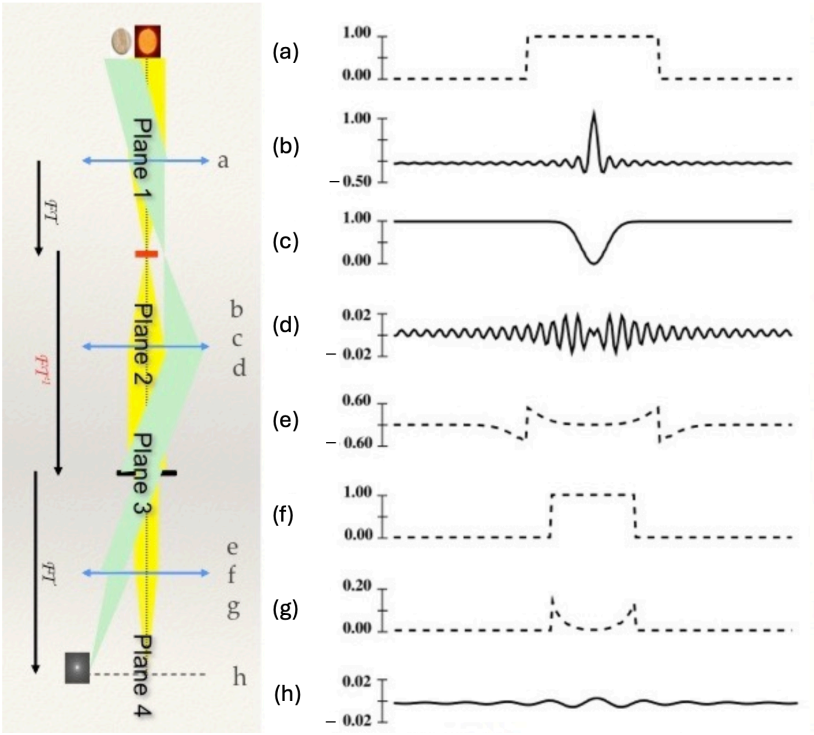

Figure 7. Coronagraphy principle and Fourier Optics.The optical scheme of a classical Lyot coronagraph (left panel). Theight coming from the star (yellow, on-axis) and from the planet (light-green, off axis) are shown. On the right, the positions and electric field or stop profiles of the following: (**a**) Primary pupil for on-axis source ; (**b**) Image before image plane stop; (**c**) Image plane stop; (**d**) Image after image plane stop; (**e**) Pupil before Lyot stop; (**f**) Lyot stop; (**g**) Pupil after Lyot stop; (**h**) Final on-axis image (right panel). Modified from [62].

In the first stage, at the focal plane, the image of the target star is focalized at the center of a circular opaque mask that absorbs most of the starlight and also diffracts part of theight around it. After that, in the following pupil, the residual starlight has been concentrated into a bright outer and inner ring around the conjugateocation of the secondary mirror of the telescope. Thisight can be filtered out without greatly affecting theight from the fainter companion posing a diaphragm (named Lyot mask) here. Finally, an image is formed by optics after this Lyot mask, and the intensity of the host star has been reduced by about 99%, while the companion is only affected at aevel of a few percent. The goodness and efficiency of a coronagraph are defined by four different parameters that take into account its ability to obscure the central star by affecting the smallest possible region around the star. The main parameter is the inner working angle (IWA) that defines the passage between the obscured and the transmitted region. It is generally treated as a hardowerimit in the modeling of coronagraphic instruments, also if it is not normally a sharp function of the detection sensibility [63]. Typically, IWA can range between $\sim 2\lambda/D$ and $\sim 4\lambda/D$. Another important parameter is the fraction of the planet'sight that is not suppressed by the coronagraph. Most of them have a throughput of ∼80%. The other two parameters

concern the sensitivity of the coronagraph toow-order wavefront errors (aberrationsike tilt, focus, astigmatism, etc.) and the chromaticity, which is the capacity to suppress theight on aarge range of wavelength:ower the chromaticity better the behavior of the coronagraph.

There are ateast four broad categories of coronagraphs: amplitude-based Lyot coronagraphs, phase-based Lyot coronagraphs, interferometric coronagraphs, and pupil-apodization coronagraphs. Moreover, for each of these categories, there are aot of different concepts. The interested reader can refer to the [62–64] reviews. Two variants of the classical Lyot coronagraph scheme (see Figure 7) are the band-limited coronagraph (BLC) [65] and the Apodized-Pupil Lyot Coronagraph (APLC). The main difference between the two is the manufacturing of the focal mask. The BLC has a focal mask with a transmission profile carefully tailored to confine the residual diffractedight to a finite outer region of the pupil. Instead, APLC modifies the entrance pupil with a tapered transmission mask that allows for a reduction of the sharp discontinuity in the transmitted wavefront at the edge of the pupil, which reduces the amplitude of the secondary maxima of the diffraction figure. Those coronagraphs perform similarly, achieving a throughput of 20–40% for an IWA $> 4\lambda/D$. Both coronagraphs are easily adapted to conventional telescopes with on-axis secondary mirrors, and they have been selected by the major ground-based coronagraph projects. In the Lyot class of coronagraph, there are also alternative designs that make use of phase shift focal devices to block the starlight (e.g., [66]). In theory, this technique removes all of the starlight and has no effect on anything else in the field of view. The best-known Phase Based Lyot Coronagraph concept is the 4-quadrant phase-mask (4QPM) coronagraph [67]. The phase mask positioned in the focal plane consists of four contiguous quadrants of transparent material on which the star is focused in the center. The adjacent quadrants differ in optical thickness by a half-wavelength (Figure 8 left panel). The transmitted beam will be nulled on the axis, but whatever object is focused on one of the quadrants will be transmitted.

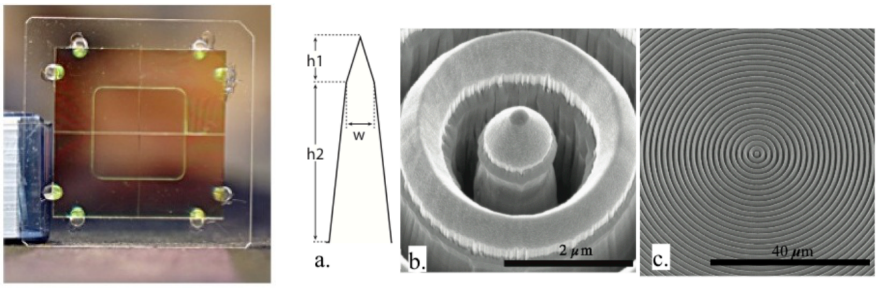

Figure 8. Examples of phase focal mask for phase-based Lyot coronagraphs. Left: the 4QPM phase mask of SPHERE (described in [66]). Right: the Annular Groove Phase Mask (AGPM) mounted on NACO at VLT. (**a**) Schematic view of the AGPM, (**b**) zoom of the central part of the AGPM, (**c**) overview of the structure of the device (for details see [68]).

A variant of the 4QPM is the Annular Groove Phase Mask (AGPM) (see Figure 8 right panel), which consists of a spiral-staircase phase mask that generates aongitudinal phase delay by operating on both polarizations. The center of the optical vortex is a phase singularity in an optical field, which generates a point of zero intensity [34]. These coronagraphs achieve near-theoretical performances with IWA of $1\lambda/D$ and high throughput. Nevertheless, they are really sensible to the position of the image of the star in the focal plane, with performances degrading for small tip/tilt errors or partially resolved stars.

3. High-Contrast Imaging and Speckle Suppression

The main goal of high-contrast imaging is primarily to discover and characterizeow-mass companions close orbiting brighter stars. In the previous section, we described the

main problematics and the techniques to mitigate them for direct imaging of faint companions. At first, we needarge telescopes to acquire high angular resolution. Furthermore, the use of AO modules allows us to restore the diffraction figure of these telescopes. But this is still not enough. In fact, we have to eliminate the restored diffraction peak to eliminate the glare of the star, and we achieve this with a coronagraphic device. But also now it is not enough to reach the contrast necessary to reveal the faint companion that is drowned in that variable, not smooth background, due to speckles. These image artifacts are caused by quasi-static optical aberrations within the telescope, AO system, coronagraph, or camera that are not correctly calibrated or corrected. Unfortunately, a speckle has the same appearance as an exoplanet, and persistent speckles can easily overwhelm a faint exoplanet image. Generally, there are two approaches to dealing with speckles: control them or remove them through special data collection and processing techniques. Even better, one could use both approaches. So, we can break these techniques into three main groups, each based on the comparison of simultaneous images at different wavelengths or images of the same star at different orientations. In particular, we discuss the Angular Differential Imaging, the spectral differential imaging, and the polarization method.

3.1. Angular Differential Imaging

The angular differential imaging (ADI) method is implemented, allowing the rotation of the field of view (FoV) centered around the target star during an observation. In such a way each physical object in the FoV will have a different position in each frame obtained during the observing period (see the red spot in Figure 9). On the contrary, the speckle pattern present in the image will not rotate during the observations. This type of observation is also said pupil stabilized as the telescope pupil does not rotate. In principle, a median image of such a datacube should contain all the information about the speckle pattern, excluding any signal of the planets, and subtracting it from the original data should eliminate the speckle noise while retaining and highlighting the signal from any physical object (e.g., a low-mass planet) present in the FoV at the same time. In practice, however, the speckle pattern is stable only for a few minutes, so a simple median of all the datasets will result in an imperfect reconstruction of the speckle pattern and, as a consequence, an imperfect subtraction of the speckle noise. When creating the image with the speckle pattern model to be subtracted from a science image we have to select just those images of the dataset near enough in time that the speckle pattern does not evolve in a substantial way. A second difficulty to be overcome is that for images taken at a small angular separation from the science one (less than $\sim\lambda/D$), we will experience a subtraction of the signal of theow mass companion (referred to as self-subtraction). The choice of the images to be used to create the speckle pattern model to be subtracted from the science image has then to be a careful trade-off between choosing images near enough in time to the science image to avoid substantial speckle pattern evolution and with sufficient different rotation to avoid self-subtraction. This trade-off is normally different at different separations from the host star. It is, however, important to stress that some self-subtraction of theow-mass companion signal is unavoidable, and it has to be carefully corrected to correctly evaluate the photometric signal from this object. One of the most common methods for performing this is the introduction of the original dataset of simulated companions at a known position and with known brightness. After performing the same data reduction procedure on this simulated dataset, it is possible to calculate the self-subtraction due to the method at different separations from the host star.

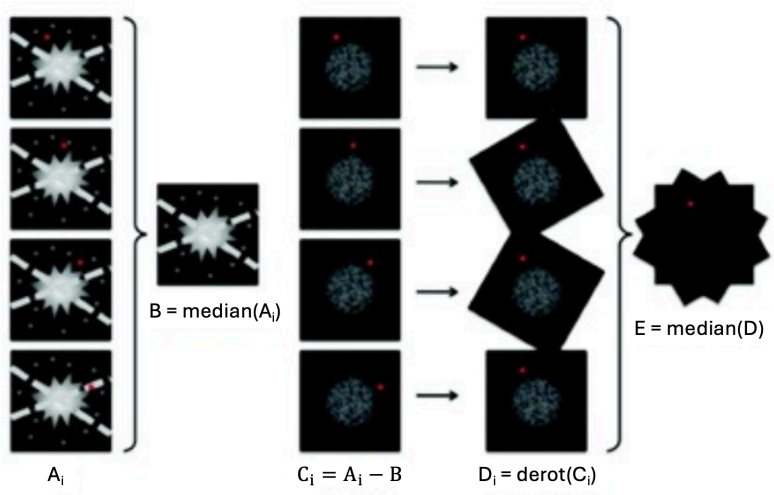

Figure 9. Graphical representation of the angular differential imaging method. The red dot indicates the position of a possible planet. The figure is taken from http://web.archive.org/web/20150915005746/http://www.mpia.de/homes/thalmann/adi.htm (accessed on 31 August 2024) by Thalmann.

3.2. Spectral Differential Imaging

Spectral differential imaging (SDI) is performed when a dataset obtained simultaneously at different wavelengths is available. Indeed, as shown in Figure 10, the speckle pattern scales with the wavelength, while a physical object does not change its position with the wavelength. It is then possible to rescale each image of a dataset taken at the same time to a single reference wavelength and subtract the speckle pattern. Once this is performed, each single image can be rescaled back to the original wavelength dimension and appropriately combined. As for the case of ADI, SDI also introduces some self-subtraction that has to be appropriately calculated and corrected using methods similar to those described for ADI.

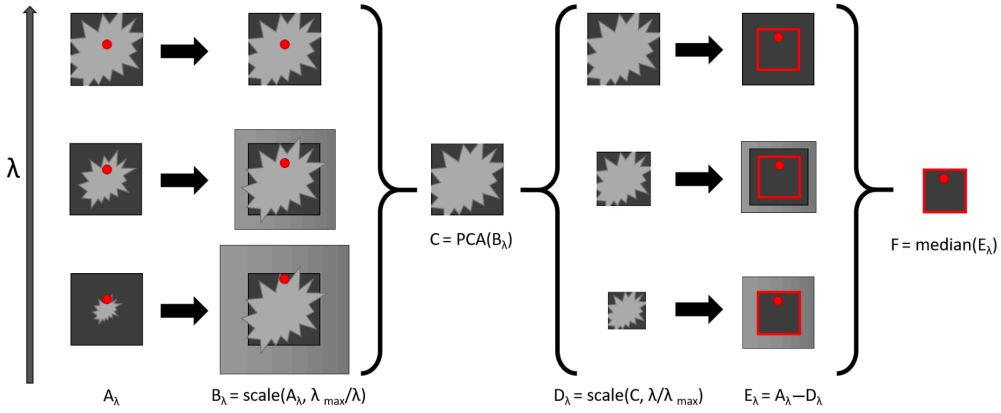

Figure 10. Graphical representation of the spectral differential imaging method. The red dot indicates the position of a possible planet. Figure is taken from (Figure 1 Kiefer et al. [69]).

3.3. Polarization

Polarimetry is useful for observations of circumstellar disks and extra-solar planets because theight reflected from disks and planets is polarized. The reflectedight polarization from extrasolar planets is typically high, >10% even forarge separations, mainly if the phase angle is in the range 60–120° (e.g., [70,71]). On the contrary, no polarization is expected from the central star [72]. This situation makes dual-mode polarimetric imaging perhaps the most effective technique for speckle suppression. In particular, the polarization is high at wavelengths < 1 µm due to Rayleigh scattering by atoms and molecules and scattering

by aerosol particles in planetary atmospheres and dust grains in circumstellar disks. This case defines the visible as the working wavelength range for this kind of instrumentation (e.g., ZIMPOL [73]). In dual-mode polarimetric imaging, the image is split by a Wollaston prism with perpendicular polarization vectors in slightly different directions, forming two simultaneous images. If each image is subtracted from the other, only theight that is actually polarized remains in the resulting image. Because speckles are formed by unpolarized starlight, they will be removed along with the unpolarized starlight. This technique achieved good results in imaging disks of dust that polarizeight through the scattering process [74–76].

3.4. Other Methods

The possibility to image young accreting planets allows us to detect these objects during their formation phase. The most important tracer for the accretion is the hydrogenines emission coming from the accretion shock (e.g., [77]). Up to now the most used of theseines is that from the H_α emission as it displays the strongest signal. Detailed models of this emission were recently presented, e.g., by Aoyama et al. [78] and Aoyama et al. [77] resulting in a different behavior with respect to what shown by protostars (e.g., [79]). The mainimitation of the H_α emission, however, is the strong expected absorption mainly due to the dust opacity that can be 10 times higher a these wavelengths than for the NIR [80]. This absorption could explain theow number of objects detected up to now using this technique. A possible solution to overcome this problem could be to observe hydrogenines in the NIR where theower absorption could compensate for theower expected flux as in the case of the $Br\alpha$ or of the $Br\gamma$ines in the K- and in the L-spectral bands, respectively.

As seen above, one of the main difficulties in the imaging of planets still embedded in the protoplanetary disk is due to the strong absorption of the signal from the planets. In recent years, a technique allowing to overcome this problem has emerged exploiting kinematics signatures caused by planet-disk interactions (see, e.g., [81] for a review). While this is not strictly an HCI method, it allows us to define both a rough position of the companion and its mass relying mainly on the capability of ALMA to image molecular emission at high both spatial and spectral resolution. Recently, this techniqueed to the detection, e.g., of aow mass companion around HD 142666 [82] and RXJ1604.3-2130 A [83].

4. Instrumentation

The development of the search for exoplanets through HCI has involved the preparation of an increasing number of instruments that are completely or in part dedicated to this type of observation. In this Section, we will present some of the ground-based instruments that are at the moment in activity (see Table 1), with, when they exist, their planned upgrades. We also discuss space-based instruments and future instrumentation.

Table 1. High-contrast imagers on duty.

Instrument	Tel.	Wavel. (μm)	Ang. Resol. (mas)	N λ/D	IWA arcsec	Coronagraph
ERIS-NIX	VLT-UT4	1–5	25.0–129.0	0.5–3.0	0.013–0.37	SAM/APP
GPI	Gemini S.	0.9–2.4	24–62	4	0.092–0.248	Lyot/APLC
GPI2.0	Gemini N.	0.9–2.4	24–62	3	0.092–0.248	Lyot/APLC
MagAO-X	Magellan II	0.5–1.0	∼20–32	2–5.5	0.032–0.177	Lyot/PIAACLC/vAPP
MIRI	JWST	10.0–23.0	317.0–730.0	1–3.3	0.33–2.16	Lyot/4QPM
NIRCam	JWST	2.0–5.0	63.0–159.0	2, 4, 6	0.14–0.89	Lyot
NIRISS	JWST	2.8–4.8	88.0–152.0	1	0.12–0.15	AMI
NIRC2	Keck-II	1.0–5.0	23.0–114.0	1.4	0.125	Lyot/VVc
SCExAO	Subaru	0.4–2.4	10–62	1	0.010–0.062	Lyot/PIAACMC/vAPP/vortex
SHARK-VIS	LBT	0.4–0.9	11–20	2.5–10	0.050–0.200	Lyot/Gauss

Table 1. *Cont.*

Instrument	Tel.	Wavel. (μm)	Ang. Resol. (mas)	N λ/D	IWA arcsec	Coronagraph
SHARK-NIR	LBT	0.96–1.7	24–42		0.050–0.150	Lyot/SP/4QPM
SPHERE	VLT -UT3	0.95–2.32	24–62	1, 2, 3	0.072–0.180	Lyot/APLC/4QPM

4QPM: 4 Quadrants Phase Mask; AMI: Aperture Masking Interferometry; APLC: Apodized Pupil Lyot Coronagraph; APP: Apodizing Phase Plate; PIAACLC: Phase Induced Amplitude Apodization Classic Lyot Coronagraph; PIAACMC: Phase Induced Amplitude Apodization Complex Mask Coronagraph; SAM: Sparse Aperture Mask; SP: Shaped pupil; vAPP: vector Apodizing Phase Plate; VVc: Vector Vortex Coronagraphic mask.

4.1. Present Instrumentation

4.1.1. GPI and GPI2.0

The Gemini planet imager (GPI; [84]) was installed at the Gemini South telescope (8.2 m) between 2014 and 2020. It operated in the NIR with a wavelength range between 0.9 and 2.4 μm. It had an integral Field Spectrograph (IFS) with R∼40, and it also provided the possibility to perform dual-channel polarimetry on the full field in Y, J, H, and K spectral bands. Also, this instrument is equipped with an ExAO with a DM of 50 actuators per beam diameter and a Shack-Hartmann wavefront sensor (1 $\leq$ speed $\leq$ 2 kHz) as primary WFS. GPI, decommissioned in August 2020, is currently in the process of being upgraded to a new version named GPI 2.0, and the firstight is expected at the Gemini—North telescope inate 2024 or early 2025 [85]. This new version will have new coronagraphs with smaller inner working angles, a new wavefront sensor at higher sensitivity, and the possibility to use new spectroscopic observing modes. The goal of the new instrument is to obtain contrasts of the order of 10^{-7} at separationsower than 1″ from the target star.

4.1.2. SPHERE and SPHERE+

SPHERE (Spectro-Polarimetic High-contrast imager for Exoplanets REsearch, [53]) is a planet imager installed at ESO/VLT (8.2 m) since 2015. It is composed of three different scientific modules. The first one is the IFS [86] that operates between the Y and the J band (0.95–1.35 μm) with a spectral resolution of R∼50 or R∼30 in the Y and the H spectral bands (0.95–1.65 μm), according to the observing mode. The second instrument is the Infra-Red Dual-beam Imager and Spectrograph (IRDIS; [87]) that can operate both together with the IFS or as a stand-alone instrument. IRDIS has both narrow- and broad-band spectral filters ranging between the J and the K spectral bands. IRDIS can operate as a dual-band imager adopting two narrow-band filters at adjacent wavelengths [88], as a classical imager on a single spectral filter, and also as a polarimetric instrument (see, e.g., [89,90]). Finally,ong-slit spectroscopy (LSS; [91]) allows one to obtain medium resolution (R∼350) spectra of bright companions at a separation of a few tenths of an arcsec from the host star. The third instrument is ZIMPOL (Zurich Imaging Polarimeter; [73]), a polarimeter operating in the visible between 500 and 900 nm. SPHERE is also equipped with an ExAO system called SAXO (SPHERE extreme AO system) with a DM of 50 actuators per beam diameter and a Shack-Hartmann WFS (1 $\leq$ speed $\leq$ 2 kHz) as primary WFS [92,93]. In the next years, SPHERE will upgrade to SPHERE+ [94] that consists of a new XAO system stage named SAXO+. The new AO stage will operate in the NIR and at a higher frequency (2–3 kHz) than the SAXO system. It has been designed to operate with both IRDIS and IFS but it will be able to do the same also for other future instrumentation. The second element of the upgrade should be a medium-resolution IFS named MEDRES [95], which should provide medium-resolution (R∼1000) spectra on aimited FoV (∼0.4″ squared) and a wavelength ranging between 1.2 and 1.65 μm. This will allow us to reach a contrast of 10^{-5}–10^{-6} down to separations of 0.1″–0.2″. However, this second element is in stand-by waiting for a future approval.

4.2. NIRC2 and KPIC

NIRC2 is a near-infrared instrument operating since Summer 2001on the Keck II telescope (10.0 m). The instrument [3] operates from 1 to 5 μm, with three observing modes (OM). Imaging OM exploits three different cameras that provide scales of 0.01, 0.02, and 0.04 arcsec/pixel close to the Keck diffraction size at J, K, and M bands. The coronagraphic OM is characterized by the presence of several Lyot masks and two vector vortex coronagraphic (VVC) masks, one optimized for the L-/M-band, and the second for the K-band. Finally, the third OM is the grism spectroscopy with severalow and medium dispersion grisms. The NIRC2 underwent the two phases upgrade named Keck Planet Imager and Characterizer (KPIC; [96]) with the installation of an infrared pyramid WFS (PyWFS) based on a fast,ow-noise SAPHIRA IR-APD array, and an array of single-mode fibers with the aid of an active fiber injection unit (FIU) which feed the NIRSPEC spectrograph with R > 30,000 (first Phase). The second phase of the upgrade consisted of the installation of a 1000-actuator deformable mirror, beam-shaping optics, a vortex coronagraph, and other upgrades to the FIU/FEU [96].

4.2.1. ERIS

ERIS (Enhanced Resolution Imaging Spectrograph; [97]) is an imager and a spectrograph recently installed at VLT (the firstight was in February 2022). It was conceived to replace two ESO instruments SINFONI and NACO. One of the science cases of ERIS is the detection of very planets and the characterization of the giant gaseous planet atmospheres [97]. ERIS is composed of two science sub-systems. The first one, called NIX [98], is an imager operating between 1 and 5 μm. NIX operates both in coronagraphic and not coronagraphic mode allowing the choice between aarge selection of both broad- and narrow-band filters. Finally, it has an LSS mode with R∼450. The second scientific subsystem is SPIFFER, which operates at wavelengths between 1 and 2.5 μm at spectral resolution R∼5000 over the full band or R∼10,000 over the half band. Furthermore, an updated AO system based on the UT4 Adaptive Optics facility (AOF, [99]) feeds ERIS.

4.2.2. SCExAO

Subaru Coronagraphic Extreme Adaptive optics (SCExAO; [100]) is installed at the Subaru Telescope (8.3 m) with the main goal of imaging exoplanets and disks around nearby stars. The light is first processed by the AO188 adaptive optics system to remove most of the optical aberrations induced by atmospheric turbulence. The optical beam is then processed by SCExAO (with a DM of 48 actuators per beam diameter [101]), which performs fine wavefront correction (ExAO) and removes the bright starlight exploiting a suite of high efficiency andow inner working angle (IWA) coronagraphs. The light from SCExAO is then provided to different scientific modules, amidst which the Coronagraphic High Angular Resolution Imaging Spectrograph (CHARIS; [102]) is an IFS covering a wavelength range in the J, H, and K spectral bands. Its spectral resolution is R∼20 using all three spectral bands and between 70 and 90 for each singular spectral band alone. CHARIS can also operate in the spectro-polarimetric observing mode. SCExAO can feed other instrumentsike the Visible Aperture Masking Polarimetric Imager for Resolved Exoplanetary Structures (VAMPIRES [103]) that operates in the visible spectrum at wavelengths between 600 and 800 nm.

4.2.3. SHARK

SHARK (System for coronagraphy with High order Adaptive optics from R to K band) is one of the Large Binocular Telescope (LBT, 2 × 8 m) instruments and consists of a

pair of instruments working in visible (0.4–0.9 μm, SHARK-VIS) and in the near-infrared (0.96–1.7 μm, SHARK-NIR), with the possibility of working in parallel.

The main innovation of SHARK-VIS [104], installed at LBT in 2023, is the implementation of a high-cadence-imaging observing mode ranging from 1 KHz to 65 Hz. This observing mode has been tested at the telescope with a forerunner instrument [105,106] that demonstrates the capability of the method to obtain a contrast of the order of 10^{-5} down to separations of the order of 100 mas around bright stars.

SHARK-NIR [107] is a high-contrast imager installed on theeft arm of the LBT. SHARK-NIR takes full advantage of the extreme AO correction delivered by SOUL (Single Conjugated Adaptive Optics Upgrade for LBT; [108]) that has recently been installed on the LBT. This new AO system is based on a Pyramid WFS allowing to obtain a SR∼70% for as faint stars as R∼13 mag. SHARK-NIR will operate in the Y, J, and H spectral bands. A suite of different coronagraphs is available for different types of scientific cases. The instrument is also equipped with both wide and narrow band filters with the possibility to perform dual-band imaging. Finally, the instrument performsow-resolution (R∼100) and medium-resolution (R∼700) spectroscopy using the LSS mode with the possibility of spectrally characterizing the atmospheres of bright substellar companions with a contrast of the order of $\sim 10^{-5}$ at separationsarger than a few tenths of arcsec.

4.2.4. MagAO-X

MagAO-X is the extreme adaptive optics system for the 6.3 m Magellan II (Clay) with a high-order controloop $>$ 2 kHz consisting of a 97 actuator woofer deformable mirror (DM), a 2040 actuator tweeter DM, and a modulated pyramid wavefront sensor (WFS) [109,110]. MagAO-X is equipped with several coronagraphs and two science cameras, so it is possible to carry out science observations in two filters simultaneously (dual-band imaging). The main science goal of MagAO-X is the search for and the characterization of young accreting planets in H_α orbiting nearby T Tauri and Herbig Ae/Be stars [111].

4.2.5. Medium and High Resolution IFSs

On several 8 m class telescopes are mounted NIR IFS instruments with medium and high resolution. Some of them are (theist is not complete): MUSE@VLT, OSIRIS@Keck, NIFs@Gemini. These instruments have been used to characterize spectroscopically, among others, early L-type companions at an angular separation $> 0.5''$ ([36] and reference therein).

4.3. Space Based HCI

Even though it was not built for HCI observations, the Hubble Space Telescope (HST) has proven to be a tool for HCI due to its relatively stable point-spread-function (PSF) which allows for the subtraction ofight from the central source using a variety of methods [112]. In 2005, Lowrance et al. [113] (see Section 7) planned to use a Near-Infrared Camera and Multi-Object Spectrometer (NICMOS) to discover substellar companions to young, nearby stars. NICMOS is a second-generation instrument for the HST and has three available cameras. Camera 2 was equipped with a coronagraph, which is a hole in the field divider mirror that is baffled with a cold pupil plane mask. The NICMOS was noonger offered after cycle18 (2010) for observations. Nevertheless, people also continued to use HST instrumentation for HCI observations in theast few years; for example, Cugno et al. [114] used data from Mag AO-X together with HST/WFC3 data to observe the emission of H_α from a candidate circumplantary disk orbiting the young K5 star V 1121 Oph. The Wide Field Camera 3 (WFC3) has been in operation since 2009. It has two channels; one UVIS operates from about 200 to 1000 nm. The second is an IR channel that operates from 900 to 1700 nm.

At the end of 2021, the James Webb Space Telescope (JWST) wasaunched toward a solar orbit near the Sun-Earth L2 Lagrange point, where it finished its commissioning phase in the summer of 2022. The JWST has a focal plane assembly composed of four scientific modules operating in NIR and MIR wavelength range. Three of them have OMs configured also for HCI observations. Two of them operate in the NIR: the NIRCam coronagraphic imaging OM [115] with five different Lyot-type coronagraphs allowing IWA between 0.14″ and 0.89″, and NIRISS Aperture masking interferometry [116] working in the wavelength range between 2.8 and 4.8 µm.Thisatter mode turns the full aperture of JWST into an interferometric array as theight is admitted by seven sub-apertures to produce an interferogram on the detector. This mode allows to detect and characterize planetary or stellar companions that are up to 9 magnitudes fainter than their host star and separated by ∼70–400 mas. The MIRI coronagraphic imaging mode [117] operates in the MIR exploiting 4QPM coronographs with IWA of 0.33″, 0.36″, 0.49″, and 2.16″ for a Lyot mask.

4.4. Future HCI Instrumentation

In the next years, in addition to the several upgrades of existing instrumentations discussed in the previous section, several brand new high-contrast imagers will be mounted on 8–10 m and on the extremelyarge class (∼40 m) telescopes. For the former, it worths to mention the IFS FRIDA (inFRared Imager and Dissector for Adaptive optics) at the Grantecan telescope (10 m) that will be in operation at mid 2025[4]. FRIDA will work in the near-infrared wavelength ranges (0.9–2.5 µm) with imaging capability. It will make use of the GTC Adaptive Optics system (GTCAO). The IFS spectral resolution, depending on the wavelength, ranges between 1000 and 32,000.

The extremelyarge telescopes, both the TMT (Thirty Meter Telescope)[5], and the E-ELT (European Extremelyarge Telescope)[6] are foreseen to have high-contrast imagers. For the TMT, the second generation set of instrumentation is foreseen for two planet imagers. The first is a mid-IR spectrometer imager IFU named bMICHI (Mid-IR Camera, High-disperser and IFU spectrograph), that will operate an IFS mode in the 3–14 µm with R∼1000, and aong slit and polarimetric mode with resolution ranging between R∼600 and 120,000 [118]. The second is the Planetary System Instrument (PSI; [119]), which is a high-contrast instrument that will work between 0.6 and 14 µm (three arms PSI-Blue: 0.6–1.8 µm, PSI-Red: 2.0–5.1 µm, and PSI-10: 7.0–14 µm) with a resolution from R∼50 to R∼6700. PSI will be equipped with several coronagraphs (vAPP, Vector-Vortex + Lyot Stop).

The first generation instrumentation of the E-ELT will comprise two planet imagers and spectrographs: METIS (Mid Infrared ELT Imager and Spectrograph), and HARMONI (High Angular Resolution Monolithic Optical and Near—Infrared Integral field spechtrograph). METIS will work with a set of four different focal planes grouped in three different subsystems: the imager (IMG) and the spectrograph (LMS) are the two scientific focal planes, and theast one, SCAO, is the dedicated adaptive optics system [120]. METIS will be encased in a cryostat and will work between 3 µm and 13.5 µm with its imaging arm, while the spectroscopic arm, an IFS with R∼100,000, will work between 3 µm and 5 µm, assisted by a coronagraph. HARMONI will cover [121] a spectral range from 0.450 µm to 2.450 µm with R from 3500 to 18,000 and spatial sampling from 60 mas to 4 mas. It can operate in two Adaptive Optics modes—SCAO (including a high-contrast capability) and LTAO—or with noAO (no use of AO). Further in time, the second generation of E-ELT instrumentation foresee the Planetary Camera and Spectrograph (PCS), a concept that is the combination of eXtreme Adaptive Optics (XAO), coronagraphy and spectroscopy [122] to detecting and characterizing nearby exoplanets with sizes from sub-Neptune to Earth-size in the neighborhood of the Sun.

Scheduled toaunch in the mid-2020s, the Nancy Grace Roman Space Telescope[7] will mount an HCI. It is a NASA observatory with a primary mirror of 2.4 m. It will have two instruments: the wide field instrument (WFI), and a coronagraphic instrument technology demonstration which will perform HCI and spectroscopy for the discovering and charaterization of extrasolar planets [123].

Figure 11 compares the measured and predicted performances of most of the instruments described previously in several wavelength regimes. Moreover, both detected (red squares) and simulated (orange diamonds) planets are also over-plotted to allow us to understand theimits of these instruments in planet detection. The future ELT and new space-based instruments will allow us to reach the contrast value necessary to observe planets in reflectedight (grey triangles), even at short angular separations.

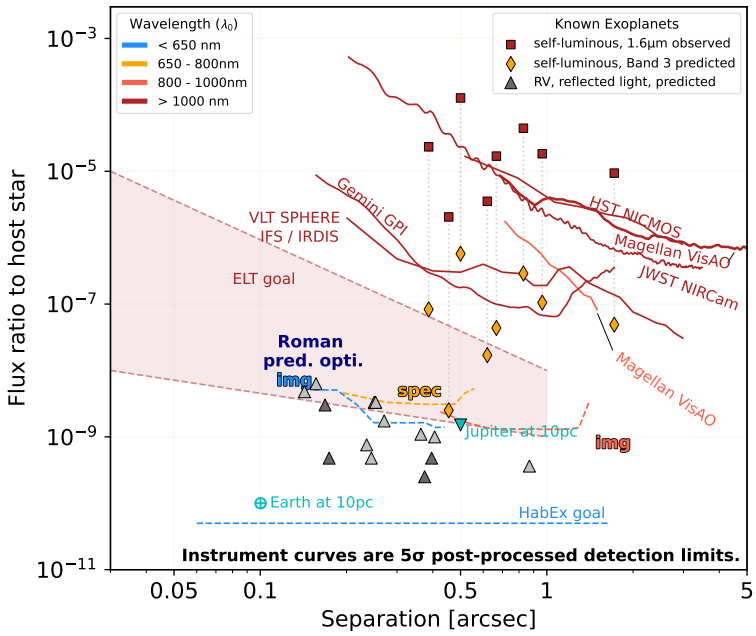

Figure 11. The 5 σ post-processed contrast curves of several both ground- and space-based high-contrast imagers. Code and data source by V. Bailey and S. Hildebrandt Rafels (https://github.com/nasavbailey/DI-flux-ratio-plot, accessed on 30 September 2024).

5. Algorithms

A number of different algorithms have been created in order to implement the high-contrast imaging methods described above. Here, we will give a short description of some of them with the advice that, given the huge development of this field in recent times, the list could beess than complete.

One of the first algorithms adopted for the subtraction of the speckle noise and one of the most widely used in the past years for HCI is theocally optimized combination of images (LOCI; [124]). The aim of the method is to construct an optimized reference image to be subtracted from the science image, maximizing the speckle subtraction and minimizing the self-subtraction of possible companions. This is obtained by dividing the image into subsections and creating, independently for each subsection, a linear combination of reference images in such a way that their subtraction from the science image could minimize the speckle noise. A correct optimization of the weights of each reference image can, moreover, help in reducing the self-subtraction of any science target in the FoV. While LOCI is particularly well optimized to reduce data using the ADI method, it can createarge self-subtraction when also spectral information is introduced using SDI data. To that end, an update of this algorithm has been introduced with TLOCI (template LOCI; [125]).

This algorithm takes into account the possiblearge flux variation at different wavelengths present in a planetary spectrum. Moreover, it couples to the original LOCI algorithm with the possibility of maximizing the SNR of a companion with a specific spectrum adopted as a template by the algorithm itself. A further update of the algorithm was proposed with MLOCI (matched LOCI; [126]) that included in the science data simulated point source used to maximize the detection SNR.

An alternative and widely used algorithm is based on the principal components analysis (PCA) of the Karhunen–Loeve (KL) transformation of aibrary of reference PSF images. It was described for the first time in Soummer et al. [127] together with the Karhunen–Loeve image projection (KLIP) algorithm. After selecting them in an appropriate way for the PSFibrary, the algorithm calculates their KL transform, selects the number of modes to be retained, and uses them to reconstruct the PSF image that will be subtracted from the science image. An alternative method to implement the PCA is to use the single value decomposition (SVD) to generate three arrays, which, if combined correctly,ead to the eigenvectors and the eigenvalues used to reconstruct the original data. A first implementation of this method has been used for the Python-based tool called PYINPOINT [128]. The same method was also used in Mesa et al. [129] for the reduction of the data of the IFS of SPHERE andater included in the SPHERE data reduction pipeline called SpeCal [130]. Independent of the technique used to implement it, PCA needs a careful choice of the number of principal components to be used to create the reference image that will be subtracted from the science data. Indeed, when using aarge number of principal components, the speckle pattern will be reconstructed with very good precision, allowing a good subtraction of the speckle pattern, but, at the same time, it will result in a strong self-subtraction. On the contrary, using a too-low number of principal components will result in a bad speckle subtraction, impeding the detection of point sources with acceptable SNR. A trade-off in the choice of the number of principal components is then fundamental, and it can depend on several different factors, e.g., the separation from the central star and if we want to image a point source or an extended structure (e.g., a protoplanetary disk). A possible solution to such a problem is the introduction of an annular PCA procedure that performs different PCA at different separations from the host star, as performed in the VIP (Vortex imaging processing; [131]) pipeline.

Different alternative algorithms have been proposed in the past few years with the aim to enhance the SNR of the detection reducing (or nulling) at the same time the self-subtractioninked to the ADI method. One such algorithm is the PAtch COvariance (PACO; [132]) method that is based on the definition of a nonstationary multi-variate Gaussian model of the background directly from the data. Once this is performed, a binary hypothesis test is applied to decide on the presence of a planet. An update of the same algorithm (PACO ASDI; [133]) also allowed its application to collect data with spectral informationike those from an IFS. More recently, the algorithm was also applied to the detection of extended structuresike circumstellar disks (REXPACO; [134]). Finally, very recently the same authors developed a further improvement of the method coupling the original PACO algorithm with supervised deepearning (deep PACO; [135]) with the aim to reduce the uncertaintiesinked to the approximate fidelity of the PACO statistical model to the time evolving observations.

The detection of substellar companions in a dataset previously reduced using the ADI technique is an objective that can be achieved by exploiting apposite algorithmsike ANDROMEDA (ANgular Differential OptiMal Exoplanet Detection Algorithm; [136]). This algorithm searches for the signature of a companion in ADI-reduced differential images by applying a maximumikelihood estimation of its position and intensity. A similar approach was followed for the reduction of the GPI data previously reduced using the KLIP algorithm

by Ruffio et al. [137]. They demonstrated that the application of a forward model matched filter (FMMF) allowed for a most effective recovery of a planetary signal while reducing the false-alarm probability at the same time.

A similar approach is followed by the regime-switching model (RSM; [138,139]) detection map. It is based on a model developed more than thirty years ago in the field of econometrics, and it allows one to use the residual cubes obtained by applying different ADI-based techniques to create a single detection map. The algorithm was then further improved by the same authors by allowing an automated optimal selection of the parameters to be used in the algorithm itself (Auto-RSM; [140]). The creation of a reliable detection map is also the main objective of the standardized trajectory intensity mean map (STIM map [141]) algorithm. It is different from the detection map normally found initerature as they assume that the residual noise in an ADI-reduced image is Gaussian. As the authors point out, this canead to aarge number of false-positive detections. To solve this problem they assume for the speckle noise a Modified Rician distribution, which allows for a strong reduction of false-positives.

Recently, some algorithms were developed to solve some specific problems of the HCI. One of these is the Morphological Analysis Yielding separated Objects in Near infrAred usIng Sources Estimation (MAYONNAISE; [142]) algorithm. It is mainly devoted to the imaging of circumstellar disks, avoiding the distortion normally induced by the ADI technique and preserving their shapes and flux distribution. Another one is the Temporal Reference Analysis of Planets (TRAP; [143]), which is mainly aimed at detecting planetary mass companions at short ($<3\lambda/D$) separation from the host star.

6. Results

In 1995, Nakajima et al. [144] announced the discovery of a sub-stellar object around a nearby M1V star GJ 229 obtained with the Adaptive Optics Coronagraph (AOC) and the Palomar 60-inch telescope. GJ 299 B is a brown dwarf with a mass of 20–50 M_{Jup}, and a spectral type of T7, and a veryow T_{eff} of 900 K. It worths to be mentioned because, also if it is not a planetary mass companion, it was the first object discovered with a high-contrast instrumental set-up[8]. After quite a decade, the HCI technique discovered the first planetary-mass object orbiting the brown dwarf 2M 1207 (short for 2MASSWJ 1207334-393254) in the TW Hydrae association [2]. The companion, at an angular separation of $\sim$0.78″, had an estimated mass of around 5 M_{Jup} and a spectral type between L5 and L9. Since this first discovery, over 30 planets and several BD companions have been discovered with the HCI technique. Most of these planets are in unexpectedly wide orbits with hundreds and thousands of au. These wide companions resulted in a critical review of the canonical theories of planet formation via disk instability and core accretion and introduced the possibility that it represents the tail of the brown dwarf formation [35,36] as opacity-limited fragments of turbolent, which collapse molecular clouds [146–149]. Planets are identified as bodies with masses below the deuterium burning mass threshold (13 M_J), as stated by the IAU Working Group Definition. Nevertheless, the recentow mass companion discoveries show that thisimit could not sharply define a boundary between planets and sub-stellar objects but rather that it should be incorporated with the tail-end of the stellar formation. As matter of fact, there are objects with masses below the deuterium burning threshold found in systems with an architecture that instead suggest the cloud-fragmentation formation, and viceversa (e.g., [150–152]). Another possible scenario is that a planet forms in a circumstellar disk around a young star, and its mass could be proportioned to the primary mass [153]. Furthermore, the distribution of the protopalenetary disk radii has a peak at around 200 au and suddenly decreases at around 300 au. Both those situations draw some authors to define the followingimits for the planet—BDs boundary:

mass < 25 M_J, $a_P \leq 300$ au, and the ratio between the companion and the primary mass q < 0.025 [36]. In any case, the matter is already under debate.

The connection between young planets and the protoplanetary disks is very important, and in particular, several efforts have been devoted to the observations of young stars with transitional disks with cavities depleted of dust (e.g., [154–156]). This approached to the discovery of several companions of the gaps, from the stellar to the planetary mass regime (two examples for all: HD142527 [157–161], and HD100546 [162–165]).

Due to the complexity of this technique, the systems with confirmed HCI companions are fewer than the other indirect methods. Also, the surveys conducted with theast-generation instruments resulted in the detection of aow frequency of giant planets at separationsarger than 10 au from the host star [17,166] that are the main targets for such instruments. As a result, blind surveys such as the SHINE survey performed with SPHERE [15,16,167] need to observe hundreds of stars to be able to detect a handful of companion. Coupling HCI with other techniques can help in increasing the probability of detecting a sub-stellar companion. An example of this type is the survey undertaken in the past years to detect companions discovered through RV data. Despite theow overlapping of these two methods (RV prefers older objects at small separation from their host star), this technique allowed for the detection of objects in the past few years, including, e.g., β Pic c [168] and HD 206893 c [11]. In theast years, some authors demonstrated that coupling HCI with astrometric data deriving from the comparison of different catalogsike those from Hipparcos and Gaia to obtain the proper motion anomaly could be a new technique to discover planets (PMa; see, e.g., [169,170]). Furthermore, coupling these data allows us to determine the companion dynamical mass together with important orbital parameters while using aow number of DI epochs. This technique allowed for the detection of new sub-stellar companions in the past few years, including those detected in the BD regime by the COPAINS survey [171] down to objects just above the deuterium limit.

In Table 2 areisted the more remarkable (at the flavor of the authors) objects found with HCI and DI. In the following a short description of each object is given. Some completeists of these objects are in the already cited review of Bowler [35] and Currie et al. [36].

Table 2. Some remarkable planetary systems discovered or characterized with DI and HCI. The discovery year is indicated in theast column.

Name	Description	Comments	Discovery
GJ 229 B [1]	1 Brown Dwarf	1st BD discovered with HCI method	1995
2M 1207 [2]	1 Planet	1st PMC found around a BD	2004
GQ Lup [3]	1 Planet or BD	1st PMC found around a young star	2005
AB Pic [4]	1 Planet	PMC at planet/ BD boundary	2005
HR8799 [5,6]	4 Planets	1st Planetary system identified with HCI and benchmark in understanding young planetary atmospheres	2008–2010
β Pic [7,8]	2 Planets	1st bona fide planet discovered in NIR and MIR in Thermal Emission	2008
Ross 458 (AB) [9,10,11]	1 Planet	1st circumbinary planet imaged	2010
LkCa 15 [12,13,14,15]	2 Protoplanets [a]	1st protoplanet seen in process of active accretion	2011
51 Eri [16]	1 Planet	1st planet discovered with XAO system (GPI)	2015
2MJ2126 [17,18]	1 Planet	The widest orbit planetary-mass object known	2016
HIP 65426 [19,20]	1 Planet	1st Planetary system observed with JWST (ERSP)	2017
PDS 70 [21,22,23]	2 protoplanets	1st detection of jovian protoplanets	2018–2019
HIP 99770 [24]	1 Planet	1st Planet found with Astrometry and HCI synergy	2023
AF Lep [25,26,27]	1 Planet	1st Planet under the D-burningimit and a < 10 au	2023

Table 2. *Cont.*

Name	Description	Comments	Discovery
ϵ Ind [28]	1 Planet	found with Astrometry and HCI synergy 1st planet discovered with JWST	2024

[a] the number of protoplanets in this system is controversial, see Currie et al. [172]. [1] Nakajima et al. [144]; [2] Chauvin et al. [2]; [3] Mugrauer and Neuhäuser [173]; [4] Chauvin et al. [174]; [5] Marois et al. [3]; [6] Marois et al. [175]; [7] Lagrange et al. [176]; [8] Lagrange et al. [177]; [9] Dupuy and Kraus [178]; [10] Goldman et al. [179]; [11] Scholz [180]; [12] Kraus and Ireland [181]; [13] Sallum et al. [182]; [14] Bowler [35]; [15] Currie et al. [172]; [16] Macintosh et al. [14]; [17] Faherty et al. [183]; [18] Deacon et al. [184]; [19] Chauvin et al. [185]; [20] Carter et al. [186]; [21] Müller et al. [187]; [22] Keppler et al. [188]; [23] Haffert et al. [189]; [24] Currie et al. [190]; [25] Mesa et al. [191]; [26] De Rosa et al. [192]; [27] Franson et al. [193]; [28] Matthews et al. [194].

6.1. GQ Lup b

The classical T Tauri star GQ Lup (K7eV) in the Lupus star-forming region (D = 140 $\pm$ 50 pc, age $\leq$ 2 Myr) is the primary of a wide binary system (a = 2400 au, [195]) with the secondary, GQ Lup B with M$\sim$ 0.15 $M_{\odot}$. In 2005 around the GQ Lup A, Neuhäuser et al. [196] discovered aow mass companion using VLT/NACO (see Figure 12). The companion, 6 mag fainter than GQ Lup A, has a semi-major axis of 32.0 $\pm$ 2.25 au (angular separation = 0.7 arcsec). The mass of GQ Lup b has been debated ever since its discovery, with inferred masses of $\sim$10–40 M_J (e.g., [197–199]). GQ Lup A has a circumstellar disk with a gap detected at $\sim$10 au, which could be the evidence of a hidden planet on a solar-system scale [200].

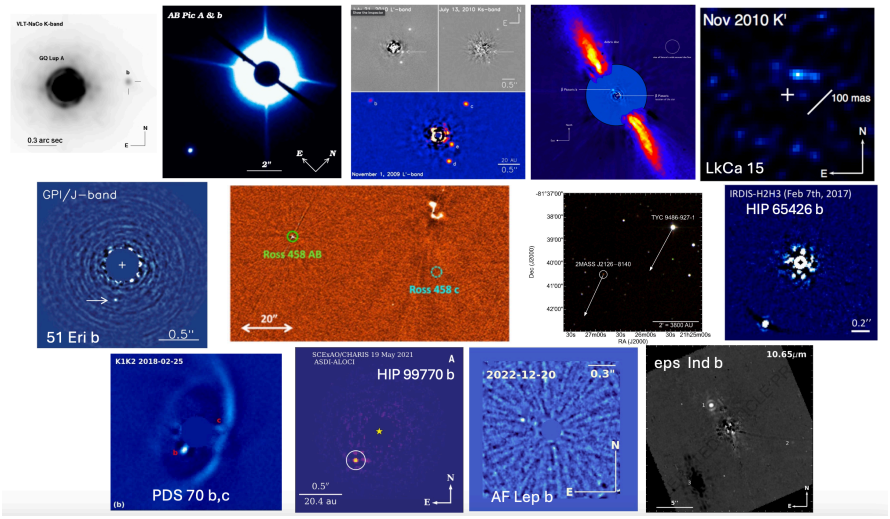

Figure 12. Discovering images of all the planets described in the Section 6 and the reference of each discovery paper. Starting fromeft top to bottom right, there is the following: GQ Lup [196]; AB Pic A b [174]; HR 8799 b,c,d,e [175]; β Pic b [176]; Ross 458 (AB) b (VLA-C band images [201]); LkCa 15 b [181]; 51 Eri b [14]; 2MJ2126 [184]; HIP 66426 [185]; PDS 70 [202]; HIP 99770 b [190]; AF Lep b [191–193]; ϵ Ind b [194].

6.2. AB Pic b

In 2005, Chauvin et al. [174] using both the Adonis/SHARPII@ESO3.6 telescope and VLT/NACO found a companion orbiting the young K2V star ($\sim$30 Myr) member of thearge Tucane-Horologium association (see Figure 12). The companion has been detected in the J, H, and K bands at an angular separation of 5.5 arcsec. Comparing the photometry of AB Pic b with theoretical models [203–205] the authors stated a mass of about 13–14 M_J and a value for the temperature ranging between 1513 and 1856 K allowing the authors to derive a spectral type $L1^{+2}_{-1}$. This object was the first object observed with the HCI technique with the mass at the deuterium burningimit. Is it a planet or a BD? The object became

part of a debate relating to the two criteria of the definition of a planet (the massimit of 13 M_J or the formation scenario). Following the formation scenario criterion, the apparent absence of companions ofow masses in the results of the major surveys suggests that wide companionsike AB Pic b (∼260 au) have formed by gravitational instability [174]. In a further analysis of AB Pic b observations with SPHERE, Palma-Bifani et al. [206] confirmed the AB Pic b parameters and found an obliquity of the planet between 45 and 135 deg, which is evidence of a misalignment between the stellar spin and the planetary orbit. Moreover, by mixing the HARPS-N radial velocity measurements by Grandjean et al. [207] with the proper motion anomaly, these authors suggested the presence of a second inner planet (AB Pic c) with a mass of ∼6 M_J orbiting between 2.5 and 10 au.

6.3. HR 8799 b,c,d,e

The huge forwardeap in HCI was the discovery of the first and for many years the only multi planetary system using direct imaging techniques with Keck and Gemini telescopes around the star HR 8799 [3,175] (see Figure 12). The host star is an A5 spectral type with a mass of around 1.5 $M_\odot$ and an estimated age of around 30 Myr. The star is at a distance of 39.4 pc from the Sun, and it is proposed to be part of the Columba moving group [208]. The three planets *b*, *c*, and *d* were discovered in 2008 at a separation of 1.70″, 0.94″, and 0.64″, which correspond to projected separations of ∼68 au, ∼38 au, and ∼24 au, respectively. Later, in 2010, a fourth inner planet, HR 8799 e, was discovered at a separation of 0.37″, which corresponds to around 14 au. The masses of these planets had aot of different estimates also according to the very uncertain age of the system. Anyway, at the moment, the most accepted values are in the range of 5–7 M_{Jup}. A wealth of different studies have been carried out in the following years both on the characteristics of every single planet and on the architecture and the stability of the system (e.g., [209–223]).

In particular, Konopacky et al. [216], after aong astrometric monitoring at Keck observatory, showed that the whole system is close to a 1:2:4:8 resonance and the b,c,d planetsay on a quite coplanar (∼27°) orbits with the disk. Instead, planet e appears not to be in a coplanar orbit with the b,c, and d planets [224]. The planets have wide separation from the host star, allowing extensive and wide wavelength range spectroscopy observation of the planets without contamination from the host star. Skemer et al. [212] shown that all planets are bright at 3.3 µm compared with equilibrium chemistry model used for field BDs. Oppenheimer et al. [225] were able to tentatively identify in all the planets of the system CH_4, NH_3, C_2H_2 and possibly CO_2 or HCN, using Project1640 at Palomar Hale 5 m Telescope. The interested reader could find other spectroscopical results in the following references: Marley et al. [213], Ingraham et al. [215], Greenbaum et al. [219], Biller et al. [226], Wang et al. [227].

6.4. β Pic b,c

Another important system is that of β Pic an A6 V star at a distance of 19.3 pc from the Sun and with an estimated age of ∼24 Myr. It hosts a well-studied edge-on dust disk that since its discovery [228] was thought to be an ideal environment to host a planetary system (see Figure 12). The planetary mass companion was finally discovered at a separation of around 10 au and with an estimated mass just above 10 M_{Jup} [176]. Its relativelyow orbital period of just above 20 years allowed for a good characterization of its orbit parameters (e.g., [229]), and it also made it possible to evaluate its interaction with the debris disk [230]. Moreover, coupling the astrometric data from Hipparcos and Gaia with those from HCI [231] were able for the first time to obtain a model-independent estimate of the mass of β Pic b obtaining a value of 11 ± 2 M_{Jup}. The orbit of the planet was further constrained thanks to the possibility of observing it before and after its conjunction [232]. Finally, evidence for a second inner planet in the system (β Pic c) was found through

radial velocity data [177]. From astrometric and RV data, the two planet masses have been estimated as $9.3^{+2.5}_{-2.6}$ M_J for β Pic b and 8.3 ± 1 M_J for β Pic c . Theatter was directly imaged by Nowak et al. [168] with high-contrast interferometric imaging by VLT/GRAVITY [233]. β Pic c has been the first planet found with the RV technique and confirmed with DI.

6.5. Ross 458 (AB) b

The binary system Ross 458 (AB) consits of a M0.5 primary and a M7 secondary orbiting at 5.4 au (in February 2000, [234]) with a period of 14.5 yr (see Figure 12). In 2010, Goldman et al. [179] identified a wide orbit companion (1168.0 au) of Ross 458 (AB) with GROND (Gamma-ray Burst Optical/Near-infrared Detector) at the 2.2 m ESO/MPG telescope and Omega 2000 NIR wide-field imager on the Calar Alto 3.5-m telescope. Ross 458 (AB) b shares its proper motion with the binary, forming, in this way, a hierarchicalow-mass star plus PMC system. The authors estimated an age ≤ 1 Gyr and M$\sim$14 M_J identifying Ross 458 (AB) b as the first circumbinary companion with a mass close to the deuterium burningimit ever discovered. Further observations of Ross 458 (AB) b show the presence of clouds (e.g., [235] and references therein) that are opacity sources expected from the condensation of species at the temperature of these sub-stellar objects (650 ± 25 K [236]). It is worth noting that Ross (AB) b is another object under discussion for its belonging, or not, to the realm of planets. Its mass is just close to the deuterium burningimit, its surface temperature isower that that of well know planets (e.g., AB Pic b, HR 8799 b). However, its wide separation raises doubts about its planetary character [236].

6.6. Lk Ca 15 b,c

The central star of Lk Ca 15 is a K5 spectral type T-Tauri star with an age of $\sim$2 Myr and at a distance of around 157 pc from the Sun. The star is known to host a transitional proto-planetary disk [237,238], and it is thought to be an ideal place for the search for planetary-mass companions caught during their formation. Different searches for these companions were performed since the discovery of the disk (e.g., [239]), and the first detection of a possible companion was for the first time proposed by Kraus and Ireland [181] at a separation of 71.9 ± 1.6 mas, corresponding to a projected separation of $\sim$20 au from the host star well into the gap of the disk (see Figure 12). Later, the presence of three accreting companions embedded in the disk was also proposed by Sallum et al. [182]. The nature of such objects was, however, widely disputed, with other authors proposing that such structures could have been explained with scatteredight by extended structures of the disk [240–243]. The presence of possible companions embedded in the disk of such a star is still strongly debated, and its case could be taken as an example of the extreme difficulty in directly imaging young giant planets embedded in proto-planetary disks.

6.7. 51 Eri b

A further step forward was obtained with the beginning of the operativity of the new generation of high-contrast imagersike GPI and SPHERE in 2014 and 2015 that allowed both the detection of new sub-stellar companions and a better characterization of those that were previously known. The first companion detected using one of these new instruments with extreme adaptive optics modules was 51 Eri b (GPI, [14]). In this case the host star is a F0 star with a mass of 1.75 $M_\odot$ and at a distance of 29.4 pc from the Sun. The companion was detected at a separation of $\sim$0.450″, which corresponded to a projected physical separation of around 13 au (see Figure 12). Its mass was estimated to be $\sim$2 M_{Jup}, assuming for the system an age of 20 Myr. Macintosh et al. [14] also reported spectral observation made with NIRC2 at Keck telescope, with the spectra recalling those of a field brown dwarf of spectral type T4.5 to T6, with the presence of strong methane absorption, similar to that of Jupiter.

6.8. 2MJ2126

Short for 2MASS J21265040?8140293, 2MJ2126, formerly identified as standalone object [183], is the fainter (J = 15.5 mag) component of a very wide separation (∼217 arcsec) common proper motion system [184] (see Figure 12). The brighter companion (J = 8.2 mag) is TYC 9486-927-1, an active, rapidly rotating early (1–45 Myr) M1 dwarf [244]. Deacon et al. [184] evaluated the 2MJ2126's mass ranging from 11.6 to 15.0 M_J, using theoretical models by Baraffe et al. [42], placing this object on the deuterium burning threshold. Actually, 2MJ2126 is not one of the results obtained with the HCI, but it isikely the widest orbit planetary-mass object known (>4500 au), and its estimated mass, age, spectral type, and T_{eff} are similar to the well-studied planet β Pictoris b [184].

6.9. HIP 65426 b

Chauvin et al. [185] discovered the first SPHERE sub-stellar companion around the 17 Myr old, A2 spectral type star HIP 65426 at a distance of 111.4 pc from the Sun. The companion, HIP 65426 b, was detected at a separation of 0.83", which corresponded to a projected separation of 92 au, and such aarge separation, together with the unusuallyarge rotation rate of the central star, suggested a planet-planet scattering mechanism with the engulfment of one of the two planets (see Figure 12). The mass of the companion was estimated to be of the order of 6–12 M_{Jup}. The analysis of the IFS spectra confirms aow-surface-gravity atmosphere of spectral type L6 $\pm$ 1 for HIP 65426 b consistent with a young massive planet at the age of the Lower Centaurus–Crux association. Recently, the ERS program high-contrast Imaging of Exoplanets and Exoplanetary Systems with JWST (ERS-01386; [245]) tested the high-contrast exoplanet imaging of both NIRCam and MIRI and coronagraphic imaging ($2 \leq \lambda \leq 16$ μm) modes of JWST, observing exoplanet HIP 65426b [186]. HIP 65426b has been clearly detected in all seven observational filters (F250M, F300M, F356M, F356W, F410M, F444W, F1140C, F1550C), and it is the first-ever exoplanet detected beyond 5 μm.

6.10. PDS 70 b,c

PDS 70 is a K7 star with a mass 0.76 $M_\odot$ and at a distance of 112 pc from the Sun. The estimated age of the system is of the order of 5 Myr. This star is known to host a proto-planetary disk with a gap with a radius of the order of 70 au [246]. The first companion was detected at a separation of 0.195" corresponding to a projected separation of the order of 22 au well into the gap in the disk (see Figure 12). The mass of the companion was estimated in several works ranging from <1 M_{Jup} to more than 10 M_{Jup} (e.g., [187,202,247,248]). PDS 70 b is on eccentric orbit (e∼0.17 $\pm$ 0.06). Follow-up observations in $H\alpha$ narrow band using MUSE allowed the detection of a second accreting planet (PDS 70 c; [189]) at a separation of ∼0.250", which corresponds to around 34 au from the host star. This second companion was not detected atonger wavelengths because it was partially hidden by the disk, but once detected, it was possible to recover it also in NIR with SPHERE [202], allowing its characterization with an estimated mass of the order of 4.5 M_{Jup}. In contrast to PDS 70 b, PDS 70 c shows a circular orbit. Finally, another important result was the detection for the first time of a circum-planetary disk around PDS 70 c using ALMA at sub-millimeter wavelengths with an extension of around 1.2 au [249] and an estimated mass of 0.007–0.03 $M_\oplus$. While, as we have seen above, other systems have been proposed. This is, up to now, the only system for which the presence of directly imaged companions has been proved in the cavity of a proto-planetary disk. This is, of course, of paramount importance as it allows us to validate models for which the presence of structures as gaps and spirals areinked to the presence of forming planets embedded in the disks themselves.

6.11. HIP 99770 b

HIP 99770b could be considered the first planet found with the PMa technique. The discovery of this object has been made with the coupling of SCExAO/CHARIS and Keck/NIRC2 data with Gaia and Hypparcos astrometry [190]. The host star is an A spectral type with an age ranging between 40 Myr and 414 Myr as determined by Tess Asteroseismology. HIP 99770 b, orbiting 17 au from its star, has a dynamical mass of 13.9–16.9 M_J and a planet-to-star mass ratio $\sim 8 \times 10^{-3}$ similar to other planets discovered with DI [190].

6.12. AF Lep b

AF Lep is an F8 star with a mass of 1.2 $M_\odot$ and at a distance of 26.8 pc from the Sun. It is part of the β Pic moving group with an estimated age of 24 $\pm$3 Myr ([191] and reference therein). AF Lep was classified as an SB2 star (spectroscopic binary) with a stellar companion at a separation of 0.021 au [250,251]; this classification is questioned by further analysis by Mesa et al. [191]. Furthermore, it is known to host a debris disk belt with a radius of 54 $\pm$ 6 au. Using the PMa technique Mesa et al. [191], De Rosa et al. [192], Franson et al. [193] discovered the presence of the PMC AF Lep b (see Figure 12). The 2–5 M_{Jup} planet is orbiting its host star at a separation of 8–9 au. The analysis of the IFS spectra shows that AF Lep b is aate-L spectral type object with a T_{eff} ranging between 1000 and 1700 K. This is the first companion with a mass below the deuterium burningimit discovered by coupling direct imaging with PMa measurements. Moreover, it could be considered the first directly detected Jupiter analog orbiting an accelerating star [191].

6.13. ϵ Ind b

ϵ Ind is a triple system composed of a K2V (M = 0.76 $M_\odot$) star (ϵ Ind A) with an age of $\sim$3.5 Gyr and a binary system with two BDs: one (ϵ Ind B) is a T1.5 BD of M = 75.0 M_J and the companion (ϵ Ind C) is a T6 BD with a mass of M = 70 M_J. The two BDs are separated by a semimajor axis of 2.6 au while they are separated by ϵ Ind A by a projected distance of 1460 au [252]. ϵ Ind A b was detected by Feng et al. [253] combining RV data and Gaia astrometric data. Further, Philipot et al. [252] revised the orbital parameters of ϵ Ind A b evaluated by Feng et al. [253], finding very different values, with M = 3.0 M_J, a semimajor axis of 8.8 au and an eccentricity of 0.48. Observing ϵ Ind A with MIRI and a coronagraphy mode of JWST, Matthews et al. [194] revealed a giant planet (see Figure 12) which is consistent with the astrometric and RV measurement reported previously. Using both the RV measurement of the object, the astrometric measurement, and the images obtained by JWST, Matthews et al. [194] constrained the orbital parameter with a M = $6.31^{+0.60}_{-0.56}$ M_J, a semi-major axis of $28.4^{+10.0}_{-7.2}$ au. The orbit has an eccentricity of $0.40^{+0.15}_{-0.18}$. Also, if theatter orbital parameter is in disagreement with the findings in Philipot et al. [252], Matthews et al. [194] concluded that the data indicate that it is the only giant planet in the system and that it could be referred as b. The atmospheric modeling of the mid NIR photometry is consistent with a planet of T$\sim$300 K, which makes ϵ Ind A b not only the first planet discovered by JWST but also the coldest planet directly imaged.

Table 3. Deep imaging Surveys dedicated to the search for planets around young and intermediate-age stars. Table adapted from Chauvin et al. [254], Chauvin [255] and updated. We have indicated the telescope, the instrument, the imaging mode (Cor-I: coronagraphic imaging; Sat-I; saturated imaging; I: imaging; SDI: simultaneous differential imaging; ADI: angular differential imaging; ASDI: angular and spectral differential imaging; APP-ADI: Apodizing mask angular differential imaging), the filters, the field of view (FoV), the number of stars observed (#), their spectral types (SpT), and ages (Age).

Survey	Tel.	Instr.	Mode	Filter	FoV (arcsec^2)	#	SpT	Age (Myr)	Ref.
NA94	PALOMAR	AOC	Cor-I	I	60×60	24	G-M	FIELD	[256]
...									
CH03	ESO3.6m	ADONIS	Cor-I	H,K	13×13	29	GKM	$\lesssim$50	[257]
NE03	NTT	Sharp	Sat-I	K	11×11	23	AFGKM	$\lesssim$50	[258]
	NTT	Sofi	Sat-I	H	13×13	10	AFGKM	$\lesssim$50	–
LO05	HST	NICMOS	Cor-I	H	19×19	145	AFGKM	10–600	[113]
HMPES [a]	VLT	NaCo	Sat-I	H,K	14×14	28	KM	$\lesssim$200	[259]
BI07	VLT	NaCo	SDI	H	5×5	45	GKM	$\lesssim$300	[260]
	MMT		SDI	H	5×5	–	–	–	–
KA07	VLT	NaCo	Sat-I	L′	28×28	22	GKM	$\lesssim$50	[261]
GDPS [b]	Gemini-N	NIRI	ADI	H	22×22	85		10–5000	[12]
AP08	VLT	NaCo	SDI	H	3×3	8	FG	12–500	[262]
CH10	VLT	NaCo	Cor-I	H,K	28×28	88	BAFGKM	$\lesssim$100	[13]
HE10	MMT	Clio	ADI	L′, M	15.5×12.4	54	FGK	100–5000	[263,264]
JA11	Gemini-N	NIRI	ADI	H,K	22×22	15	BA	20–700	[265]
IDPS [c]	GEMINI-N	NIRI	ADI	J,H,K	22×22	292	BAFGKM	<1000	[266,267]
	KECK II	NIRC2	ADI	J,H,K,L	10×10	–	–	–	–
	GEMINI-S	NICI	ADI /SDI	H,K	18×18	–	–	–	–
	VLT	NaCo	ADI	H,K	14×14	–	–	–	–
DE12	VLT	NaCo	ADI	L′	28×28	16	M	$\lesssim$200	[268]
PALMS [d]	KECK II	NIRC2	ADI	H,K	10×10	72	M	$\lesssim$300	[269–271]
	SUBARU	HiCIAO	ADI	H,K	20×20	–	–	–	–
RA13	VLT	NaCo	ADI	L′	28×28	59	AF	$\lesssim$200	[272]
SEEDS [e]	SUBARU	HiCIAO	ADI	H,K	20×20	20	AFGKM	$\lesssim$1000	[273–277]
BI13	Gemini-S	NICI	Cor-ASDI	H	18×18	80	BAFGKM	$\lesssim$200	[278]
NI13	Gemini-S	NICI	Cor-ASDI	H	18×18	70	BA	50–500	[279]
WA13	Gemini-S	NICI	Cor-ASDI	H	18×18	57	AFGKM	$\lesssim$1000	[280]
LEECH [f]	LBT	LMIRCam	ADI	H,L′	11×11	136	AFGKM	$\lesssim$1000	[281–283]
SPOTS [g]	VLT	NaCo	ADI	H	14×14	26	AFGKM	$\lesssim$200	[284–286]

Table 3. *Cont.*

Survey	Tel.	Instr.	Mode	Filter	FoV (arcsec^2)	#	SpT	Age (Myr)	Ref.
	–	SPH/IRDIFS (IFS)	ADI	Y,J	1.77 × 1.77	34	–	–	–
	–	SPH/IRDIFS (IRDIS)	ADI	H	11 × 11	–	–	–	–
ME15	VLT	NaCo	APP-ADI	L′	28 × 28	20	AF	$\lesssim$200	[287,288]
DU16	Spitzer	IRAC	I	4.5 μm	312 × 312	73	AFGKM	$\lesssim$200	[289]
NACO LP [h]	VLT	NaCo	ADI	H	14 × 14	86	FGK	$\lesssim$200	[254,290,291]
MASSIVE [i]	VLT	NaCo	ADI	L′	28 × 28	58	M	$\lesssim$100	[292]
PSYM-WIDE [j]	Gemini-S	GMOS-S	CI	i′,z′	300 × 300	95	KML	$\lesssim$200	[293]
WEIRD [k]	Spitzer	IRAC	I	3.6 & 4.5 μm	312 × 312	344	BAFGKM	10–150	[294]
	CFHT	WIRCam	CI	J	1200 × 1200	–	–	–	
	CFHT	MEGACam	CI	z	3600 × 3600	–	–	–	
	Gemini-S	GMOS-S	CI	z	300 × 300	–	–	–	
	Gemini-S	Flamingos-2	CI	J	360 × 360	–	–	–	
BEAST [l]	VLT	SPH/IRDIFS (IFS)	ADI	Y,J,H	1.77 × 1.77	85	B	10–20	[295,296]
	–	SPH/IRDIFS (IRDIS)	ADI	H,K	11 × 11	–	–	–	–
YSES [m]	VLT	SPH/IRDIS	CI/DBI	Y,J,H,K	11 × 11	70	K	∼ 15	[297–299]
	–	NaCo	CI	L′,M′	28 × 28	–	–	–	–
GPIES [n]	Gemini-s	GPI	ADI/SDI	Y,J,H,K	2.78 × 2.78	600	BAFGKM	$\lesssim$1000	[166]
SHINE [o]	VLT	SPH/IRDIFS (IFS)	ADI	Y,J	1.77 × 1.77	500	AFGKM	$\lesssim$800	[15–17]
	–	SPH/IRDIFS (IRDIS)	ADI	H	11 × 11	–	–	–	–
ISPY [p]	VLT	NaCo	ADI	L′	28 × 28	∼200	BAFGKM	<10	[300]

Notes: [a] Hot Massive Extrasolar Planets Search; [b] Gemini Deep Planet Survey; [c] International Deep Planet Survey; [d] Planets Around Low-Mass Stars; [e] Strategic Exploration of Exoplanets and disks; [f] LBTI Exozodi Exoplanet Common Hunt; [g] Search for Planets Orbiting Two Stars; [h] NaCo Long Program 184.C-0157; [i] M-dwArf Statistical Survey for direct Imaging of massiVe Exoplanets; [j] Planet Search around Young-associations; [k] Wide-orbit Exoplanet search with Infrared Direct imaging; [l] B-star Exoplanets Abundance Study; [m] Young Suns Exoplanets Survey; [n] Gemini Planets Imager Exoplanet Survey; [o] SpHere INfrared survey for Exoplanets; [p] Imaging Survey for Planets around Young Stars.

7. Occurrence Rate of Low Mass Companions on Wide Orbits

One of the main goals ofarge direct-imaging surveys (see Table 3) is the statistical definition of the frequency of exoplanets as a function of their separation from the host star. In the following we describe some of the main surveys and their results. The first example is, perhaps, the survey performed in the L′ spectral band using NACO of 22 targets in the Tucana and β-Pictoris moving groups (KA07, [261]) that, despite theack of novel detection, costrained the distribution of Jupiter-like companions with M > 3 M_J at separationarger than 30 au with aower frequency (<2%) than that stated by the HMPES (Hot Massive Extrasolar Planets Search) results. In the following years, new andarger surveys were conducted to allow for the refinement of these results. Nielsen and Close [301] exploited a survey on 118 young FGKM stars observed both with NACO in H and K spectral bands and the NIRI camera at the Gemini telescope (HMPES & BI07) and using different planetary models to infer the frequency ofow mass companions. They were able to set an upperimit of ∼20% for the presence of planetary mass companions ($\geq$4 M_J) around these stars and to put a model-dependingimit for the separation beyond which the presence of a planet was not possible. Heinze et al. [264] (HE10) prioritized the nearness of the sample selecting 54 F, G and K stars at a median distance of 11.2 pc from the Sun. Independently by distribution models, they found with a confidence of 90% thatess than 50% of FGK stars closer than 11.2 pc have a planetary companion with M $>$ 5M_J orbiting between 30 and 94 au. Janson et al. [265] (JA11) observed 18 nearby and very massive stars with spectral type between B2 and A0 and found that <30% of these stars form and retain planets, BD, and veryow mass stars of M $<$ 100 M_J within 300 au, at 99% confidence. Their conclusion took them to privilege the core accretion as the main planet formation mechanism around this type of star. The International Deep Planet Survey (IDPS, [266]) observed 54 young A and F spectral types stars at a small distance from the Sun using both NACO@VLT and NIRI@Gemini. They were able to define a frequency of 5.9–18.8% for planets with mass between 3 and 14 M_J at separations between 10 and 300 au. The Gemini-NICI planet-finding campaign (BI13, [278]) was devoted to searching forow-mass companions around 80 members of the beta Pic, TW Hya, Tucana–Horologium, AB Dor, and Hercules–Lyra moving groups. They found a frequencyower than 18% or 6% according to the adopted model for planets in the mass range of 1–20 M_J and separation of 10–150 au. The authors in [272] (RA13) performed a survey of 59 A and F spectral type stars and found a frequency between 10.8% and 24.8% for planets with masses in between 1 and 13 M_J and separation between 1 and 1000 au around these stars. A statistical analysis of different surveys (SEEDS, GDPS, and BI13) was performed by Brandt et al. [275], and they found aow frequency of 1–3.1% for companions with masses between 5 and 70 M_J and for separations from the host star between 10 and 100 au. A new analysis [267] of IDPS sample, considering a uniform distribution in planet masses and semi-major axis, demonstrated a frequency muchower than those found by previous survey with a frequency ∼1.05%. If considering a poweraw distribution, the frequency arrives at 2.3% for planets with a mass between 0.5 and 14 M_J and separations between 20 and 300 au. They also found no dependence for the frequency with the mass of the host star while this dependence is present for planets at smaller separation than that considered in their work. A relativelyess exploredow mass stellar range was considered by Lannier et al. [292] (MASSIVE) that observed 54 M spectral type stars finding a frequency of 2.3% for planetary mass companions at separations 8 and 400 au. They concluded that theow-mass stars host a different planetary mass population with respect to higher-mass host stars (A-F spectral types). The analysis of the results of the LEECH survey [283] considering 98 nearby stars with spectral types between B and M cannot exclude that planets with masses around 10 M_J are quite common around FGK stars. An analysis of a mucharger sample of

confirmed members of nearby young moving groups was performed by Baron et al. [302] (WEIRD, and PSYM-WIDE). Their sample was composed of 344 stars and considered companions with masses between 1 and 20 M_J and separations between 5 and 5000 au, with aow frequency of 0.1% in the case of the hot start model. Regarding the cold start model, they found, for the same semi-major axis and mass intervals, an upperimit of 5.2% at a 95% confidenceevel. They also found that the occurrence ofow-mass companions is negatively correlated with the orbit semi-major axis and positively correlated with the mass of the host star. In the context of thisarge number of analyses often conducted on small samples andimited to a particular subset of targets, the twoarger surveys had an important role. They were conducted with two of the most important high-contrast imagers currently in activity, namely GPI@Gemini, and SPHERE@VLT. The Gemini Planet Imager Exoplanets Survey (GPIES [166] has observed 521 nearby and young stars further confirming that the frequency of planetary mass companions declines for separationsarger than 10 au. They also found that the frequency of planets is dependent on the mass of the host star, with values of 5.3–13.9% for planets in the mass range between 5 and 13 M_J, around stars with a massarger than 1.5 $M_\odot$ compared to theower frequency of 2.1–5.4% for the same type of objects aroundower mass stars. They also concluded that the main formation mechanism for wide-separation planets should be core-accretion, while for the brown dwarf, the main mechanism should be gravitational instability. Similar results were obtained by the intermediate sample of 150 stars out of the foreseen 400 targets for the full survey for the SHINE survey performed using SPHERE@VLT and described in Vigan et al. [17]. They found a frequency of 13.3–36.5% for planets with a mass between 1 and 75 M_J at separations between 5 and 300 au from the host star to be compared to the muchower frequency of 3–10.5% for such objects around FGK stars. On the contrary, the frequency for such objects around M stars was of the order of 5.5–25.5%. The authors concluded that a planet-like formation pathway dominates for more massive host stars (B and A spectral types), while for the M spectral type, the detection is dominated by brown dwarf binaries. A combination of these two pathways is instead valid for stars of F, G, and K spectral types. The results ofarge surveys, summarized in Table 4, were confirmed by smaller surveys come after them. The Scorpion Planet Survey performed exploiting SPHERE was dedicated to searching planets around 84 A-spectral type stars in the Sco OB2 association. Their results confirmed thearger occurrence of planets atower separation from the host star and thearger probability of finding planetary mass companions at separationsarger than 100 au when observing around A stars. The survey Imaging Survey for Planets around Young stars (ISPY, [303]) exploited NACO to observe 45 young stars hosting a known protoplanetary disk. For these systems, they found a frequency forow-mass companions inine with what they found for more evolved systems. In very recent times, the possibility that the frequency of exoplanets atarge separation from their host star could have been underestimated was suggested by Gratton et al. [304]. These authors analyzed 30 stars in the β-Pic moving group coupling results from direct imaging with those from other techniquesike, e.g., astrometry, concluding that ateast 20 of these targets could host Jupiter-like planets, which suggests that the frequency of such objects could be mucharger than expected by previous analysis.

Table 4. Outcome statistics of some of the surveysisted in Table 3.

Survey	Stars Sp	a (au)	M_P (M_J)	D (pc)	Conf. Lev. (%)	Frequency (%)	Ref.
HMPES, KA07	GKM	≥30	≤5	–	–	<5	[261]
HMPES, BI07	FGKM	$22 < a < 507$ $21 < a < 479$ $82 < a < 276$	>4	–	95	20 [a]	[301]
HE10	FGK	$30 < a < 94$ $22 < a < 100$ $8 < a < 100$	>5 10 20	<11.2	90	<50 <15 <25	[264]
JA11	BA	<300	<100	–	99	<30	[265]
IDPS	AF	$5 < a < 320$ $20 < a < 300$	$3 < M_P < 14$ $0.5 < M_P < 14$	–	68	5.9–18.8 $1.0^{+2.80}_{-0.70}$	[266] [267]
BI13	BAFGKM	$10 < a < 150$ $10 < a < 50$	$1 < M_P < 20$	–	95 95.4 95.4 95.4	<18 [b] <6 [c] <21 [b] <7 [c]	[278]
RA13	AF	$1 < a < 1000$	$1 \leq M_P \leq 13$	–	68	10.8–24.8	[272]
SEEDS, GDPS, BI13	BAFGKM	$10 < a < 100$	$5 \leq M_P \leq 70$	–	68	1–3.1	[275]
IDPS	BAFGKM	$20 < a < 300$	$0.5 \leq M_P \leq 14$	–	–	$1.05^{+2.80}_{-0.70}$ [d] $2.30^{+5.95}_{-1.55}$ [e]	[267]
MASSIVE	M	$8 < a < 400$	$2 \leq M_P \leq 14$ $2 \leq M_P \leq 80$	–	68	$2.3^{+2.9}_{-0.70}$ $4.4^{+3.2}_{-1.3}$	[292]
LEECH	FGK	$5 < a < 50$	$7 \leq M_P \leq 10$	–	–	≤90	[283]
WEIRD, PSYM-WIDE	BAFGKM	$5 < a < 5000$	$1 \leq M_P \leq 20$	–	–	< 5.2 [f] 11^{+11}_{-5} [g]	[302]
GPIES	BAFGKM	$10 < a < 100$ $10 < a < 100$	$5 \leq M_P \leq 13$ $13 \leq M_P \leq 80$	–	–	9^{+5}_{-4} [h] $0.8^{+0.8}_{-0.5}$ [h]	[166]
SPHERE/SHINE	BA FGK M	$5 < a < 300$	$1 \leq M_P \leq 75$	–	–	$23^{+13.5}_{-9.7}$ $5.8^{+4.7}_{-2.8}$ $12.6^{+12.9}_{-7.1}$	[17]

Notes: a: The authors give different results for different planetary spectra models: Fortney et al. [21], Baraffe et al. [42], Burrows et al. [305] respectively. b: using DUSTY models [205]; c: using COND models [42]; d: Considering an uniform distribution; e: Using a poweraw; f: Using cold start planetary models; g: Using hot start planetary models; h: with host stars mass $< 1.5\ M_\odot$.

8. Perspective and Conclusions

In this work, we presented the recent advancement in discovering substellar objects using HCI. Up to now, the number of detections (a few tens of planets) is quiteimited with respect to the thousands found with indirect techniquesike the radial velocity (RV) or the transit technique. With the current instrumentation, the HCI method is able to explorearge separations from the host star where the expected number of massive companions is low [17], while the peak of the distribution of such objects is expected at separationsower than 10 au [166]. Nevertheless, HCI is fundamental for finding massive young exoplanets atarge separations (>10 au) from the host star, a niche not covered by other techniques, and it hints at these objects' formation mechanisms. As a matter of fact, the fundamental HCI contribution in testing, constraining, and disentangling the planetary formation mech-

anisms (core accretion, gravitational instability into a disk) is recognized by most of the authors already cited (e.g., [17,35,36]). Furthermore, this technique allows for the atmospheric characterization of these companions, detecting the photons from them at different wavelengths. In some cases, it has also been possible to obtain spectra atow or medium resolution of such objects, which allows us to determine the presence of moleculesike, e.g., H_2O and CH_4 (e.g., [36]).

With the current instrumentation, the only way to access separations <10 au is to observe targets atow distances (<50 pc) from the Sun; however, just aow number of such objects are as young (a few tens of Myr) as needed for a successful observation with HCI. Coupling the HCI with one or more different techniques, e.g., RV and astrometric measurements, can improve the scientific results of the programs aimed at searching and characterizing planetary objects. Firstly, this can improve the probability of detecting aow-mass companion with respect to the expected probability as opposed to the blind surveys conducted up to now, for which the observations of a sample of hundreds of targets were needed to detect a bunch of substellar objects (both BDs and planets). Indeed, informed surveys areimited to targets for which the probable presence of a companion is indicated by the results of other techniques, which can enhance the success expectation of each single observation. Secondly, coupling different techniques can help in constraining the physical characteristics of the companions, including their dynamical masses and their orbital parameters. The definition of the dynamical mass of the companion, at the moment possible in a few cases, also allows us to calibrate the atmospheric models that, up to now, are used for defining the photometric mass of the directly detected companions.

In addition, the predicted gain, in contrast with the future ELTs' novel instrumentation, can reach, at best, $\sim 10^{-8}$ at an angular separation of about 0.3 arcsecs (see Figure 11), allowing the observation of reflectedight planetsike, for example, Jupiter or planets caught with RV technique. The possibility of reaching closer angular separations with HCI will allow us to search into the habitable zone of F, G, and early K stars to detect giant planets with possible habitable moons or, in one more optimistic view, to distinguish technosignatures such as, for example, the flux ratio of a faintaser signal to residual scatteredight around the star as suggested by Vides et al. [306]. Much more promising is the suite of future space missions, which will be dedicated to host space coronagraphic observatoriesike the Roman Telescope, whose performance can reach $\sim 10^{-9}$ at an angular separation of 0.5 arcsecs sufficient to resolve a planetike Jupiter orbiting a star at 10 pc (see Figure 11). Since the middle of theast century, NASA and ESA have foreseen space-basedarge aperture mission concepts that will reach deeper contrasts at closer angular separations, operating at a wavelength from UV to IRike LUVOIR (NASA; [307]), HabEx (NASA; [308]), which have been merged in one mission named Habitable Worlds Observatory (HWO; [309,310]), and LIFE (an interferometric mission) (ESA; [311]) should then allow for the detection and the characterization of exoplanetary systems down to earth mass objects around nearby stars. Their goal will also be to detect possible signs of the presence ofife (biosignatures).

These instruments, together with those of the ELTs, will allow the HCI techniques to make a huge forwardeap both in detection and characterization capabilities, which will allow them to equal and, in some cases, outperform the most used indirect methods.

Author Contributions: Conceptualization, R.C. and D.M.; methodology, R.C. and D.M.; investigation, R.C. and D.M.; writing—original draft preparation, R.C. and D.M.; writing—review and editing, R.C. and D.M.; supervision, R.C. All authors have read and agreed to the published version of the manuscript.

Funding: This research received no external funding.

Institutional Review Board Statement: Not applicable.

Informed Consent Statement: Not applicable.

Data Availability Statement: No new data were created or analyzed in this study. Data sharing is not applicable to this article.

Conflicts of Interest: The authors declare no conflicts of interest.

Abbreviations

The following abbreviations are used in this manuscript:

4QPM	4-quadrant Phase-Mask
ADI	Angular Differential Imaging
AGPM	Annular Groove Phase Mask
ALMA	Atacama Large Millimeter/submillimeter Array
ANDROMEDA	ANgular Differential OptiMal Exoplanet Detection Algorithm
APLC	Apodized-Pupil Lyot Coronagraph
au	astronomical unit
BLC	Band-Limited Coronagraph
DM	Deformale Mirror
DMS	Deformable Mirror Secondary
ELT	Extremely Large Telescope
EMCCDs	Electron-Multiplying Charge-Coupled Devices
ERIS	Enhanced Resolution Imaging Spectrograph
ERSP	Early Release Science Program
FMMF	Forward Model Matched Filter
FoV	Field of View
FRIDA	inFRared Imager and Dissector for Adaptive optics
GPI	Gemini Planet Imager
GTC	Gran Telescopio Canarias
GTCAO	GTC Adaptive Optics system
HabEx	Habitable Exoplanets observatory
HCI	High-Contrast Imaging
HARMONI	High Angular Resolution Monolithic Optical and Near—Infrared IFS
HST	Hubble Space Telescope
HWO	Habitable Worlds Observatory
IFS	Integral Field Spectrograph
IRDIS	Infra-Red Dual-beam Imager and Spectrograph
IWA	Inner Working Angle
KL	Karhunen–Loeve
KLIP	Karhunen–Loeve Image Projection
JWST	James Webb Space Telescope
LGS	Laser Guide Stars
LOCI	Locally Optimized Combination of Images
LTAO	Laser Tomography Adaptive Optics
LUVOIR	Large Ultraviolet Optical Infrared Surveyor
MAYONNAISE	Morphological Analysis Yielding separated Objects in Near infrAred using Sources Estimation
METIS	Mid Infrared ELT Imager and Spectrograph
MICHI	Mid-IR Camera, High-disperser and IFU spectrograph
MIRI	Mid-Infrared Instrument
MLOCI	Matched LOCI
MUSE	Multi Unit Spectroscopic Explorer
NGS	Natural Guide Star
NIRCam	Near-infrared Camera
NIRSpec	Near-infrared Spectrograph

NIRISS	Near-Infrared Imager and Slitless Spectrograph
OM	Observing Mode
PACO	PAtch COvariance
PCA	Principal Component Analysis
PCS	Planetary Camera and Spectrograph
PMa	Proper Motion Anomaly
PMC	Planetary Mass Companion
PSI	Planetary System Instrument
PSF	Point Spread Function
RSM	Regime Switching Model
RV	Radial Velocity
SAXO	SPHERE extreme AO system
SCAO	Single-Conjugate Adaptive Optics
SCExAO	Subaru Coronagraphic Extreme Adaptive optics
SDI	Spectral Differential Imaging
SINFONI	Spectrograph for Integral Field Observation in the Near-Infrared
SPHERE	Spectro-Polarimetric High-contrast imager for Exoplanets REsearch
SPIFFI	Spectrometer for Infrared Faint Field Imaging
STIM	standardized trajectory intensity mean
SVD	Single Value Decomposition
TLOCI	Template LOCI
TRAP	Temporal Reference Analysis of Planets
VIP	Vortex Imaging Processing
WFS	WaveFront Sensor
ZIMPOL	Zurich Imaging Polarimeter

Notes

[1] http://exoplanet.eu/, accessed on 31 August 2024.
[2] https://exoplanetarchive.ipac.caltech.edu/index.html, accessed on 31 August 2024.
[3] https://www2.keck.hawaii.edu/inst/nirc2/tech_home.html, accessed on 31 August 2024.
[4] https://www.gtc.iac.es/instruments/instrumentation.php, accessed on 30 September 2024.
[5] https://www.tmt.org/page/second-generation-instruments, acccessed on 30 September 2024.
[6] https://elt.eso.org/instrument/ acccessed on 30 September 2024.
[7] https://science.nasa.gov/mission/roman-space-telescope/introducing-the-roman-space-telescope/, accessed on 30 September 2024.
[8] During the writing of this review, Xuan et al. [145] observing GJ 229 with GRAVITY interferometry resolved Gliese 229 B into two components, Gliese 229 Ba and Bb.

References

1. Dyson, F.W.; Eddington, A.S.; Davidson, C. A Determination of the Deflection of Light by the Sun's Gravitational Field, from Observations Made at the Total Eclipse of May 29, 1919. *Philos. Trans. R. Soc. Lond. Ser. A* **1920**, *220*, 291–333. [CrossRef]
2. Chauvin, G.; Lagrange, A.M.; Dumas, C.; Zuckerman, B.; Mouillet, D.; Song, I.; Beuzit, J.L.; Lowrance, P. A giant planet candidate near a young brown dwarf. Direct VLT/NACO observations using IR wavefront sensing. *Astron. Astrophys.* **2004**, *425*, L29–L32. [CrossRef]
3. Marois, C.; Macintosh, B.; Barman, T.; Zuckerman, B.; Song, I.; Patience, J.; Lafrenière, D.; Doyon, R. Direct Imaging of Multiple Planets Orbiting the Star HR 8799. *Science* **2008**, *322*, 1348. [CrossRef] [PubMed]
4. Mayor, M.; Queloz, D. A Jupiter-mass companion to a solar-type star. *Nature* **1995**, *378*, 355–359. [CrossRef]
5. Traub, W.A. Extrasolar planet characteristics in the visible wavelength range. In Proceedings of the Conference on Towards Other Earths: DARWIN/TPF and the Search for Extrasolar Terrestrial Planets, Heidelberg, Germany, 22–25 April 2003; Fridlund, M., Henning, T., Lacoste, H., Eds.; ESA Publications Division: Noordwijk, The Netherlands, 2003; Volume 539, pp. 231–239.
6. Kaltenegger, L. How to Characterize Habitable Worlds and Signs of Life. *Annu. Rev. Astron. Astrophys.* **2017**, *55*, 433–485. [CrossRef]

7. Calissendorff, P.; De Furio, M.; Meyer, M.; Albert, L.; Aganze, C.; Ali-Dib, M.; Bardalez Gagliuffi, D.C.; Baron, F.; Beichman, C.A.; Burgasser, A.J.; et al. JWST/NIRCam Discovery of the First Y+Y Brown Dwarf Binary: WISE J033605.05-014350.4. *Astrophys. J. Lett.* **2023**, *947*, L30. [CrossRef]
8. Liu, M.C.; Delorme, P.; Dupuy, T.J.; Bowler, B.P.; Albert, L.; Artigau, E.; Reylé, C.; Forveille, T.; Delfosse, X. CFBDSIR J1458+1013B: A Very Cold (>T10) Brown Dwarf in a Binary System. *Astrophys. J.* **2011**, *740*, 108. [CrossRef]
9. Garcia, E.V.; Ammons, S.M.; Salama, M.; Crossfield, I.; Bendek, E.; Chilcote, J.; Garrel, V.; Graham, J.R.; Kalas, P.; Konopacky, Q.; et al. Individual, Model-independent Masses of the Closest Known Brown Dwarf Binary to the Sun. *Astrophys. J.* **2017**, *846*, 97. [CrossRef]
10. Bedin, L.R.; Dietrich, J.; Burgasser, A.J.; Apai, D.; Libralato, M.; Griggio, M.; Fontanive, C.; Pourbaix, D. HST astrometry of the closest brown dwarfs-II. Improved parameters and constraints on a third body. *Astron. Nachrichten* **2024**, *345*, e20230158. [CrossRef]
11. Hinkley, S.; Lacour, S.; Marleau, G.D.; Lagrange, A.M.; Wang, J.J.; Kammerer, J.; Cumming, A.; Nowak, M.; Rodet, L.; Stolker, T.; et al. Direct discovery of the inner exoplanet in the HD 206893 system. Evidence for deuterium burning in a planetary-mass companion. *Astron. Astrophys.* **2023**, *671*, L5. [CrossRef]
12. Lafrenière, D.; Doyon, R.; Marois, C.; Nadeau, D.; Oppenheimer, B.R.; Roche, P.F.; Rigaut, F.; Graham, J.R.; Jayawardhana, R.; Johnstone, D.; et al. The Gemini Deep Planet Survey. *Astrophys. J.* **2007**, *670*, 1367–1390. [CrossRef]
13. Chauvin, G.; Lagrange, A.M.; Bonavita, M.; Zuckerman, B.; Dumas, C.; Bessell, M.S.; Beuzit, J.L.; Bonnefoy, M.; Desidera, S.; Farihi, J.; et al. Deep imaging survey of young, nearby austral stars. VLT/NACO near-infrared Lyot-coronographic observations. *Astron. Astrophys.* **2010**, *509*, A52. [CrossRef]
14. Macintosh, B.; Graham, J.R.; Barman, T.; De Rosa, R.J.; Konopacky, Q.; Marley, M.S.; Marois, C.; Nielsen, E.L.; Pueyo, L.; Rajan, A.; et al. Discovery and spectroscopy of the young jovian planet 51 Eri b with the Gemini Planet Imager. *Science* **2015**, *350*, 64–67. [CrossRef] [PubMed]
15. Desidera, S.; Chauvin, G.; Bonavita, M.; Messina, S.; LeCoroller, H.; Schmidt, T.; Gratton, R.; Lazzoni, C.; Meyer, M.; Schlieder, J.; et al. The SPHERE infrared survey for exoplanets (SHINE). I. Sample definition and target characterization. *Astron. Astrophys.* **2021**, *651*, A70. [CrossRef]
16. Langlois, M.; Gratton, R.; Lagrange, A.M.; Delorme, P.; Boccaletti, A.; Bonnefoy, M.; Maire, A.L.; Mesa, D.; Chauvin, G.; Desidera, S.; et al. The SPHERE infrared survey for exoplanets (SHINE). II. Observations, data reduction and analysis, detection performances, and initial results. *Astron. Astrophys.* **2021**, *651*, A71. [CrossRef]
17. Vigan, A.; Fontanive, C.; Meyer, M.; Biller, B.; Bonavita, M.; Feldt, M.; Desidera, S.; Marleau, G.D.; Emsenhuber, A.; Galicher, R.; et al. The SPHERE infrared survey for exoplanets (SHINE). III. The demographics of young giant exoplanets below 300 au with SPHERE. *Astron. Astrophys.* **2021**, *651*, A72. [CrossRef]
18. Brown, T.M. Transmission Spectra as Diagnostics of Extrasolar Giant Planet Atmospheres. *Astrophys. J.* **2001**, *553*, 1006–1026. [CrossRef]
19. Tinetti, G.; Liang, M.C.; Vidal-Madjar, A.; Ehrenreich, D.; Lecavelier des Etangs, A.; Yung, Y.L. Infrared Transmission Spectra for Extrasolar Giant Planets. *Astrophys. J. Lett.* **2007**, *654*, L99–L102. [CrossRef]
20. Charbonneau, D.; Allen, L.E.; Megeath, S.T.; Torres, G.; Alonso, R.; Brown, T.M.; Gilliland, R.L.; Latham, D.W.; Mandushev, G.; O'Donovan, F.T.; et al. Detection of Thermal Emission from an Extrasolar Planet. *Astrophys. J.* **2005**, *626*, 523–529. [CrossRef]
21. Fortney, J.J.; Marley, M.S.; Saumon, D.; Lodders, K. Synthetic Spectra and Colors of Young Giant Planet Atmospheres: Effects of Initial Conditions and Atmospheric Metallicity. *Astrophys. J.* **2008**, *683*, 1104–1116. [CrossRef]
22. Burrows, A.; Rauscher, E.; Spiegel, D.S.; Menou, K. Photometric and Spectral Signatures of Three-dimensional Models of Transiting Giant Exoplanets. *Astrophys. J.* **2010**, *719*, 341–350. [CrossRef]
23. Baraffe, I.; Chabrier, G.; Barman, T. Structure and evolution of super-Earth to super-Jupiter exoplanets. I. Heavy element enrichment in the interior. *Astron. Astrophys.* **2008**, *482*, 315–332. [CrossRef]
24. Marley, M.S.; Fortney, J.J.; Hubickyj, O.; Bodenheimer, P.; Lissauer, J.J. On the Luminosity of Young Jupiters. *Astrophys. J.* **2007**, *655*, 541–549. [CrossRef]
25. Spiegel, D.S.; Burrows, A. Spectral and Photometric Diagnostics of Giant Planet Formation Scenarios. *Astrophys. J.* **2012**, *745*, 174. [CrossRef]
26. Oppenheimer, B.R.; Hinkley, S. High-Contrast Observations in Optical and Infrared Astronomy. *Annu. Rev. Astron. Astrophys.* **2009**, *47*, 253–289. [CrossRef]
27. Davies, R.; Kasper, M. Adaptive Optics for Astronomy. *Annu. Rev. Astron. Astrophys.* **2012**, *50*, 305–351. [CrossRef]
28. Monnier, J.D. Optical interferometry in astronomy. *Rep. Prog. Phys.* **2003**, *66*, 789–857. [CrossRef]
29. Absil, O.; Mawet, D. Formation and evolution of planetary systems: The impact of high-angular resolution optical techniques. *Astron. Astrophys. Rev.* **2010**, *18*, 317–382. [CrossRef]
30. Quirrenbach, A. Optical Interferometry. *Annu. Rev. Astron. Astrophys.* **2001**, *39*, 353–401. [CrossRef]
31. Saha, S.K. Modern optical astronomy: Technology and impact of interferometry. *Rev. Mod. Phys.* **2002**, *74*, 551–600. [CrossRef]

32. GRAVITY Collaboration; Abuter, R.; Accardo, M.; Amorim, A.; Anugu, N.; Ávila, G.; Azouaoui, N.; Benisty, M.; Berger, J.P.; Blind, N.; et al. Firstight for GRAVITY: Phase referencing optical interferometry for the Very Large Telescope Interferometer. *Astron. Astrophys.* **2017**, *602*, A94. [CrossRef]
33. Defrère, D.; Absil, O.; Berger, J.P.; Danchi, W.C.; Dandumont, C.; Eisenhauer, F.; Ertel, S.; Gardner, T.; Glauser, A.; Hinz, P.; et al. Review and scientific prospects of high-contrast optical stellar interferometry. In Proceedings of the Optical and Infrared Interferometry and Imaging VII, Oline, 14–18 December 2020; Society of Photo-Optical Instrumentation Engineers (SPIE) Conference Series; Tuthill, P.G., Mérand, A., Sallum, S., Eds.; Society of Photo-Optical Instrumentation Engineers (SPIE). Bellingham, WA, USA, 2020; Volume 11446, p. 114461J. [CrossRef]
34. Traub, W.A.; Oppenheimer, B.R. Direct Imaging of Exoplanets. In *Exoplanets*; Seager, S., Ed.; The University of Arizona Press: Tucson, AZ, USA, 2010; pp. 111–156.
35. Bowler, B.P. Imaging Extrasolar Giant Planets. *Pub. Astron. Soc. Pac.* **2016**, *128*, 102001. [CrossRef]
36. Currie, T.; Biller, B.; Lagrange, A.; Marois, C.; Guyon, O.; Nielsen, E.L.; Bonnefoy, M.; De Rosa, R.J. Direct Imaging and Spectroscopy of Extrasolar Planets. In Proceedings of the Protostars and Planets VII, Kyoto, Japan, 10–15 April 2023; Astronomical Society of the Pacific Conference Series; Inutsuka, S., Aikawa, Y., Muto, T., Tomida, K., Tamura, M., Eds.; Astronomical Society of the Pacific: San Francisco, CA, USA, 2023; Volume 534, p. 799, [CrossRef]
37. Follette, K.B. An Introduction to High Contrast Differential Imaging of Exoplanets and Disks. *Pub. Astron. Soc. Pac.* **2023**, *135*, 093001. [CrossRef]
38. Oppenheimer, B.R.; Golimowski, D.A.; Kulkarni, S.R.; Matthews, K.; Nakajima, T.; Creech-Eakman, M.; Durrance, S.T. A Coronagraphic Survey for Companions of Stars within 8 Parsecs. *Astron. J.* **2001**, *121*, 2189–2211. [CrossRef]
39. Kasting, J.F.; Catling, D. Evolution of a Habitable Planet. *Annu. Rev. Astron. Astrophys.* **2003**, *41*, 429–463. [CrossRef]
40. de Pater, I.; Lissauer, J.J. *Planetary Sciences*; Cambridge University Press, Cambridge, UK, 2010.
41. Burrows, A.; Hubbard, W.B.; Lunine, J.I.; Liebert, J. The theory of brown dwarfs and extrasolar giant planets. *Rev. Mod. Phys.* **2001**, *73*, 719–765. [CrossRef]
42. Baraffe, I.; Chabrier, G.; Barman, T.S.; Allard, F.; Hauschildt, P.H. Evolutionary models for cool brown dwarfs and extrasolar giant planets. The case of HD 209458. *Astron. Astrophys.* **2003**, *402*, 701–712. [CrossRef]
43. Born, M.; Wolf, E. *Principles of Optics*; Pergamon Press, Oxford, England 1999.
44. Racine, R.; Walker, G.A.H.; Nadeau, D.; Doyon, R.; Marois, C. Speckle Noise and the Detection of Faint Companions. *Pub. Astron. Soc. Pac.* **1999**, *111*, 587–594. [CrossRef]
45. Soummer, R.; Ferrari, A.; Aime, C.; Jolissaint, L. Speckle Noise and Dynamic Range in Coronagraphic Images. *Astrophys. J.* **2007**, *669*, 642–656. [CrossRef]
46. Babcock, H.W. The Possibility of Compensating Astronomical Seeing. *Pub. Astron. Soc. Pac.* **1953**, *65*, 229. [CrossRef]
47. Merkle, F.; Kern, P.; Léna, P.; Rigaut, F.; Fontanella, J.C.; Rousset, G.; Boyer, C.; Gaffard, J.P.; Jagourel, P. Successful tests of adaptive optics. *Messenger* **1989**, *58*, 1–4.
48. Rigaut, F.; Rousset, G.; Kern, P.; Fontanella, J.C.; Gaffard, J.P.; Merkle, F.; Léna, P. Adaptive optics on a 3.6-m telescope—Results and performance. *Astron. Astrophys.* **1991**, *250*, 280–290.
49. Beckers, J.M. Adaptive Optics for Astronomy: Principles, Performance, and Applications. *Annu. Rev. Astron. Astrophys.* **1993**, *31*, 13–62. [CrossRef]
50. Rousset, G.; Fontanella, J.C.; Kern, P.; Gigan, P.; Rigaut, F. First diffraction-limited astronomical images with adaptive optics. *Astron. Astrophys.* **1990**, *230*, L29–L32.
51. Ragazzoni, R. Pupil plane wavefront sensing with an oscillating prism. *J. Mod. Opt.* **1996**, *43*, 289–293. [CrossRef]
52. Esposito, S.; Riccardi, A.; Fini, L.; Puglisi, A.T.; Pinna, E.; Xompero, M.; Briguglio, R.; Quirós-Pacheco, F.; Stefanini, P.; Guerra, J.C.; et al. Firstight AO (FLAO) system for LBT: Final integration, acceptance test in Europe, and preliminary on-sky commissioning results. In Proceedings of the Adaptive Optics Systems II, San Diego, CA, USA, 27 June 2010; Society of Photo-Optical Instrumentation Engineers (SPIE) Conference Series; Ellerbroek, B.L., Hart, M., Hubin, N., Wizinowich, P.L., Eds.; Society of Photo-Optical Instrumentation Engineers (SPIE): Bellingham, WA, USA, 2010; Volume 7736, p. 773609. [CrossRef]
53. Beuzit, J.L.; Vigan, A.; Mouillet, D.; Dohlen, K.; Gratton, R.; Boccaletti, A.; Sauvage, J.F.; Schmid, H.M.; Langlois, M.; Petit, C.; et al. SPHERE: The exoplanet imager for the Very Large Telescope. *Astron. Astrophys.* **2019**, *631*, A155. [CrossRef]
54. Macintosh, B.; Chilcote, J.K.; Bailey, V.P.; de Rosa, R.; Nielsen, E.; Norton, A.; Poyneer, L.; Wang, J.; Ruffio, J.B.; Graham, J.R.; et al. The Gemini Planet Imager: Looking back over five years and forward to the future. In Proceedings of the Adaptive Optics Systems VI, Austin, TX, USA, 10 June 2018; Society of Photo-Optical Instrumentation Engineers (SPIE) Conference Series; Close, L.M., Schreiber, L., Schmidt, D., Eds.; Society of Photo-Optical Instrumentation Engineers (SPIE): Bellingham, WA, USA, 2018; Volume 10703, p. 107030K. [CrossRef]
55. Ross, T.S. Limitations and applicability of the Maréchal approximation. *Appl. Opt.* **2009**, *48*, 1812. [CrossRef] [PubMed]

56. Wizinowich, P.L.; Le Mignant, D.; Bouchez, A.H.; Campbell, R.D.; Chin, J.C.Y.; Contos, A.R.; van Dam, M.A.; Hartman, S.K.; Johansson, E.M.; Lafon, R.E.; et al. The W. M. Keck Observatory Laser Guide Star Adaptive Optics System: Overview. *Pub. Astron. Soc. Pac.* **2006**, *118*, 297–309. [CrossRef]
57. Bonaccini Calia, D.; Allaert, E.; Alvarez, J.L.; Araujo Hauck, C.; Avila, G.; Bendek, E.; Buzzoni, B.; Comin, M.; Cullum, M.; Davies, R.; et al. Firstight of the ESO Laser Guide Star Facility. In Proceedings of the Advances in Adaptive Optics II, Orlando, FL, USA, 24 May 2006; Society of Photo-Optical Instrumentation Engineers (SPIE) Conference Series; Ellerbroek, B.L., Bonaccini Calia, D., Eds.; Society of Photo-Optical Instrumentation Engineers (SPIE): Bellingham, WA, USA, 2006; Volume 6272, p. 627207. [CrossRef]
58. Boccas, M.; Rigaut, F.; Bec, M.; Irarrazaval, B.; James, E.; Ebbers, A.; D'Orgeville, C.; Grace, K.; Arriagada, G.; Karewicz, S.; et al. Laser guide star upgrade of Altair at Gemini North. In Proceedings of the Advances in Adaptive Optics II, Orlando, FL, USA, 24 May 2006; Society of Photo-Optical Instrumentation Engineers (SPIE) Conference Series; Ellerbroek, B.L., Bonaccini Calia, D., Eds.; Society of Photo-Optical Instrumentation Engineers (SPIE): Bellingham, WA, USA, 2006; Volume 6272, p. 62723L. [CrossRef]
59. Hayano, Y.; Takami, H.; Oya, S.; Hattori, M.; Saito, Y.; Watanabe, M.; Guyon, O.; Minowa, Y.; Egner, S.E.; Ito, M.; et al. Commissioning status of Subaruaser guide star adaptive optics system. In Proceedings of the Adaptive Optics Systems II, San Diego, CA, USA, 27 June 2010; Society of Photo-Optical Instrumentation Engineers (SPIE) Conference Series; Ellerbroek, B.L., Hart, M., Hubin, N., Wizinowich, P.L., Eds.; Society of Photo-Optical Instrumentation Engineers (SPIE): Bellingham, WA, USA, 2010; Volume 7736, p. 77360N. [CrossRef]
60. Guyon, O. Extreme Adaptive Optics. *Annu. Rev. Astron. Astrophys.* **2018**, *56*, 315–355. [CrossRef]
61. Lyot, B. The study of the solar corona and prominences without eclipses (George Darwin Lecture, 1939). *Mon. Not. R. Astron. Soc.* **1939**, *99*, 580. [CrossRef]
62. Sivaramakrishnan, A.; Koresko, C.D.; Makidon, R.B.; Berkefeld, T.; Kuchner, M.J. Ground-based Coronagraphy with High-order Adaptive Optics. *Astrophys. J.* **2001**, *552*, 397–408. [CrossRef]
63. Guyon, O.; Pluzhnik, E.A.; Kuchner, M.J.; Collins, B.; Ridgway, S.T. Theoretical Limits on Extrasolar Terrestrial Planet Detection with Coronagraphs. *Astrophys. J. Suppl.* **2006**, *167*, 81–99. [CrossRef]
64. Galicher, R.; Mazoyer, J. Imaging exoplanets with coronagraphic instruments. *Comptes Rendus Phys.* **2024**, *24*, 133. [CrossRef]
65. Kuchner, M.J.; Traub, W.A. A Coronagraph with a Band-limited Mask for Finding Terrestrial Planets. *Astrophys. J.* **2002**, *570*, 900–908. [CrossRef]
66. Boccaletti, A.; Riaud, P.; Baudoz, P.; Baudrand, J.; Rouan, D.; Gratadour, D.; Lacombe, F.; Lagrange, A.M. The Four-Quadrant Phase Mask Coronagraph. IV. First Light at the Very Large Telescope. *Pub. Astron. Soc. Pac.* **2004**, *116*, 1061–1071. [CrossRef]
67. Rouan, D.; Riaud, P.; Boccaletti, A.; Clénet, Y.; Labeyrie, A. The Four-Quadrant Phase-Mask Coronagraph. I. Principle. *Pub. Astron. Soc. Pac.* **2000**, *112*, 1479–1486. [CrossRef]
68. Mawet, D.; Absil, O.; Delacroix, C.; Girard, J.H.; Milli, J.; O'Neal, J.; Baudoz, P.; Boccaletti, A.; Bourget, P.; Christiaens, V.; et al. L′-band AGPM vector vortex coronagraph's firstight on VLT/NACO. Discovery of aate-type companion at two beamwidths from an F0V star. *Astron. Astrophys.* **2013**, *552*, L13. [CrossRef]
69. Kiefer, S.; Bohn, A.J.; Quanz, S.P.; Kenworthy, M.; Stolker, T. Spectral and angular differential imaging with SPHERE/IFS. Assessing the performance of various PCA-based approaches to PSF subtraction. *Astron. Astrophys.* **2021**, *652*, A33. [CrossRef]
70. Seager, S.; Whitney, B.A.; Sasselov, D.D. Photometric Light Curves and Polarization of Close-in Extrasolar Giant Planets. *Astrophys. J.* **2000**, *540*, 504–520. [CrossRef]
71. Stam, D.M.; Hovenier, J.W.; Waters, L.B.F.M. Using polarimetry to detect and characterize Jupiter-like extrasolar planets. *Astron. Astrophys.* **2004**, *428*, 663–672. [CrossRef]
72. Schmid, H.M.; Beuzit, J.L.; Feldt, M.; Gisler, D.; Gratton, R.; Henning, T.; Joos, F.; Kasper, M.; Lenzen, R.; Mouillet, D.; et al. Search and investigation of extra-solar planets with polarimetry. In Proceedings of the IAU Colloq. 200: Direct Imaging of Exoplanets: Science & Techniques, Villefranche sur Mer, France, 3–7 October 2005; Aime, C., Vakili, F., Eds.; Cambridge University Press: Cambridge, UK, 2006; pp. 165–170. [CrossRef]
73. Schmid, H.M.; Bazzon, A.; Roelfsema, R.; Mouillet, D.; Milli, J.; Menard, F.; Gisler, D.; Hunziker, S.; Pragt, J.; Dominik, C.; et al. SPHERE/ZIMPOL high resolution polarimetric imager. I. System overview, PSF parameters, coronagraphy, and polarimetry. *Astron. Astrophys.* **2018**, *619*, A9. [CrossRef]
74. Kuhn, J.R.; Potter, D.; Parise, B. Imaging Polarimetric Observations of a New Circumstellar Disk System. *Astrophys. J. Lett.* **2001**, *553*, L189–L191. [CrossRef]
75. Perrin, M.D.; Graham, J.R.; Kalas, P.; Lloyd, J.P.; Max, C.E.; Gavel, D.T.; Pennington, D.M.; Gates, E.L. Laser Guide Star Adaptive Optics Imaging Polarimetry of Herbig Ae/Be Stars. *Science* **2004**, *303*, 1345–1348. [CrossRef] [PubMed]
76. Oppenheimer, B.R.; Brenner, D.; Hinkley, S.; Zimmerman, N.; Sivaramakrishnan, A.; Soummer, R.; Kuhn, J.; Graham, J.R.; Perrin, M.; Lloyd, J.P.; et al. The Solar-System-Scale Disk around AB Aurigae. *Astrophys. J.* **2008**, *679*, 1574–1581. [CrossRef]
77. Aoyama, Y.; Marleau, G.D.; Mordasini, C.; Ikoma, M. Spectral appearance of the planetary-surface accretion shock: Global spectra and hydrogen-line profiles and fluxes. *arXiv* **2020**, arXiv:2011.06608. [CrossRef]

78. Aoyama, Y.; Ikoma, M.; Tanigawa, T. Theoretical Model of Hydrogen Line Emission from Accreting Gas Giants. *Astrophys. J.* **2018**, *866*, 84. [CrossRef]
79. Rigliaco, E.; Natta, A.; Testi, L.; Randich, S.; Alcalà, J.M.; Covino, E.; Stelzer, B. X-shooter spectroscopy of young stellar objects. I. Mass accretion rates ofow-mass T Tauri stars in σ Orionis. *Astron. Astrophys.* **2012**, *548*, A56. [CrossRef]
80. Marleau, G.D.; Aoyama, Y.; Kuiper, R.; Follette, K.; Turner, N.J.; Cugno, G.; Manara, C.F.; Haffert, S.Y.; Kitzmann, D.; Ringqvist, S.C.; et al. Accreting protoplanets: Spectral signatures and magnitude of gas and dust extinction at H α. *Astron. Astrophys.* **2022**, *657*, A38. [CrossRef]
81. Pinte, C.; Teague, R.; Flaherty, K.; Hall, C.; Facchini, S.; Casassus, S. Kinematic Structures in Planet-Forming Disks. *arXiv* **2022**, arXiv:2203.09528. [CrossRef]
82. Terry, J.P.; Hall, C.; Abreau, S.; Gleyzer, S. Kinematic Evidence of an Embedded Protoplanet in HD 142666 Identified by Machine Learning. *Astrophys. J.* **2023**, *947*, 60. [CrossRef]
83. Stadler, J.; Benisty, M.; Izquierdo, A.; Facchini, S.; Teague, R.; Kurtovic, N.; Pinilla, P.; Bae, J.; Ansdell, M.; Loomis, R.; et al. A kinematically detected planet candidate in a transition disk. *Astron. Astrophys.* **2023**, *670*, L1. [CrossRef]
84. Macintosh, B.; Graham, J.R.; Ingraham, P.; Konopacky, Q.; Marois, C.; Perrin, M.; Poyneer, L.; Bauman, B.; Barman, T.; Burrows, A.S.; et al. Firstight of the Gemini Planet Imager. *Proc. Natl. Acad. Sci. USA* **2014**, *111*, 12661–12666. [CrossRef] [PubMed]
85. Chilcote, J.; Konopacky, Q.; Hamper, R.; Macintosh, B.; Marois, C.; Savransky, D.; Soummer, R.; Veran, J.P.; Gemini Planet Imager 2. 0. GPI 2.0: Upgrade of the Gemini Planet Imager. In Proceedings of the AAS/Division for Extreme Solar Systems, Christchurch, New Zealand, 16–21 March 2024; AAS/Division for Extreme Solar Systems Abstracts; America Astronomical Society, Washington, DC, USA, 2024; Volume 56, p. 628.07.
86. Claudi, R.U.; Turatto, M.; Gratton, R.G.; Antichi, J.; Bonavita, M.; Bruno, P.; Cascone, E.; De Caprio, V.; Desidera, S.; Giro, E.; et al. SPHERE IFS: The spectro differential imager of the VLT for exoplanets search. In Proceedings of the Ground-Based and Airborne Instrumentation for Astronomy II, Marseille, France, 23–28 June 2008; Society of Photo-Optical Instrumentation Engineers (SPIE) Conference Series; McLean, I.S., Casali, M.M., Eds., Society of Photo-Optical Instrumentation Engineers (SPIE): Bellingham, WA, USA, 2008; Volume 7014, p. 70143E. [CrossRef]
87. Dohlen, K.; Langlois, M.; Saisse, M.; Hill, L.; Origne, A.; Jacquet, M.; Fabron, C.; Blanc, J.C.; Llored, M.; Carle, M.; et al. The infrared dual imaging and spectrograph for SPHERE: Design and performance. In Proceedings of the Ground-Based and Airborne Instrumentation for Astronomy II, Marseille, France, 23–28 June 2008; Society of Photo-Optical Instrumentation Engineers (SPIE) Conference Series; McLean, I.S., Casali, M.M., Eds.; Society of Photo-Optical Instrumentation Engineers (SPIE: Bellingham, WA, USA, 2008; Volume 7014, p. 70143L. [CrossRef]
88. Vigan, A.; Moutou, C.; Langlois, M.; Allard, F.; Boccaletti, A.; Carbillet, M.; Mouillet, D.; Smith, I. Photometric characterization of exoplanets using angular and spectral differential imaging. *Mon. Not. R. Astron. Soc.* **2010**, *407*, 71–82. [CrossRef]
89. de Boer, J.; Langlois, M.; van Holstein, R.G.; Girard, J.H.; Mouillet, D.; Vigan, A.; Dohlen, K.; Snik, F.; Keller, C.U.; Ginski, C.; et al. Polarimetric imaging mode of VLT/SPHERE/IRDIS. I. Description, data reduction, and observing strategy. *Astron. Astrophys.* **2020**, *633*, A63. [CrossRef]
90. van Holstein, R.G.; Girard, J.H.; de Boer, J.; Snik, F.; Milli, J.; Stam, D.M.; Ginski, C.; Mouillet, D.; Wahhaj, Z.; Schmid, H.M.; et al. Polarimetric imaging mode of VLT/SPHERE/IRDIS. II. Characterization and correction of instrumental polarization effects. *Astron. Astrophys.* **2020**, *633*, A64. [CrossRef]
91. Vigan, A.; Langlois, M.; Moutou, C.; Dohlen, K. Exoplanet characterization withong slit spectroscopy. *Astron. Astrophys.* **2008**, *489*, 1345–1354. [CrossRef]
92. Fusco, T.; Rousset, G.; Sauvage, J.F.; Petit, C.; Beuzit, J.L.; Dohlen, K.; Mouillet, D.; Charton, J.; Nicolle, M.; Kasper, M.; et al. High-order adaptive optics requirements for direct detection of extrasolar planets: Application to the SPHERE instrument. *Opt. Express* **2006**, *14*, 7515. [CrossRef] [PubMed]
93. Fusco, T.; Sauvage, J.F.; Petit, C.; Costille, A.; Dohlen, K.; Mouillet, D.; Beuzit, J.L.; Kasper, M.; Suarez, M.; Soenke, C.; et al. Final performance andesson-learned of SAXO, the VLT-SPHERE extreme AO: From early design to on-sky results. In Proceedings of the Adaptive Optics Systems IV, Montréal, QC, Canada, 22–27 June 2014; Society of Photo-Optical Instrumentation Engineers (SPIE) Conference Series; Marchetti, E., Close, L.M., Vran, J.P., Eds.; Society of Photo-Optical Instrumentation Engineers (SPIE): Bellingham, WA, USA, 2014; Volume 9148, p. 91481U. [CrossRef]
94. Boccaletti, A.; Chauvin, G.; Wildi, F.; Milli, J.; Stadler, E.; Diolaiti, E.; Gratton, R.; Vidal, F.; Loupias, M.; Langlois, M.; et al. Upgrading the high contrast imaging facility SPHERE: Science drivers and instrument choices. In Proceedings of the Ground-Based and Airborne Instrumentation for Astronomy IX, Montréal, QC, Canada, 17–23 July 2022; Society of Photo-Optical Instrumentation Engineers (SPIE) Conference Series; Evans, C.J., Bryant, J.J., Motohara, K., Eds.; Society of Photo-Optical Instrumentation Engineers (SPIE): Bellingham, WA, USA, 2022; Volume 12184, p. 121841S. [CrossRef]

95. Gratton, R.; Keller, C.; Diolaiti, E.; Baruffolo, A.; Bonnefoy, M.; D'Orazi, V.; Langlois, M.; Loupias, M.; N'Diaye, M.; Pantin, E.; et al. MedRes: A new MEDium RESolution integral field spectrograph for SPHERE. In Proceedings of the Ground-Based and Airborne Instrumentation for Astronomy IX, Montréal, QC, Canada, 17–23 July 2022; Society of Photo-Optical Instrumentation Engineers (SPIE) Conference Series; Evans, C.J., Bryant, J.J., Motohara, K., Eds.; Society of Photo-Optical Instrumentation Engineers (SPIE): Bellingham, WA, USA, 2022; Volume 12184, p. 121844F. [CrossRef]
96. Wang, J.J.; Mawet, D.; Xuan, J.W.; Hsu, C.C.; Ruffio, J.B.; Horstman, K.; Xin, Y.; Delorme, J.R.; Jovanovic, N.; Zhang, Y.; et al. The high-contrast performance of the Keck Planet Imager and Characterizer. *arXiv* **2024**, arXiv:2406.15028. [CrossRef]
97. Davies, R.; Absil, O.; Agapito, G.; Agudo Berbel, A.; Baruffolo, A.; Biliotti, V.; Black, M.; Bonaglia, M.; Bonse, M.; Briguglio, R.; et al. The Enhanced Resolution Imager and Spectrograph for the VLT. *Astron. Astrophys.* **2023**, *674*, A207. [CrossRef]
98. Pearson, D.; Taylor, W.; Davies, R.; MacIntosh, M.; Henry, D.; Lunney, D.; Waring, C.; Gao, X.; Lightfoot, J.; Glauser, A.M.; et al. NIX, the imager for ERIS: The AO instrument for the VLT. In Proceedings of the Ground-Based and Airborne Instrumentation for Astronomy VI, Edinburgh, UK, 26 June–1 July 2016; Society of Photo-Optical Instrumentation Engineers (SPIE) Conference Series; Evans, C.J., Simard, L., Takami, H., Eds.; Society of Photo-Optical Instrumentation Engineers (SPIE): Bellingham, WA, USA, 2016; Volume 9908, p. 99083F. [CrossRef]
99. Riccardi, A.; Puglisi, A.; Grani, P.; Briguglio, R.; Esposito, S.; Agapito, G.; Biliotti, V.; Bonaglia, M.; Carbonaro, L.; Xompero, M.; et al. The ERIS Adaptive Optics System: First on-sky results of the ongoing commissioning at the VLT-UT4. In Proceedings of the Adaptive Optics Systems VIII, Montréal, QC, Canada, 17–23 July 2022; Schreiber, L., Schmidt, D., Vernet, E., Eds.; International Society for Optics and Photonics, SPIE; Society of Photo-Optical Instrumentation Engineers (SPIE): Bellingham, WA, USA, 2022; Volume 12185, p. 1218508. [CrossRef]
100. Martinache, F.; Guyon, O. The Subaru Coronagraphic Extreme-AO Project. In Proceedings of the Techniques and Instrumentation for Detection of Exoplanets IV, San Diego, CA, USA, 4–5 August 2009; Society of Photo-Optical Instrumentation Engineers (SPIE) Conference Series; Shaklan, S.B., Ed.; Society of Photo-Optical Instrumentation Engineers (SPIE): Bellingham, WA, USA, 2009; Volume 7440, p. 74400O. [CrossRef]
101. Jovanovic, N.; Martinache, F.; Guyon, O.; Clergeon, C.; Singh, G.; Kudo, T.; Garrel, V.; Newman, K.; Doughty, D.; Lozi, J.; et al. The Subaru Coronagraphic Extreme Adaptive Optics System: Enabling High-Contrast Imaging on Solar-System Scales. *Pub. Astron. Soc. Pac.* **2015**, *127*, 890. [CrossRef]
102. Groff, T.D.; Kasdin, N.J.; Limbach, M.A.; Galvin, M.; Carr, M.A.; Knapp, G.; Brandt, T.; Loomis, C.; Jarosik, N.; Mede, K.; et al. The CHARIS IFS for high contrast imaging at Subaru. In Proceedings of the Techniques and Instrumentation for Detection of Exoplanets VII, San Diego, CA, USA, 10–13 August 2015; Society of Photo-Optical Instrumentation Engineers (SPIE) Conference Series; Shaklan, S., Ed.; Society of Photo-Optical Instrumentation Engineers (SPIE): Bellingham, WA, USA, 2015; Volume 9605, p. 96051C. [CrossRef]
103. Norris, B.R.M.; Tuthill, P.G.; Jovanovic, N.; Schworer, G.; Guyon, O.; Martinache, F.; Stewart, P.N. VAMPIRES: Probing the innermost regions of protoplanetary systems with polarimetric aperture-masking. In Proceedings of the Optical and Infrared Interferometry IV, Montréal, QC, Canada, 22–27 June 2014; Society of Photo-Optical Instrumentation Engineers (SPIE) Conference Series; Rajagopal, J.K., Creech-Eakman, M.J., Malbet, F., Eds.; Society of Photo-Optical Instrumentation Engineers (SPIE): Bellingham, WA, USA, 2014; Volume 9146, p. 91460U. [CrossRef]
104. Mattioli, M.; Pedichini, F.; Antoniucci, S.; Li Causi, G.; Piazzesi, R.; Stangalini, M.; Testa, V. SHARK-VIS the LBT high contrast imager at visible wavelengths. In Proceedings of the Ground-based and Airborne Instrumentation for Astronomy VII, Austin, TX, USA, 10–15 June 2018; Society of Photo-Optical Instrumentation Engineers (SPIE) Conference Series; Evans, C.J., Simard, L., Takami, H., Eds.; Society of Photo-Optical Instrumentation Engineers (SPIE): Bellingham, WA, USA, 2018; Volume 10702, p. 107024F. [CrossRef]
105. Pedichini, F.; Stangalini, M.; Ambrosino, F.; Puglisi, A.; Pinna, E.; Bailey, V.; Carbonaro, L.; Centrone, M.; Christou, J.; Esposito, S.; et al. High Contrast Imaging in the Visible: First Experimental Results at the Large Binocular Telescope. *Astron. J.* **2017**, *154*, 74. [CrossRef]
106. Li Causi, G.; Stangalini, M.; Antoniucci, S.; Pedichini, F.; Mattioli, M.; Testa, V.; Piazzesi, R. Fast cadence speckle-free high-contrast imaging: SFADI and SFI. In Proceedings of the Adaptive Optics Systems VI, Austin, TX, USA, 10–15 June 2018; Society of Photo-Optical Instrumentation Engineers (SPIE) Conference Series; Close, L.M., Schreiber, L., Schmidt, D., Eds.; Society of Photo-Optical Instrumentation Engineers (SPIE): Bellingham, WA, USA, 2018; Volume 10703, p. 107032U. [CrossRef]
107. Farinato, J.; Baruffolo, A.; Bergomi, M.; Bianco, A.; Biondi, F.; Briegel, F.; Carolo, E.; Carlotti, A.; Chavan, S.; Chinellato, S.; et al. SHARK-NIR, ready to "swim" in the LBT Northern Hemisphere "ocean". In Proceedings of the Adaptive Optics Systems VIII, Montréal, QC, Canada, 17–23 July 2022; Society of Photo-Optical Instrumentation Engineers (SPIE) Conference Series; Schreiber, L., Schmidt, D., Vernet, E., Eds.; Society of Photo-Optical Instrumentation Engineers (SPIE): Bellingham, WA, USA, 2022; Volume 12185, p. 1218522. [CrossRef]
108. Pinna, E.; Rossi, F.; Puglisi, A.; Agapito, G.; Bonaglia, M.; Plantet, C.; Mazzoni, T.; Briguglio, R.; Carbonaro, L.; Xompero, M.; et al. Bringing SOUL on sky. *arXiv* **2021**, arXiv:2101.07091. [CrossRef]

109. Males, J.R.; Close, L.M.; Guyon, O.; Hedglen, A.D.; Van Gorkom, K.; Long, J.D.; Kautz, M.; Lumbres, J.; Schatz, L.; Rodack, A.; et al. MagAO-X firstight. In Proceedings of the Adaptive Optics Systems VII, Online, 14–18 December 2020; Society of Photo-Optical Instrumentation Engineers (SPIE) Conference Series; Schreiber, L., Schmidt, D., Vernet, E., Eds.; Society of Photo-Optical Instrumentation Engineers (SPIE): Bellingham, WA, USA, 2020; Volume 11448, p. 114484L. [CrossRef]
110. Close, L.M.; Males, J.R.; Durney, O.; Sauve, C.; Kautz, M.; Hedglen, A.; Schatz, L.; Lumbres, J.; Miller, K.; Van Gorkom, K.; et al. Optical and mechanical design of the extreme AO coronagraphic instrument MagAO-X. In Proceedings of the Adaptive Optics Systems VI, Austin, TX, USA, 10–15 June 2018; Society of Photo-Optical Instrumentation Engineers (SPIE) Conference Series; Close, L.M., Schreiber, L., Schmidt, D., Eds.; Society of Photo-Optical Instrumentation Engineers (SPIE): Bellingham, WA, USA, 2018; Volume 10703, p. 107034Y, [CrossRef]
111. Close, L.M. The Separation and Hα Contrasts of Massive Accreting Planets in the Gaps of Transitional Disks: Predicted Hα Protoplanet Yields for Adaptive Optics Surveys. *Astron. J.* **2020**, *160*, 221. [CrossRef]
112. Krist, J.E. High-contrast imaging with the Hubble Space Telescope: Performance andessonsearned. In Proceedings of the Optical, Infrared, and Millimeter Space Telescopes, Glasgow, UK, 21–25 June 2004; Society of Photo-Optical Instrumentation Engineers (SPIE) Conference Series; Mather, J.C., Ed.; Society of Photo-Optical Instrumentation Engineers (SPIE): Bellingham, WA, USA, 2004; Volume 5487, pp. 1284–1295. [CrossRef]
113. Lowrance, P.J.; Becklin, E.E.; Schneider, G.; Kirkpatrick, J.D.; Weinberger, A.J.; Zuckerman, B.; Dumas, C.; Beuzit, J.L.; Plait, P.; Malumuth, E.; et al. An Infrared Coronagraphic Survey for Substellar Companions. *Astron. J.* **2005**, *130*, 1845–1861. [CrossRef]
114. Cugno, G.; Zhou, Y.; Thanathibodee, T.; Calissendorff, P.; Meyer, M.R.; Edwards, S.; Bae, J.; Benisty, M.; Bergin, E.; De Furio, M.; et al. MagAO-X and HST High-contrast Imaging of the AS209 Disk at Hα. *Astron. J.* **2023**, *166*, 162. [CrossRef]
115. Krist, J.E.; Balasubramanian, K.; Muller, R.E.; Shaklan, S.B.; Kelly, D.M.; Wilson, D.W.; Beichman, C.A.; Serabyn, E.; Mao, Y.; Echternach, P.M.; et al. The JWST/NIRCam coronagraph flight occulters. In Proceedings of the Space Telescopes and Instrumentation 2010: Optical, Infrared, and Millimeter Wave, San Diego, CA, USA, 27 June–2 July 2010; Society of Photo-Optical Instrumentation Engineers (SPIE) Conference Series; Oschmann Jacobus, M.J., Clampin, M.C., MacEwen, H.A., Eds.; Society of Photo-Optical Instrumentation Engineers (SPIE): Bellingham, WA, USA, 2010; Volume 7731, p. 77313J. [CrossRef]
116. Sivaramakrishnan, A.; Tuthill, P.; Lloyd, J.P.; Greenbaum, A.Z.; Thatte, D.; Cooper, R.A.; Vandal, T.; Kammerer, J.; Sanchez-Bermudez, J.; Pope, B.J.S.; et al. The Near Infrared Imager and Slitless Spectrograph for the James Webb Space Telescope. IV. Aperture Masking Interferometry. *Pub. Astron. Soc. Pac.* **2023**, *135*, 015003. [CrossRef]
117. Boccaletti, A.; Lagage, P.O.; Baudoz, P.; Beichman, C.; Bouchet, P.; Cavarroc, C.; Dubreuil, D.; Glasse, A.; Glauser, A.M.; Hines, D.C.; et al. The Mid-Infrared Instrument for the James Webb Space Telescope, V: Predicted Performance of the MIRI Coronagraphs. *Pub. Astron. Soc. Pac.* **2015**, *127*, 633. [CrossRef]
118. Packham, C.; Honda, M.; Chun, M.; Sakon, I.; Richter, M.; Okamoto, Y.; Kataza, H.; Marois, C.; Meyer, M.; Puravankara, M.; et al. The key science drivers for MICHI: A thermal-infrared instrument for the TMT. In Proceedings of the Ground-Based and Airborne Instrumentation for Astronomy VII, Online, 14–18 December 2020; Society of Photo-Optical Instrumentation Engineers (SPIE) Conference Series; Evans, C.J., Simard, L., Takami, H., Eds.; Society of Photo-Optical Instrumentation Engineers (SPIE): Bellingham, WA, USA, 2018; Volume 10702, p. 10702A0. [CrossRef]
119. Jensen-Clem, R.; Hinz, P.; von Kooten, M.; Fitzgerald, M.P.; Sallum, S.; Mazin, B.; Chun, M.; Max, C.; Millar-Blanchaer, M.; Guyon, O.; et al. The Planetary Systems Imager adaptive optics system: An initial optical design and performance analysis tool for the PSI-Red AO system. In Proceedings of the Techniques and Instrumentation for Detection of Exoplanets X, San Diego, CA, USA, 1–5 August 2021; Society of Photo-Optical Instrumentation Engineers (SPIE) Conference Series; Shaklan, S.B., Ruane, G.J., Eds., Society of Photo-Optical Instrumentation Engineers (SPIE): Bellingham, WA, USA, 2021; Volume 11823, p. 1182309. [CrossRef]
120. Serra, B.; Ives, D.J.; Accardo, M.; Conzelmann, R.D.; Leveratto, S.; Mueller, E.; George, E.M.; Bezawada, N.N.; Alvarez, D.; Sedghi, B.; et al. METIS firstight imager and spectrograph for the ELT: Overview of the near and mid-infrared detector subsystems. In Proceedings of the X-Ray, Optical, and Infrared Detectors for Astronomy XI, Yokohama, Japan, 16–22 June 2024; Society of Photo-Optical Instrumentation Engineers (SPIE) Conference Series; Holland, A.D., Minoglou, K., Eds.; Society of Photo-Optical Instrumentation Engineers (SPIE): Bellingham, WA, USA, 2024; Volume 13103, p. 131031U. [CrossRef]
121. Thatte, N.A.; Melotte, D.; Neichel, B.; Le Mignant, D.; Rees, P.; Clarke, F.; Ferraro-Wood, V.; Gonzalez, O.; Jones, M.; Álvarez Urueña, A.; et al. HARMONI at ELT: Project status and instrument overview. In Proceedings of the Ground-Based and Airborne Instrumentation for Astronomy X, 17-23 July 2022 in Montréal, Québec, Canada Society of Photo-Optical Instrumentation Engineers (SPIE) Conference Series; Bryant, J.J., Motohara, K., Vernet, J.R.D., Eds.; Society of Photo-Optical Instrumentation Engineers (SPIE): Bellingham, WA, USA, 2024; Volume 13096, p. 1309614. [CrossRef]
122. Kasper, M.; Cerpa Urra, N.; Pathak, P.; Bonse, M.; Nousiainen, J.; Engler, B.; Heritier, C.T.; Kammerer, J.; Leveratto, S.; Rajani, C.; et al. PCS—A Roadmap for Exoearth Imaging with the ELT. *Messenger* **2021**, *182*, 38–43. [CrossRef]
123. Spergel, D.; Gehrels, N.; Breckinridge, J.; Donahue, M.; Dressler, A.; Gaudi, B.S.; Greene, T.; Guyon, O.; Hirata, C.; Kalirai, J.; et al. WFIRST-2.4: What Every Astronomer Should Know. *arXiv* **2013**, arXiv:1305.5425. [CrossRef]

124. Lafrenière, D.; Marois, C.; Doyon, R.; Nadeau, D.; Artigau, É. A New Algorithm for Point-Spread Function Subtraction in High-Contrast Imaging: A Demonstration with Angular Differential Imaging. *Astrophys. J.* **2007**, *660*, 770–780. [CrossRef]
125. Marois, C.; Correia, C.; Véran, J.P.; Currie, T. TLOCI: A Fully Loaded Speckle Killing Machine. In Proceedings of the Exploring the Formation and Evolution of Planetary Systems, 2 June 2013 in Victoria, Canada Booth, M., Matthews, B.C., Graham, J.R., Eds.; Cambridge University Press, Cambridge, England 2014; Volume 299, pp. 48–49. [CrossRef]
126. Wahhaj, Z.; Cieza, L.A.; Mawet, D.; Yang, B.; Canovas, H.; de Boer, J.; Casassus, S.; Ménard, F.; Schreiber, M.R.; Liu, M.C.; et al. Improving signal-to-noise in the direct imaging of exoplanets and circumstellar disks with MLOCI. *Astron. Astrophys.* **2015**, *581*, A24. [CrossRef]
127. Soummer, R.; Pueyo, L.; Larkin, J. Detection and Characterization of Exoplanets and Disks Using Projections on Karhunen-Loève Eigenimages. *Astrophys. J. Lett.* **2012**, *755*, L28. [CrossRef]
128. Amara, A.; Quanz, S.P. PYNPOINT: An image processing package for finding exoplanets. *Mon. Not. R. Astron. Soc.* **2012**, *427*, 948–955. [CrossRef]
129. Mesa, D.; Gratton, R.; Zurlo, A.; Vigan, A.; Claudi, R.U.; Alberi, M.; Antichi, J.; Baruffolo, A.; Beuzit, J.L.; Boccaletti, A.; et al. Performance of the VLT Planet Finder SPHERE. II. Data analysis and results for IFS inaboratory. *Astron. Astrophys.* **2015**, *576*, A121. [CrossRef]
130. Galicher, R.; Boccaletti, A.; Mesa, D.; Delorme, P.; Gratton, R.; Langlois, M.; Lagrange, A.M.; Maire, A.L.; Le Coroller, H.; Chauvin, G.; et al. Astrometric and photometric accuracies in high contrast imaging: The SPHERE speckle calibration tool (SpeCal). *Astron. Astrophys.* **2018**, *615*, A92. [CrossRef]
131. Gomez Gonzalez, C.A.; Wertz, O.; Absil, O.; Christiaens, V.; Defrère, D.; Mawet, D.; Milli, J.; Absil, P.A.; Van Droogenbroeck, M.; Cantalloube, F.; et al. VIP: Vortex Image Processing Package for High-contrast Direct Imaging. *Astron. J.* **2017**, *154*, 7. [CrossRef]
132. Flasseur, O.; Denis, L.; Thiébaut, É.; Langlois, M. Exoplanet detection in angular differential imaging by statistical earning of the nonstationary patch covariances. The PACO algorithm. *Astron. Astrophys.* **2018**, *618*, A138. [CrossRef]
133. Flasseur, O.; Denis, L.; Thiébaut, É.; Langlois, M. PACO ASDI: An algorithm for exoplanet detection and characterization in direct imaging with integral field spectrographs. *Astron. Astrophys.* **2020**, *637*, A9. [CrossRef]
134. Flasseur, O.; Thé, S.; Denis, L.; Thiébaut, É.; Langlois, M. REXPACO: An algorithm for high contrast reconstruction of the circumstellar environment by angular differential imaging. *Astron. Astrophys.* **2021**, *651*, A62. [CrossRef]
135. Flasseur, O.; Bodrito, T.; Mairal, J.; Ponce, J.; Langlois, M.; Lagrange, A.M. deep PACO: Combining statistical models with deepearning for exoplanet detection and characterization in direct imaging at high contrast. *arXiv* **2023**, arXiv:2303.02461. [CrossRef]
136. Cantalloube, F.; Mouillet, D.; Mugnier, L.M.; Milli, J.; Absil, O.; Gomez Gonzalez, C.A.; Chauvin, G.; Beuzit, J.L.; Cornia, A. Direct exoplanet detection and characterization using the ANDROMEDA method: Performance on VLT/NaCo data. *Astron. Astrophys.* **2015**, *582*, A89. [CrossRef]
137. Ruffio, J.B.; Macintosh, B.; Wang, J.J.; Pueyo, L.; Nielsen, E.L.; De Rosa, R.J.; Czekala, I.; Marley, M.S.; Arriaga, P.; Bailey, V.P.; et al. Improving and Assessing Planet Sensitivity of the GPI Exoplanet Survey with a Forward Model Matched Filter. *Astrophys. J.* **2017**, *842*, 14. [CrossRef]
138. Dahlqvist, C.H.; Cantalloube, F.; Absil, O. Regime-switching model detection map for direct exoplanet detection in ADI sequences. *Astron. Astrophys.* **2020**, *633*, A95. [CrossRef]
139. Dahlqvist, C.H.; Louppe, G.; Absil, O. Improving the RSM map exoplanet detection algorithm. PSF forward modelling and optimal selection of PSF subtraction techniques. *Astron. Astrophys.* **2021**, *646*, A49. [CrossRef]
140. Dahlqvist, C.H.; Cantalloube, F.; Absil, O. Auto-RSM: An automated parameter-selection algorithm for the RSM map exoplanet detection algorithm. *Astron. Astrophys.* **2021**, *656*, A54. [CrossRef]
141. Pairet, B.; Cantalloube, F.; Gomez Gonzalez, C.A.; Absil, O.; Jacques, L. STIM map: Detection map for exoplanets imaging beyond asymptotic Gaussian residual speckle noise. *Mon. Not. R. Astron. Soc.* **2019**, *487*, 2262–2277. [CrossRef]
142. Pairet, B.; Cantalloube, F.; Jacques, L. MAYONNAISE: A morphological components analysis pipeline for circumstellar discs and exoplanets imaging in the near-infrared. *Mon. Not. R. Astron. Soc.* **2021**, *503*, 3724–3742. [CrossRef]
143. Samland, M.; Bouwman, J.; Hogg, D.W.; Brandner, W.; Henning, T.; Janson, M. TRAP: A temporal systematics model for improved direct detection of exoplanets at small angular separations. *Astron. Astrophys.* **2021**, *646*, A24. [CrossRef]
144. Nakajima, T.; Oppenheimer, B.R.; Kulkarni, S.R.; Golimowski, D.A.; Matthews, K.; Durrance, S.T. Discovery of a cool brown dwarf. *Nature* **1995**, *378*, 463–465. [CrossRef]
145. Xuan, J.W.; Mérand, A.; Thompson, W.; Zhang, Y.; Lacour, S.; Blakely, D.; Mawet, D.; Oppenheimer, R.; Kammerer, J.; Batygin, K.; et al. The cool brown dwarf Gliese 229 B is a close binary. *arXiv* **2024**, arXiv:2410.11953. [CrossRef]
146. Low, C.; Lynden-Bell, D. The minimum Jeans mass or when fragmentation must stop. *Mon. Not. R. Astron. Soc.* **1976**, *176*, 367–390. [CrossRef]
147. Silk, J. On the fragmentation of cosmic gas clouds. II. Opacity-limited star formation. *Astrophys. J.* **1977**, *214*, 152–160. [CrossRef]

148. Boss, A.P. Formation of Planetary-Mass Objects by Protostellar Collapse and Fragmentation. *Astrophys. J. Lett.* **2001**, *551*, L167–L170. [CrossRef]
149. Bate, M.R. Stellar, brown dwarf and multiple star properties from hydrodynamical simulations of star cluster formation. *Mon. Not. R. Astron. Soc.* **2009**, *392*, 590–616. [CrossRef]
150. Todorov, K.; Luhman, K.L.; McLeod, K.K. Discovery of a Planetary-mass Companion to a Brown Dwarf in Taurus. *Astrophys. J. Lett.* **2010**, *714*, L84–L88. [CrossRef]
151. Liu, M.C.; Magnier, E.A.; Deacon, N.R.; Allers, K.N.; Dupuy, T.J.; Kotson, M.C.; Aller, K.M.; Burgett, W.S.; Chambers, K.C.; Draper, P.W.; et al. The Extremely Red, Young L Dwarf PSO J318.5338-22.8603: A Free-floating Planetary-mass Analog to Directly Imaged Young Gas-giant Planets. *Astrophys. J. Lett.* **2013**, *777*, L20. [CrossRef]
152. Quirrenbach, A.; Trifonov, T.; Lee, M.H.; Reffert, S. Precise radial velocities of giant stars. XI. Two brown dwarfs in 6:1 mean motion resonance around the K giant star ν Ophiuchi. *Astron. Astrophys.* **2019**, *624*, A18. [CrossRef]
153. Grether, D.; Lineweaver, C.H. How Dry is the Brown Dwarf Desert? Quantifying the Relative Number of Planets, Brown Dwarfs, and Stellar Companions around Nearby Sun-like Stars. *Astrophys. J.* **2006**, *640*, 1051–1062. [CrossRef]
154. Dodson-Robinson, S.E.; Salyk, C. Transitional Disks as Signposts of Young, Multiplanet Systems. *Astrophys. J.* **2011**, *738*, 131. [CrossRef]
155. Espaillat, C.; Muzerolle, J.; Najita, J.; Andrews, S.; Zhu, Z.; Calvet, N.; Kraus, S.; Hashimoto, J.; Kraus, A.; D'Alessio, P. An Observational Perspective of Transitional Disks. In Proceedings of the Protostars and Planets VI, Heidelberg, Germany, 14–20 July 2013; Beuther, H., Klessen, R.S., Dullemond, C.P., Henning, T., Eds.; University of Arizona Press: Tucson, AZ, USA, 2014; pp. 497–520. [CrossRef]
156. Owen, J.E. The Origin and Evolution of Transition Discs: Successes, Problems, and Open Questions. *Pub. Astron. Soc. Aust.* **2016**, *33*, e005. [CrossRef]
157. Biller, B.; Lacour, S.; Juhász, A.; Benisty, M.; Chauvin, G.; Olofsson, J.; Pott, J.U.; Müller, A.; Sicilia-Aguilar, A.; Bonnefoy, M.; et al. A Likely Close-in Low-mass Stellar Companion to the Transitional Disk Star HD 142527. *Astrophys. J. Lett.* **2012**, *753*, L38. [CrossRef]
158. Close, L.M.; Follette, K.B.; Males, J.R.; Puglisi, A.; Xompero, M.; Apai, D.; Najita, J.; Weinberger, A.J.; Morzinski, K.; Rodigas, T.J.; et al. Discovery of Hα Emission from the Close Companion inside the Gap of Transitional Disk HD 142527. *Astrophys. J. Lett.* **2014**, *781*, L30. [CrossRef]
159. Rodigas, T.J.; Follette, K.B.; Weinberger, A.; Close, L.; Hines, D.C. Polarized Light Imaging of the HD 142527 Transition Disk with the Gemini Planet Imager: Dust around the Close-in Companion. *Astrophys. J. Lett.* **2014**, *791*, L37. [CrossRef]
160. Lacour, S.; Biller, B.; Cheetham, A.; Greenbaum, A.; Pearce, T.; Marino, S.; Tuthill, P.; Pueyo, L.; Mamajek, E.E.; Girard, J.H.; et al. An M-dwarf star in the transition disk of Herbig HD 142527. Physical parameters and orbital elements. *Astron. Astrophys.* **2016**, *590*, A90. [CrossRef]
161. Claudi, R.; Maire, A.L.; Mesa, D.; Cheetham, A.; Fontanive, C.; Gratton, R.; Zurlo, A.; Avenhaus, H.; Bhowmik, T.; Biller, B.; et al. SPHERE dynamical and spectroscopic characterization of HD 142527B. *Astron. Astrophys.* **2019**, *622*, A96. [CrossRef]
162. Quanz, S.P.; Amara, A.; Meyer, M.R.; Girard, J.H.; Kenworthy, M.A.; Kasper, M. Confirmation and Characterization of the Protoplanet HD 100546 b—Direct Evidence for Gas Giant Planet Formation at 50 AU. *Astrophys. J.* **2015**, *807*, 64. [CrossRef]
163. Currie, T.; Cloutier, R.; Brittain, S.; Grady, C.; Burrows, A.; Muto, T.; Kenyon, S.J.; Kuchner, M.J. Resolving the HD 100546 Protoplanetary System with the Gemini Planet Imager: Evidence for Multiple Forming, Accreting Planets. *Astrophys. J. Lett.* **2015**, *814*, L27. [CrossRef]
164. Garufi, A.; Quanz, S.P.; Schmid, H.M.; Mulders, G.D.; Avenhaus, H.; Boccaletti, A.; Ginski, C.; Langlois, M.; Stolker, T.; Augereau, J.C.; et al. The SPHERE view of the planet-forming disk around HD 100546. *Astron. Astrophys.* **2016**, *588*, A8. [CrossRef]
165. Sissa, E.; Gratton, R.; Garufi, A.; Rigliaco, E.; Zurlo, A.; Mesa, D.; Langlois, M.; de Boer, J.; Desidera, S.; Ginski, C.; et al. High-contrast study of the candidate planets and protoplanetary disk around HD 100546. *Astron. Astrophys.* **2018**, *619*, A160. [CrossRef]
166. Nielsen, E.L.; De Rosa, R.J.; Macintosh, B.; Wang, J.J.; Ruffio, J.B.; Chiang, E.; Marley, M.S.; Saumon, D.; Savransky, D.; Ammons, S.M.; et al. The Gemini Planet Imager Exoplanet Survey: Giant Planet and Brown Dwarf Demographics from 10 to 100 au. *Astron. J.* **2019**, *158*, 13. [CrossRef]
167. Chauvin, G.; Desidera, S.; Lagrange, A.M.; Vigan, A.; Feldt, M.; Gratton, R.; Langlois, M.; Cheetham, A.; Bonnefoy, M.; Meyer, M. SHINE, The SpHere INfrared survey for Exoplanets. In Proceedings of the SF2A-2017: Proceedings of the Annual Meeting of the French Society of Astronomy and Astrophysics, Paris, France, 4–7 July 2017; Reylé, C., Di Matteo, P., Herpin, F., Lagadec, E., Lançon, A., Meliani, Z., Royer, F., Eds.; Société Française d'Astronomie et d'Astrophysique (SF2A): Paris, France, 2017; p. 331
168. Nowak, M.; Lacour, S.; Lagrange, A.M.; Rubini, P.; Wang, J.; Stolker, T.; Abuter, R.; Amorim, A.; Asensio-Torres, R.; Bauböck, M.; et al. Direct confirmation of the radial-velocity planet β Pictoris c. *Astron. Astrophys.* **2020**, *642*, L2. [CrossRef]
169. Brandt, T.D. The Hipparcos-Gaia Catalog of Accelerations: Gaia EDR3 Edition. *Astrophys. J. Suppl.* **2021**, *254*, 42. [CrossRef]

170. Kervella, P.; Arenou, F.; Thévenin, F. Stellar and substellar companions from Gaia EDR3. Proper-motion anomaly and resolved common proper-motion pairs. *Astron. Astrophys.* **2022**, *657*, A7. [CrossRef]
171. Bonavita, M.; Fontanive, C.; Gratton, R.; Mužić, K.; Desidera, S.; Mesa, D.; Biller, B.; Scholz, A.; Sozzetti, A.; Squicciarini, V. Results from The COPAINS Pilot Survey: Four new BDs and a high companion detection rate for accelerating stars. *Mon. Not. R. Astron. Soc.* **2022**, *513*, 5588–5605. [CrossRef]
172. Currie, T.; Marois, C.; Cieza, L.; Mulders, G.D.; Lawson, K.; Caceres, C.; Rodriguez-Ruiz, D.; Wisniewski, J.; Guyon, O.; Brandt, T.D.; et al. No Clear, Direct Evidence for Multiple Protoplanets Orbiting LkCa 15: LkCa 15 bcd are Likely Inner Disk Signals. *Astrophys. J. Lett.* **2019**, *877*, L3. [CrossRef]
173. Mugrauer, M.; Neuhäuser, R. GQ Lup and its common proper motion companion. *Astron. Nachrichten* **2005**, *326*, 701–708. [CrossRef]
174. Chauvin, G.; Lagrange, A.M.; Zuckerman, B.; Dumas, C.; Mouillet, D.; Song, I.; Beuzit, J.L.; Lowrance, P.; Bessell, M.S. A companion to AB Pic at the planet/brown dwarf boundary. *Astron. Astrophys.* **2005**, *438*, L29–L32. [CrossRef]
175. Marois, C.; Zuckerman, B.; Konopacky, Q.M.; Macintosh, B.; Barman, T. Images of a fourth planet orbiting HR 8799. *Nature* **2010**, *468*, 1080–1083. [CrossRef]
176. Lagrange, A.M.; Gratadour, D.; Chauvin, G.; Fusco, T.; Ehrenreich, D.; Mouillet, D.; Rousset, G.; Rouan, D.; Allard, F.; Gendron, É.; et al. A probable giant planet imaged in the β Pictoris disk. VLT/NaCo deep L′-band imaging. *Astron. Astrophys.* **2009**, *493*, L21–L25. [CrossRef]
177. Lagrange, A.M.; Meunier, N.; Rubini, P.; Keppler, M.; Galland, F.; Chapellier, E.; Michel, E.; Balona, L.; Beust, H.; Guillot, T.; et al. Evidence for an additional planet in the β Pictoris system. *Nat. Astron.* **2019**, *3*, 1135–1142. [CrossRef]
178. Dupuy, T.J.; Kraus, A.L. Distances, Luminosities, and Temperatures of the Coldest Known Substellar Objects. *Science* **2013**, *341*, 1492–1495. [CrossRef] [PubMed]
179. Goldman, B.; Marsat, S.; Henning, T.; Clemens, C.; Greiner, J. A new benchmark T8-9 brown dwarf and a couple of new mid-T dwarfs from the UKIDSS DR5+ LAS. *Mon. Not. R. Astron. Soc.* **2010**, *405*, 1140–1152. [CrossRef]
180. Scholz, R.D. Hip 63510C, Hip 73786B, and nine new isolated high proper motion T dwarf candidates from UKIDSS DR6 and SDSS DR7. *Astron. Astrophys.* **2010**, *515*, A92. [CrossRef]
181. Kraus, A.L.; Ireland, M.J. LkCa 15: A Young Exoplanet Caught at Formation? *Astrophys. J.* **2012**, *745*, 5. [CrossRef]
182. Sallum, S.; Follette, K.B.; Eisner, J.A.; Close, L.M.; Hinz, P.; Kratter, K.; Males, J.; Skemer, A.; Macintosh, B.; Tuthill, P.; et al. Accreting protoplanets in the LkCa 15 transition disk. *Nature* **2015**, *527*, 342–344. [CrossRef] [PubMed]
183. Faherty, J.K.; Rice, E.L.; Cruz, K.L.; Mamajek, E.E.; Núñez, A. 2MASS J035523.37+113343.7: A Young, Dusty, Nearby, Isolated Brown Dwarf Resembling a Giant Exoplanet. *Astron. J.* **2013**, *145*, 2. [CrossRef]
184. Deacon, N.R.; Schlieder, J.E.; Murphy, S.J. A nearby young M dwarf with a wide, possibly planetary-mass companion. *Mon. Not. R. Astron. Soc.* **2016**, *457*, 3191–3199. [CrossRef]
185. Chauvin, G.; Desidera, S.; Lagrange, A.M.; Vigan, A.; Gratton, R.; Langlois, M.; Bonnefoy, M.; Beuzit, J.L.; Feldt, M.; Mouillet, D.; et al. Discovery of a warm, dusty giant planet around HIP 65426. *Astron. Astrophys.* **2017**, *605*, L9. [CrossRef]
186. Carter, A.L.; Hinkley, S.; Kammerer, J.; Skemer, A.; Biller, B.A.; Leisenring, J.M.; Millar-Blanchaer, M.A.; Petrus, S.; Stone, J.M.; Ward-Duong, K.; et al. The JWST Early Release Science Program for Direct Observations of Exoplanetary Systems I: High-contrast Imaging of the Exoplanet HIP 65426 b from 2 to 16 μm. *Astrophys. J. Lett.* **2023**, *951*, L20. [CrossRef]
187. Müller, A.; Keppler, M.; Henning, T.; Samland, M.; Chauvin, G.; Beust, H.; Maire, A.L.; Molaverdikhani, K.; van Boekel, R.; Benisty, M.; et al. Orbital and atmospheric characterization of the planet within the gap of the PDS 70 transition disk. *Astron. Astrophys.* **2018**, *617*, L2. [CrossRef]
188. Keppler, M.; Benisty, M.; Müller, A.; Henning, T.; van Boekel, R.; Cantalloube, F.; Ginski, C.; van Holstein, R.G.; Maire, A.L.; Pohl, A.; et al. Discovery of a planetary-mass companion within the gap of the transition disk around PDS 70. *Astron. Astrophys.* **2018**, *617*, A44. [CrossRef]
189. Haffert, S.Y.; Bohn, A.J.; de Boer, J.; Snellen, I.A.G.; Brinchmann, J.; Girard, J.H.; Keller, C.U.; Bacon, R. Two accreting protoplanets around the young star PDS 70. *Nat. Astron.* **2019**, *3*, 749–754. [CrossRef]
190. Currie, T.; Brandt, G.M.; Brandt, T.D.; Lacy, B.; Burrows, A.; Guyon, O.; Tamura, M.; Liu, R.Y.; Sagynbayeva, S.; Tobin, T.; et al. Direct imaging and astrometric detection of a gas giant planet orbiting an accelerating star. *Science* **2023**, *380*, 198–203. [CrossRef] [PubMed]
191. Mesa, D.; Gratton, R.; Kervella, P.; Bonavita, M.; Desidera, S.; D'Orazi, V.; Marino, S.; Zurlo, A.; Rigliaco, E. AF Lep b: Theowest-mass planet detected by coupling astrometric and direct imaging data. *Astron. Astrophys.* **2023**, *672*, A93. [CrossRef]
192. De Rosa, R.J.; Nielsen, E.L.; Wahhaj, Z.; Ruffio, J.B.; Kalas, P.G.; Peck, A.E.; Hirsch, L.A.; Roberson, W. Direct imaging discovery of a super-Jovian around the young Sun-like star AF Leporis. *Astron. Astrophys.* **2023**, *672*, A94. [CrossRef]
193. Franson, K.; Bowler, B.P.; Zhou, Y.; Pearce, T.D.; Bardalez Gagliuffi, D.C.; Biddle, L.I.; Brandt, T.D.; Crepp, J.R.; Dupuy, T.J.; Faherty, J.; et al. Astrometric Accelerations as Dynamical Beacons: A Giant Planet Imaged inside the Debris Disk of the Young Star AF Lep. *Astrophys. J. Lett.* **2023**, *950*, L19. [CrossRef]

194. Matthews, E.C.; Carter, A.L.; Pathak, P.; Morley, C.V.; Phillips, M.W.; Krishanth, P.M.S.; Feng, F.; Bonse, M.J.; Boogaard, L.A.; Burt, J.A.; et al. A temperate super-Jupiter imaged with JWST in the mid-infrared. *Nature* **2024**. [CrossRef]
195. Alcalá, J.M.; Majidi, F.Z.; Desidera, S.; Frasca, A.; Manara, C.F.; Rigliaco, E.; Gratton, R.; Bonnefoy, M.; Covino, E.; Chauvin, G.; et al. 2MASS J15491331-3539118: A newow-mass wide companion of the GQ Lup system. *Astron. Astrophys.* **2020**, *635*, L1. [CrossRef]
196. Neuhäuser, R.; Guenther, E.W.; Wuchterl, G.; Mugrauer, M.; Bedalov, A.; Hauschildt, P.H. Evidence for a co-moving sub-stellar companion of GQ Lup. *Astron. Astrophys.* **2005**, *435*, L13–L16. [CrossRef]
197. Marois, C.; Macintosh, B.; Barman, T. GQ Lup B Visible and Near-Infrared Photometric Analysis. *Astrophys. J. Lett.* **2007**, *654*, L151–L154. [CrossRef]
198. McElwain, M.W.; Metchev, S.A.; Larkin, J.E.; Barczys, M.; Iserlohe, C.; Krabbe, A.; Quirrenbach, A.; Weiss, J.; Wright, S.A. First High-Contrast Science with an Integral Field Spectrograph: The Substellar Companion to GQ Lupi. *Astrophys. J.* **2007**, *656*, 505–514. [CrossRef]
199. Seifahrt, A.; Neuhäuser, R.; Hauschildt, P.H. Near-infrared integral-field spectroscopy of the companion to GQ Lupi. *Astron. Astrophys.* **2007**, *463*, 309–313. [CrossRef]
200. Long, D.E.; Zhang, K.; Teague, R.; Bergin, E.A. Hints of a Population of Solar System Analog Planets from ALMA. *Astrophys. J. Lett.* **2020**, *895*, L46. [CrossRef]
201. Cendes, Y.; Williams, P.K.G.; Berger, E. A Pilot Radio Search for Magnetic Activity in Directly Imaged Exoplanets. *Astron. J.* **2022**, *163*, 15. [CrossRef]
202. Mesa, D.; Keppler, M.; Cantalloube, F.; Rodet, L.; Charnay, B.; Gratton, R.; Langlois, M.; Boccaletti, A.; Bonnefoy, M.; Vigan, A.; et al. VLT/SPHERE exploration of the young multiplanetary system PDS70. *Astron. Astrophys.* **2019**, *632*, A25. [CrossRef]
203. Burrows, A.; Marley, M.; Hubbard, W.B.; Lunine, J.I.; Guillot, T.; Saumon, D.; Freedman, R.; Sudarsky, D.; Sharp, C. A Nongray Theory of Extrasolar Giant Planets and Brown Dwarfs. *Astrophys. J.* **1997**, *491*, 856–875. [CrossRef]
204. Chabrier, G.; Baraffe, I.; Allard, F.; Hauschildt, P. Evolutionary Models for Very Low-Mass Stars and Brown Dwarfs with Dusty Atmospheres. *Astrophys. J.* **2000**, *542*, 464–472. [CrossRef]
205. Baraffe, I.; Chabrier, G.; Allard, F.; Hauschildt, P.H. Evolutionary models forow-mass stars and brown dwarfs: Uncertainties andimits at very young ages. *Astron. Astrophys.* **2002**, *382*, 563–572. [CrossRef]
206. Palma-Bifani, P.; Chauvin, G.; Bonnefoy, M.; Rojo, P.M.; Petrus, S.; Rodet, L.; Langlois, M.; Allard, F.; Charnay, B.; Desgrange, C.; et al. Peering into the young planetary system AB Pic. Atmosphere, orbit, obliquity, and second planetary candidate. *Astron. Astrophys.* **2023**, *670*, A90. [CrossRef]
207. Grandjean, A.; Lagrange, A.M.; Keppler, M.; Meunier, N.; Mignon, L.; Borgniet, S.; Chauvin, G.; Desidera, S.; Galland, F.; Messina, S.; et al. A HARPS RV search for planets around young nearby stars. *Astron. Astrophys.* **2020**, *633*, A44. [CrossRef]
208. Torres, C.A.O.; Quast, G.R.; Melo, C.H.F.; Sterzik, M.F. Young Nearby Loose Associations. In *Handbook of Star Forming Regions; Volume II*; Reipurth, B., Ed.; Astronomical Society of the Pacific: San Francisco, CA, USA, 2008; Volume 5. p. 757. [CrossRef]
209. Janson, M.; Bergfors, C.; Goto, M.; Brandner, W.; Lafrenière, D. Spatially Resolved Spectroscopy of the Exoplanet HR 8799 c. *Astrophys. J. Lett.* **2010**, *710*, L35–L38. [CrossRef]
210. Fabrycky, D.C.; Murray-Clay, R.A. Stability of the Directly Imaged Multiplanet System HR 8799: Resonance and Masses. *Astrophys. J.* **2010**, *710*, 1408–1421. [CrossRef]
211. Bergfors, C.; Brandner, W.; Janson, M.; Köhler, R.; Henning, T. VLT/NACO astrometry of the HR 8799 planetary system. L′-band observations of the three outer planets. *Astron. Astrophys.* **2011**, *528*, A134. [CrossRef]
212. Skemer, A.J.; Hinz, P.M.; Esposito, S.; Burrows, A.; Leisenring, J.; Skrutskie, M.; Desidera, S.; Mesa, D.; Arcidiacono, C.; Mannucci, F.; et al. First Light LBT AO Images of HR 8799 bcde at 1.6 and 3.3 μm: New Discrepancies between Young Planets and Old Brown Dwarfs. *Astrophys. J.* **2012**, *753*, 14. [CrossRef]
213. Marley, M.S.; Saumon, D.; Cushing, M.; Ackerman, A.S.; Fortney, J.J.; Freedman, R. Masses, Radii, and Cloud Properties of the HR 8799 Planets. *Astrophys. J.* **2012**, *754*, 135. [CrossRef]
214. Esposito, S.; Mesa, D.; Skemer, A.; Arcidiacono, C.; Claudi, R.U.; Desidera, S.; Gratton, R.; Mannucci, F.; Marzari, F.; Masciadri, E.; et al. LBT observations of the HR 8799 planetary system. First detection of HR 8799e in H band. *Astron. Astrophys.* **2013**, *549*, A52. [CrossRef]
215. Ingraham, P.; Marley, M.S.; Saumon, D.; Marois, C.; Macintosh, B.; Barman, T.; Bauman, B.; Burrows, A.; Chilcote, J.K.; De Rosa, R.J.; et al. Gemini Planet Imager Spectroscopy of the HR 8799 Planets c and d. *Astrophys. J. Lett.* **2014**, *794*, L15. [CrossRef]
216. Konopacky, Q.M.; Marois, C.; Macintosh, B.A.; Galicher, R.; Barman, T.S.; Metchev, S.A.; Zuckerman, B. Astrometric Monitoring of the HR 8799 Planets: Orbit Constraints from Self-consistent Measurements. *Astron. J.* **2016**, *152*, 28. [CrossRef]
217. Zurlo, A.; Vigan, A.; Galicher, R.; Maire, A.L.; Mesa, D.; Gratton, R.; Chauvin, G.; Kasper, M.; Moutou, C.; Bonnefoy, M.; et al. Firstight of the VLT planet finder SPHERE. III. New spectrophotometry and astrometry of the HR 8799 exoplanetary system. *Astron. Astrophys.* **2016**, *587*, A57. [CrossRef]

218. Bonnefoy, M.; Zurlo, A.; Baudino, J.L.; Lucas, P.; Mesa, D.; Maire, A.L.; Vigan, A.; Galicher, R.; Homeier, D.; Marocco, F.; et al. Firstight of the VLT planet finder SPHERE. IV. Physical and chemical properties of the planets around HR8799. *Astron. Astrophys.* **2016**, *587*, A58. [CrossRef]
219. Greenbaum, A.Z.; Pueyo, L.; Ruffio, J.B.; Wang, J.J.; De Rosa, R.J.; Aguilar, J.; Rameau, J.; Barman, T.; Marois, C.; Marley, M.S.; et al. GPI Spectra of HR 8799 c, d, and e from 1.5 to 2.4 μm with KLIP Forward Modeling. *Astron. J.* **2018**, *155*, 226. [CrossRef]
220. Goździewski, K.; Migaszewski, C. The Orbital Architecture and Debris Disks of the HR 8799 Planetary System. *Astrophys. J. Suppl.* **2018**, *238*, 6. [CrossRef]
221. Petit dit dea Roche, D.J.M.; van den Ancker, M.E.; Kissler-Patig, M.; Ivanov, V.D.; Fedele, D. New constraints on the HR 8799 planetary system from mid-infrared direct imaging. *Mon. Not. R. Astron. Soc.* **2020**, *491*, 1795–1799. [CrossRef]
222. Wang, J.; Wang, J.J.; Ma, B.; Chilcote, J.; Ertel, S.; Guyon, O.; Ilyin, I.; Jovanovic, N.; Kalas, P.; Lozi, J.; et al. On the Chemical Abundance of HR 8799 and the Planet c. *Astron. J.* **2020**, *160*, 150. [CrossRef]
223. Zurlo, A.; Goździewski, K.; Lazzoni, C.; Mesa, D.; Nogueira, P.; Desidera, S.; Gratton, R.; Marzari, F.; Langlois, M.; Pinna, E.; et al. Orbital and dynamical analysis of the system around HR 8799. New astrometric epochs from VLT/SPHERE and LBT/LUCI. *Astron. Astrophys.* **2022**, *666*, A133. [CrossRef]
224. GRAVITY Collaboration; Lacour, S.; Nowak, M.; Wang, J.; Pfuhl, O.; Eisenhauer, F.; Abuter, R.; Amorim, A.; Anugu, N.; Benisty, M.; et al. First direct detection of an exoplanet by optical interferometry. Astrometry and K-band spectroscopy of HR 8799 e. *Astron. Astrophys.* **2019**, *623*, L11. [CrossRef]
225. Oppenheimer, B.R.; Baranec, C.; Beichman, C.; Brenner, D.; Burruss, R.; Cady, E.; Crepp, J.R.; Dekany, R.; Fergus, R.; Hale, D.; et al. Reconnaissance of the HR 8799 Exosolar System. I. Near-infrared Spectroscopy. *Astrophys. J.* **2013**, *768*, 24. [CrossRef]
226. Biller, B.A.; Apai, D.; Bonnefoy, M.; Desidera, S.; Gratton, R.; Kasper, M.; Kenworthy, M.; Lagrange, A.M.; Lazzoni, C.; Mesa, D.; et al. A high-contrast search for variability in HR 8799bc with VLT-SPHERE. *Mon. Not. R. Astron. Soc.* **2021**, *503*, 743–767. [CrossRef]
227. Wang, J.J.; Gao, P.; Chilcote, J.; Lozi, J.; Guyon, O.; Marois, C.; De Rosa, R.J.; Sahoo, A.; Groff, T.D.; Vievard, S.; et al. Atmospheric Monitoring and Precise Spectroscopy of the HR 8799 Planets with SCExAO/CHARIS. *Astron. J.* **2022**, *164*, 143. [CrossRef]
228. Smith, B.A.; Terrile, R.J. A Circumstellar Disk around β Pictoris. *Science* **1984**, *226*, 1421–1424. [CrossRef] [PubMed]
229. Chauvin, G.; Lagrange, A.M.; Beust, H.; Bonnefoy, M.; Boccaletti, A.; Apai, D.; Allard, F.; Ehrenreich, D.; Girard, J.H.V.; Mouillet, D.; et al. Orbital characterization of the β Pictoris b giant planet. *Astron. Astrophys.* **2012**, *542*, A41. [CrossRef]
230. Lagrange, A.M.; Boccaletti, A.; Milli, J.; Chauvin, G.; Bonnefoy, M.; Mouillet, D.; Augereau, J.C.; Girard, J.H.; Lacour, S.; Apai, D. The position of β Pictoris b position relative to the debris disk. *Astron. Astrophys.* **2012**, *542*, A40. [CrossRef]
231. Snellen, I.A.G.; Brown, A.G.A. The mass of the young planet Beta Pictoris b through the astrometric motion of its host star. *Nat. Astron.* **2018**, *2*, 883–886. [CrossRef]
232. Lagrange, A.M.; Boccaletti, A.; Langlois, M.; Chauvin, G.; Gratton, R.; Beust, H.; Desidera, S.; Milli, J.; Bonnefoy, M.; Cheetham, A.; et al. Post-conjunction detection of β Pictoris b with VLT/SPHERE. *Astron. Astrophys.* **2019**, *621*, L8. [CrossRef]
233. GRAVITY Collaboration; Nowak, M.; Lacour, S.; Mollière, P.; Wang, J.; Charnay, B.; van Dishoeck, E.F.; Abuter, R.; Amorim, A.; Berger, J.P.; et al. Peering into the formation history of β Pictoris b with VLTI/GRAVITYong-baseline interferometry. *Astron. Astrophys.* **2020**, *633*, A110. [CrossRef]
234. Beuzit, J.L.; Ségransan, D.; Forveille, T.; Udry, S.; Delfosse, X.; Mayor, M.; Perrier, C.; Hainaut, M.C.; Roddier, C.; Roddier, F.; et al. New neighbours. III. 21 new companions to nearby dwarfs, discovered with adaptive optics. *Astron. Astrophys.* **2004**, *425*, 997–1008. [CrossRef]
235. Morley, C.V.; Fortney, J.J.; Marley, M.S.; Visscher, C.; Saumon, D.; Leggett, S.K. Neglected Clouds in T and Y Dwarf Atmospheres. *Astrophys. J.* **2012**, *756*, 172. [CrossRef]
236. Burgasser, A.J.; Simcoe, R.A.; Bochanski, J.J.; Saumon, D.; Mamajek, E.E.; Cushing, M.C.; Marley, M.S.; McMurtry, C.; Pipher, J.L.; Forrest, W.J. Clouds in the Coldest Brown Dwarfs: Fire Spectroscopy of Ross 458C. *Astrophys. J.* **2010**, *725*, 1405–1420. [CrossRef]
237. Piétu, V.; Dutrey, A.; Guilloteau, S.; Chapillon, E.; Pety, J. Resolving the inner dust disks surrounding LkCa 15 and MWC 480 at mm wavelengths. *Astron. Astrophys.* **2006**, *460*, L43–L47. [CrossRef]
238. Espaillat, C.; Calvet, N.; Luhman, K.L.; Muzerolle, J.; D'Alessio, P. Confirmation of a Gapped Primordial Disk around LkCa 15. *Astrophys. J. Lett.* **2008**, *682*, L125. [CrossRef]
239. Bonavita, M.; Chauvin, G.; Boccaletti, A.; Pietu, V.; Baudoz, P.; Beuzit, J.L.; Dutrey, A.; Guilloteau, S.; Lagrange, A.M.; Mouillet, D.; et al. Searching for the sub-stellar companions in the LkCa15 proto-planetary disk. *Astron. Astrophys.* **2010**, *522*, A2. [CrossRef]
240. Thalmann, C.; Janson, M.; Garufi, A.; Boccaletti, A.; Quanz, S.P.; Sissa, E.; Gratton, R.; Salter, G.; Benisty, M.; Bonnefoy, M.; et al. Resolving the Planet-hosting Inner Regions of the LkCa 15 Disk. *Astrophys. J. Lett.* **2016**, *828*, L17. [CrossRef]
241. Mendigutía, I.; Oudmaijer, R.D.; Schneider, P.C.; Huélamo, N.; Baines, D.; Brittain, S.D.; Aberasturi, M. Spectro-astrometry of the pre-transitional star LkCa 15 does not reveal an accreting planet but extended Hα emission. *Astron. Astrophys.* **2018**, *618*, L9. [CrossRef]

242. Blakely, D.; Francis, L.; Johnstone, D.; Soulain, A.; Tuthill, P.; Cheetham, A.; Sanchez-Bermudez, J.; Sivaramakrishnan, A.; Dong, R.; van der Marel, N.; et al. Two Rings and a Marginally Resolved, 5 au Disk around LkCa 15 Identified via Near-infrared Sparse Aperture Masking Interferometry. *Astrophys. J.* **2022**, *931*, 3. [CrossRef]
243. Sallum, S.; Eisner, J.; Skemer, A.; Murray-Clay, R. Systematic Multiepoch Monitoring of LkCa 15: Dynamic Dust Structures on Solar System Scales. *Astrophys. J.* **2023**, *953*, 55. [CrossRef]
244. Torres, C.A.O.; Quast, G.R.; da Silva, L.; de La Reza, R.; Melo, C.H.F.; Sterzik, M. Search for associations containing young stars (SACY). I. Sample and searching method. *Astron. Astrophys.* **2006**, *460*, 695–708. [CrossRef]
245. Hinkley, S.; Carter, A.L.; Ray, S.; Skemer, A.; Biller, B.; Choquet, E.; Millar-Blanchaer, M.A.; Sallum, S.; Miles, B.; Whiteford, N.; et al. The JWST Early Release Science Program for the Direct Imaging and Spectroscopy of Exoplanetary Systems. *Pub. Astron. Soc. Pac.* **2022**, *134*, 095003. [CrossRef]
246. Hashimoto, J.; Dong, R.; Kudo, T.; Honda, M.; McClure, M.K.; Zhu, Z.; Muto, T.; Wisniewski, J.; Abe, L.; Brandner, W.; et al. Polarimetric Imaging of Large Cavity Structures in the Pre-transitional Protoplanetary Disk around PDS 70: Observations of the Disk. *Astrophys. J. Lett.* **2012**, *758*, L19. [CrossRef]
247. Wang, J.J.; Ginzburg, S.; Ren, B.; Wallack, N.; Gao, P.; Mawet, D.; Bond, C.Z.; Cetre, S.; Wizinowich, P.; De Rosa, R.J.; et al. Keck/NIRC2 L′-band Imaging of Jovian-mass Accreting Protoplanets around PDS 70. *Astron. J.* **2020**, *159*, 263. [CrossRef]
248. Stolker, T.; Marleau, G.D.; Cugno, G.; Mollière, P.; Quanz, S.P.; Todorov, K.O.; Kühn, J. MIRACLES: Atmospheric characterization of directly imaged planets and substellar companions at 4-5 μm. II. Constraints on the mass and radius of the enshrouded planet PDS 70 b. *Astron. Astrophys.* **2020**, *644*, A13. [CrossRef]
249. Benisty, M.; Bae, J.; Facchini, S.; Keppler, M.; Teague, R.; Isella, A.; Kurtovic, N.T.; Pérez, L.M.; Sierra, A.; Andrews, S.M.; et al. A Circumplanetary Disk around PDS70c. *Astrophys. J. Lett.* **2021**, *916*, L2. [CrossRef]
250. Nordström, B.; Mayor, M.; Andersen, J.; Holmberg, J.; Pont, F.; Jørgensen, B.R.; Olsen, E.H.; Udry, S.; Mowlavi, N. The Geneva-Copenhagen survey of the Solar neighbourhood. Ages, metallicities, and kinematic properties of ∼14 000 F and G dwarfs. *Astron. Astrophys.* **2004**, *418*, 989–1019. [CrossRef]
251. Eker, Z.; Ak, N.F.; Bilir, S.; Doğru, D.; Tüysüz, M.; Soydugan, E.; Bakış, H.; Uğraş, B.; Soydugan, F.; Erdem, A.; et al. A catalogue of chromospherically active binary stars (third edition). *Mon. Not. R. Astron. Soc.* **2008**, *389*, 1722–1726. [CrossRef]
252. Philipot, F.; Lagrange, A.M.; Rubini, P.; Kiefer, F.; Chomez, A. Updated characterization ofong-period single companion by combining radial velocity, relative astrometry, and absolute astrometry. *Astron. Astrophys.* **2023**, *670*, A65. [CrossRef]
253. Feng, F.; Anglada-Escudé, G.; Tuomi, M.; Jones, H.R.A.; Chanamé, J.; Butler, P.R.; Janson, M. Detection of the nearest Jupiter analogue in radial velocity and astrometry data. *Mon. Not. R. Astron. Soc.* **2019**, *490*, 5002–5016. [CrossRef]
254. Chauvin, G.; Vigan, A.; Bonnefoy, M.; Desidera, S.; Bonavita, M.; Mesa, D.; Boccaletti, A.; Buenzli, E.; Carson, J.; Delorme, P.; et al. The VLT/NaCoarge program to probe the occurrence of exoplanets and brown dwarfs at wide orbits. II. Survey description, results, and performances. *Astron. Astrophys.* **2015**, *573*, A127. [CrossRef]
255. Chauvin, G. Two decades of exoplanetary science with adaptive optics. In Proceedings of the Adaptive Optics Systems VI, Austin, TX, USA, 10–15 June 2018; Society of Photo-Optical Instrumentation Engineers (SPIE) Conference Series; Close, L.M., Schreiber, L., Schmidt, D., Eds.; Society of Photo-Optical Instrumentation Engineers (SPIE): Bellingham, WA, USA, 2018; Volume 10703, p. 1070305. [CrossRef]
256. Nakajima, T.; Durrance, S.T.; Golimowski, D.A.; Kulkarni, S.R. A Coronagraphic Search for Brown Dwarfs around Nearby Stars. *Astrophys. J.* **1994**, *428*, 797. [CrossRef]
257. Chauvin, G.; Thomson, M.; Dumas, C.; Beuzit, J.L.; Lowrance, P.; Fusco, T.; Lagrange, A.M.; Zuckerman, B.; Mouillet, D. Adaptive optics imaging survey of the Tucana-Horologium association. *Astron. Astrophys.* **2003**, *404*, 157–162. [CrossRef]
258. Neuhäuser, R.; Guenther, E.W.; Alves, J.; Huélamo, N.; Ott, T.; Eckart, A. An infrared imaging search forow-mass companions to members of the young nearby β Pic and Tucana/Horologium associations. *Astron. Nachrichten* **2003**, *324*, 535–542. [CrossRef]
259. Masciadri, E.; Mundt, R.; Henning, T.; Alvarez, C.; Barrado y Navascués, D. A Search for Hot Massive Extrasolar Planets around Nearby Young Stars with the Adaptive Optics System NACO. *Astrophys. J.* **2005**, *625*, 1004–1018. [CrossRef]
260. Biller, B.A.; Close, L.M.; Masciadri, E.; Nielsen, E.; Lenzen, R.; Brandner, W.; McCarthy, D.; Hartung, M.; Kellner, S.; Mamajek, E.; et al. An Imaging Survey for Extrasolar Planets around 45 Close, Young Stars with the Simultaneous Differential Imager at the Very Large Telescope and MMT. *Astrophys. J. Suppl.* **2007**, *173*, 143–165. [CrossRef]
261. Kasper, M.; Apai, D.; Janson, M.; Brandner, W. A novel L-band imaging search for giant planets in the Tucana and β Pictoris moving groups. *Astron. Astrophys.* **2007**, *472*, 321–327. [CrossRef]
262. Apai, D.; Janson, M.; Moro-Martín, A.; Meyer, M.R.; Mamajek, E.E.; Masciadri, E.; Henning, T.; Pascucci, I.; Kim, J.S.; Hillenbrand, L.A.; et al. A Survey for Massive Giant Planets in Debris Disks with Evacuated Inner Cavities. *Astrophys. J.* **2008**, *672*, 1196–1201. [CrossRef]
263. Heinze, A.N.; Hinz, P.M.; Sivanandam, S.; Kenworthy, M.; Meyer, M.; Miller, D. Constraints on Long-period Planets from an L′- and M-band Survey of Nearby Sun-like Stars: Observations. *Astrophys. J.* **2010**, *714*, 1551–1569. [CrossRef]

264. Heinze, A.N.; Hinz, P.M.; Kenworthy, M.; Meyer, M.; Sivanandam, S.; Miller, D. Constraints on Long-period Planets from an L′- and M-band Survey of Nearby Sun-like Stars: Modeling Results. *Astrophys. J.* **2010**, *714*, 1570–1581. [CrossRef]
265. Janson, M.; Bonavita, M.; Klahr, H.; Lafrenière, D.; Jayawardhana, R.; Zinnecker, H. High-contrast Imaging Search for Planets and Brown Dwarfs around the Most Massive Stars in the Solar Neighborhood. *Astrophys. J.* **2011**, *736*, 89. [CrossRef]
266. Vigan, A.; Patience, J.; Marois, C.; Bonavita, M.; De Rosa, R.J.; Macintosh, B.; Song, I.; Doyon, R.; Zuckerman, B.; Lafrenière, D.; et al. The International Deep Planet Survey. I. The frequency of wide-orbit massive planets around A-stars. *Astron. Astrophys.* **2012**, *544*, A9. [CrossRef]
267. Galicher, R.; Marois, C.; Macintosh, B.; Zuckerman, B.; Barman, T.; Konopacky, Q.; Song, I.; Patience, J.; Lafrenière, D.; Doyon, R.; et al. The International Deep Planet Survey. II. The frequency of directly imaged giant exoplanets with stellar mass. *Astron. Astrophys.* **2016**, *594*, A63. [CrossRef]
268. Delorme, P.; Lagrange, A.M.; Chauvin, G.; Bonavita, M.; Lacour, S.; Bonnefoy, M.; Ehrenreich, D.; Beust, H. High-resolution imaging of young M-type stars of the solar neighbourhood: Probing for companions down to the mass of Jupiter. *Astron. Astrophys.* **2012**, *539*, A72. [CrossRef]
269. Bowler, B.P.; Liu, M.C.; Shkolnik, E.L.; Dupuy, T.J.; Cieza, L.A.; Kraus, A.L.; Tamura, M. Planets around Low-mass Stars (PALMS). I. A Substellar Companion to the Young M Dwarf 1RXS J235133.3+312720. *Astrophys. J.* **2012**, *753*, 142. [CrossRef]
270. Bowler, B.P.; Liu, M.C.; Shkolnik, E.L.; Tamura, M. Planets around Low-mass Stars (PALMS). II. A Low-mass Companion to the Young M Dwarf GJ 3629 Separated by 0.2″. *Astrophys. J.* **2012**, *756*, 69. [CrossRef]
271. Bowler, B.P.; Liu, M.C.; Shkolnik, E.L.; Tamura, M. Planets around Low-mass Stars (PALMS). IV. The Outer Architecture of M Dwarf Planetary Systems. *Astrophys. J. Suppl.* **2015**, *216*, 7. [CrossRef]
272. Rameau, J.; Chauvin, G.; Lagrange, A.M.; Klahr, H.; Bonnefoy, M.; Mordasini, C.; Bonavita, M.; Desidera, S.; Dumas, C.; Girard, J.H. A survey of young, nearby, and dusty stars conducted to understand the formation of wide-orbit giant planets. VLT/NaCo adaptive optics thermal and angular differential imaging. *Astron. Astrophys.* **2013**, *553*, A60. [CrossRef]
273. Tamura, M. Subaru Strategic Exploration of Exoplanets and Disks with HiCIAO/AO188 (SEEDS). In Proceedings of the Exoplanets and Disks: Their Formation and Diversity, Kailua-Kona, HI, USA, 9–12 March 2009; American Institute of Physics Conference Series; Usuda, T., Tamura, M., Ishii, M., Eds.; AIP: Long Island, NY, USA, 2009; Volume 1158, pp. 11–16. [CrossRef]
274. Yamamoto, K.; Matsuo, T.; Shibai, H.; Itoh, Y.; Konishi, M.; Sudo, J.; Tanii, R.; Fukagawa, M.; Sumi, T.; Kudo, T.; et al. Direct Imaging Search for Extrasolar Planets in the Pleiades. *Pub. Astron. Soc. Japan* **2013**, *65*, 90. [CrossRef]
275. Brandt, T.D.; McElwain, M.W.; Turner, E.L.; Mede, K.; Spiegel, D.S.; Kuzuhara, M.; Schlieder, J.E.; Wisniewski, J.P.; Abe, L.; Biller, B.; et al. A Statistical Analysis of SEEDS and Other High-contrast Exoplanet Surveys: Massive Planets or Low-mass Brown Dwarfs? *Astrophys. J.* **2014**, *794*, 159. [CrossRef]
276. Janson, M.; Brandt, T.D.; Moro-Martín, A.; Usuda, T.; Thalmann, C.; Carson, J.C.; Goto, M.; Currie, T.; McElwain, M.W.; Itoh, Y.; et al. The SEEDS Direct Imaging Survey for Planets and Scattered Dust Emission in Debris Disk Systems. *Astrophys. J.* **2013**, *773*, 73. [CrossRef]
277. Tamura, M. SEEDS—Strategic explorations of exoplanets and disks with the Subaru Telescope. *Proc. Jpn. Acad. Ser. B* **2016**, *92*, 45–55. [CrossRef] [PubMed]
278. Biller, B.A.; Liu, M.C.; Wahhaj, Z.; Nielsen, E.L.; Hayward, T.L.; Males, J.R.; Skemer, A.; Close, L.M.; Chun, M.; Ftaclas, C.; et al. The Gemini/NICI Planet-Finding Campaign: The Frequency of Planets around Young Moving Group Stars. *Astrophys. J.* **2013**, *777*, 160. [CrossRef]
279. Nielsen, E.L.; Liu, M.C.; Wahhaj, Z.; Biller, B.A.; Hayward, T.L.; Close, L.M.; Males, J.R.; Skemer, A.J.; Chun, M.; Ftaclas, C.; et al. The Gemini NICI Planet-Finding Campaign: The Frequency of Giant Planets around Young B and A Stars. *Astrophys. J.* **2013**, *776*, 4. [CrossRef]
280. Wahhaj, Z.; Liu, M.C.; Nielsen, E.L.; Biller, B.A.; Hayward, T.L.; Close, L.M.; Males, J.R.; Skemer, A.; Ftaclas, C.; Chun, M.; et al. The Gemini Planet-finding Campaign: The Frequency Of Giant Planets around Debris Disk Stars. *Astrophys. J.* **2013**, *773*, 179. [CrossRef]
281. Skemer, A.J.; Hinz, P.; Esposito, S.; Skrutskie, M.F.; Defrère, D.; Bailey, V.; Leisenring, J.; Apai, D.; Biller, B.; Bonnefoy, M.; et al. High contrast imaging at the LBT: The LEECH exoplanet imaging survey. In Proceedings of the Adaptive Optics Systems IV, Montréal, QC, Canada, 22–27 June 2014; Society of Photo-Optical Instrumentation Engineers (SPIE) Conference Series; Marchetti, E., Close, L.M., Vran, J.P., Eds.; Society of Photo-Optical Instrumentation Engineers (SPIE): Bellingham, WA, USA, 2014; Volume 9148, p. 91480L. [CrossRef]
282. Maire, A.L.; Skemer, A.J.; Hinz, P.M.; Desidera, S.; Esposito, S.; Gratton, R.; Marzari, F.; Skrutskie, M.F.; Biller, B.A.; Defrère, D.; et al. The LEECH Exoplanet Imaging Survey. Further constraints on the planet architecture of the HR 8799 system (Corrigendum). *Astron. Astrophys.* **2015**, *579*, C2. [CrossRef]
283. Stone, J.M.; Skemer, A.J.; Hinz, P.M.; Bonavita, M.; Kratter, K.M.; Maire, A.L.; Defrere, D.; Bailey, V.P.; Spalding, E.; Leisenring, J.M.; et al. The LEECH Exoplanet Imaging Survey: Limits on Planet Occurrence Rates under Conservative Assumptions. *Astron. J.* **2018**, *156*, 286. [CrossRef]

284. Thalmann, C.; Desidera, S.; Bonavita, M.; Janson, M.; Usuda, T.; Henning, T.; Köhler, R.; Carson, J.; Boccaletti, A.; Bergfors, C.; et al. SPOTS: The Search for Planets Orbiting Two Stars. I. Survey description and first observations. *Astron. Astrophys.* **2014**, *572*, A91. [CrossRef]
285. Bonavita, M.; Desidera, S.; Thalmann, C.; Janson, M.; Vigan, A.; Chauvin, G.; Lannier, J. SPOTS: The Search for Planets Orbiting Two Stars. II. First constraints on the frequency of sub-stellar companions on wide circumbinary orbits. *Astron. Astrophys.* **2016**, *593*, A38. [CrossRef]
286. Asensio-Torres, R.; Janson, M.; Bonavita, M.; Desidera, S.; Thalmann, C.; Kuzuhara, M.; Henning, T.; Marzari, F.; Meyer, M.R.; Calissendorff, P.; et al. SPOTS: The Search for Planets Orbiting Two Stars. III. Complete sample and statistical analysis. *Astron. Astrophys.* **2018**, *619*, A43. [CrossRef]
287. Meshkat, T.; Bailey, V.P.; Su, K.Y.L.; Kenworthy, M.A.; Mamajek, E.E.; Hinz, P.M.; Smith, P.S. Searching for Planets in Holey Debris Disks with the Apodizing Phase Plate. *Astrophys. J.* **2015**, *800*, 5. [CrossRef]
288. Meshkat, T.; Kenworthy, M.A.; Reggiani, M.; Quanz, S.P.; Mamajek, E.E.; Meyer, M.R. Searching for gas giant planets on Solar system scales—A NACO/APP L′-band survey of A- and F-type main-sequence stars. *Mon. Not. R. Astron. Soc.* **2015**, *453*, 2533–2539. [CrossRef]
289. Durkan, S.; Janson, M.; Carson, J.C. High Contrast Imaging with Spitzer: Constraining the Frequency of Giant Planets out to 1000 au Separations. *Astrophys. J.* **2016**, *824*, 58. [CrossRef]
290. Desidera, S.; Covino, E.; Messina, S.; Carson, J.; Hagelberg, J.; Schlieder, J.E.; Biazzo, K.; Alcalá, J.M.; Chauvin, G.; Vigan, A.; et al. The VLT/NaCoarge program to probe the occurrence of exoplanets and brown dwarfs in wide orbits. I. Sample definition and characterization. *Astron. Astrophys.* **2015**, *573*, A126. [CrossRef]
291. Vigan, A.; Bonavita, M.; Biller, B.; Forgan, D.; Rice, K.; Chauvin, G.; Desidera, S.; Meunier, J.C.; Delorme, P.; Schlieder, J.E.; et al. The VLT/NaCoarge program to probe the occurrence of exoplanets and brown dwarfs at wide orbits. IV. Gravitational instability rarely forms wide, giant planets. *Astron. Astrophys.* **2017**, *603*, A3. [CrossRef]
292. Lannier, J.; Delorme, P.; Lagrange, A.M.; Borgniet, S.; Rameau, J.; Schlieder, J.E.; Gagné, J.; Bonavita, M.A.; Malo, L.; Chauvin, G.; et al. MASSIVE: A Bayesian analysis of giant planet populations around ow-mass stars. *Astron. Astrophys.* **2016**, *596*, A83. [CrossRef]
293. Naud, M.E.; Artigau, É.; Doyon, R.; Malo, L.; Gagné, J.; Lafrenière, D.; Wolf, C.; Magnier, E.A. PSYM-WIDE: A Survey for Large-separation Planetary-mass Companions to Late Spectral Type Members of Young Moving Groups. *Astron. J.* **2017**, *154*, 129. [CrossRef]
294. Baron, F.; Artigau, É.; Rameau, J.; Lafrenière, D.; Gagné, J.; Malo, L.; Albert, L.; Naud, M.E.; Doyon, R.; Janson, M.; et al. WEIRD: Wide-orbit Exoplanet Search with InfraRed Direct Imaging. *Astron. J.* **2018**, *156*, 137. [CrossRef]
295. Janson, M.; Asensio-Torres, R.; André, D.; Bonnefoy, M.; Delorme, P.; Reffert, S.; Desidera, S.; Langlois, M.; Chauvin, G.; Gratton, R.; et al. The B-Star Exoplanet Abundance Study: A co-moving 16–25 M_{Jup} companion to the young binary system HIP 79098. *Astron. Astrophys.* **2019**, *626*, A99. [CrossRef]
296. Janson, M.; Squicciarini, V.; Delorme, P.; Gratton, R.; Bonnefoy, M.; Reffert, S.; Mamajek, E.E.; Eriksson, S.C.; Vigan, A.; Langlois, M.; et al. BEAST begins: Sample characteristics and survey performance of the B-star Exoplanet Abundance Study. *Astron. Astrophys.* **2021**, *646*, A164. [CrossRef]
297. Bohn, A.J.; Kenworthy, M.A.; Ginski, C.; Manara, C.F.; Pecaut, M.J.; de Boer, J.; Keller, C.U.; Mamajek, E.E.; Meshkat, T.; Reggiani, M.; et al. The Young Suns Exoplanet Survey: Detection of a wide-orbit planetary-mass companion to a solar-type Sco-Cen member. *Mon. Not. R. Astron. Soc.* **2020**, *492*, 431–443. [CrossRef]
298. Bohn, A.J.; Kenworthy, M.A.; Ginski, C.; Rieder, S.; Mamajek, E.E.; Meshkat, T.; Pecaut, M.J.; Reggiani, M.; de Boer, J.; Keller, C.U.; et al. Two Directly Imaged, Wide-orbit Giant Planets around the Young, Solar Analog TYC 8998-760-1. *Astrophys. J. Lett.* **2020**, *898*, L16. [CrossRef]
299. Bohn, A.J.; Ginski, C.; Kenworthy, M.A.; Mamajek, E.E.; Pecaut, M.J.; Mugrauer, M.; Vogt, N.; Adam, C.; Meshkat, T.; Reggiani, M.; et al. Discovery of a directly imaged planet to the young solar analog YSES 2. *Astron. Astrophys.* **2021**, *648*, A73. [CrossRef]
300. Launhardt, R.; Henning, T.; Quirrenbach, A.; Ségransan, D.; Avenhaus, H.; van Boekel, R.; Brems, S.S.; Cheetham, A.C.; Cugno, G.; Girard, J.; et al. ISPY-NACO Imaging Survey for Planets around Young stars. Survey description and results from the first 2.5 years of observations. *Astron. Astrophys.* **2020**, *635*, A162. [CrossRef]
301. Nielsen, E.L.; Close, L.M. A Uniform Analysis of 118 Stars with High-contrast Imaging: Long-period Extrasolar Giant Planets are Rare Around Sun-like Stars. *Astrophys. J.* **2010**, *717*, 878–896. [CrossRef]
302. Baron, F.; Lafrenière, D.; Artigau, É.; Gagné, J.; Rameau, J.; Delorme, P.; Naud, M.E. Constraints on the Occurrence and Distribution of 1–20 M $_{Jup}$ Companions to Stars at Separations of 5–5000 au from a Compilation of Direct Imaging Surveys. *Astron. J.* **2019**, *158*, 187. [CrossRef]
303. Cugno, G.; Pearce, T.D.; Launhardt, R.; Bonse, M.J.; Ma, J.; Henning, T.; Quirrenbach, A.; Ségransan, D.; Matthews, E.C.; Quanz, S.P.; et al. ISPY: NACO Imaging Survey for Planets around Young stars. The demographics of forming planets embedded in protoplanetary disks. *Astron. Astrophys.* **2023**, *669*, A145. [CrossRef]

304. Gratton, R.; Mesa, D.; Bonavita, M.; Zurlo, A.; Marino, S.; Kervella, P.; Desidera, S.; D'Orazi, V.; Rigliaco, E. Jupiter-like planets might be common in aow-density environment. *Nat. Commun.* **2023**, *14*, 6232. [CrossRef] [PubMed]
305. Burrows, A.; Sudarsky, D.; Lunine, J.I. Beyond the T Dwarfs: Theoretical Spectra, Colors, and Detectability of the Coolest Brown Dwarfs. *Astrophys. J.* **2003**, *596*, 587–596. [CrossRef]
306. Vides, C.L.; Macintosh, B.; Binder, B.A.; De Rosa, R.J.; Ruffio, J.B.; Savransky, D. Model of the Search for Extraterrestrial Intelligence with Coronagraphic Imaging. *Astron. J.* **2019**, *158*, 207. [CrossRef]
307. Roberge, A.; Fischer, D.; Peterson, B.; Bean, J.; Calzetti, D.; Dawson, R.; Dressing, C.; Feinberg, L.; France, K.; Guyon, O.; et al. The Large UV / Optical / Infrared Surveyor (LUVOIR) Telling the Story of Life in the Universe. *Proc. Bull. Am. Astron. Soc.* **2021**, *53*, 332. [CrossRef]
308. Gaudi, B.S.; Seager, S.; Mennesson, B.; Kiessling, A.; Warfield, K.; Cahoy, K.; Clarke, J.T.; Domagal-Goldman, S.; Feinberg, L.; Guyon, O.; et al. The Habitable Exoplanet Observatory (HabEx) Mission Concept Study Final Report. *arXiv* **2020**, arXiv:2001.06683. [CrossRef]
309. Vaughan, S.R.; Gebhard, T.D.; Bott, K.; Casewell, S.L.; Cowan, N.B.; Doelman, D.S.; Kenworthy, M.; Mazoyer, J.; Millar-Blanchaer, M.A.; Trees, V.J.H.; et al. Chasing rainbows and ocean glints: Inner working angle constraints for the Habitable Worlds Observatory. *Mon. Not. R. Astron. Soc.* **2023**, *524*, 5477–5485. [CrossRef]
310. Stark, C.C.; Mennesson, B.; Bryson, S.; Ford, E.B.; Robinson, T.D.; Belikov, R.; Bolcar, M.R.; Feinberg, L.D.; Guyon, O.; Latouf, N.; et al. Paths to robust exoplanet science yield margin for the Habitable Worlds Observatory. *J. Astron. Telesc. Instrum. Syst.* **2024**, *10*, 034006. [CrossRef]
311. Quanz, S.P.; Absil, O.; Benz, W.; Bonfils, X.; Berger, J.P.; Defrère, D.; van Dishoeck, E.; Ehrenreich, D.; Fortney, J.; Glauser, A.; et al. Atmospheric characterization of terrestrial exoplanets in the mid-infrared: Biosignatures, habitability, and diversity. *Exp. Astron.* **2022**, *54*, 1197–1221. [CrossRef] [PubMed]